UNIVERSITÀ DEGLI STUDI DI NAPOLI FEDERICO II

Dottorato di Ricerca in Ingegneria Elettronica e delle Telecomunicazioni (XVIII ciclo)

SYNCHRONIZATION TECHNICS FOR OFDM SYSTEMS

TILDE FUSCO

Il Coordinatore
Ch.mo Prof. Giovanni POGGI

Il Tutore
Ch.mo Prof. Mario TANDA

A.A. 2004-2005

A Silverio e alla mia famiglia

Acknowledgements

I wish to thank my advisor, Prof. Mario Tanda, for giving me constant trust during the entire course of my PH.D. studies, for his helpful suggestions, for his continuous support and his teachings essential to achieve this goal.

Tanks are also due to all staff of the Dipartimento di Ingegneria Elettronica e delle Telecomunicazioni at the Università di Napoli Federico II for their kind availability.

Contents

List of Figures

Notations

j imaginary unit

a scalar

a^* complex conjugate of a scalar a

$|a|$ absolute value of the number a

$\Re\{a\}$ real part of a complex scalar a

$\Im\{a\}$ imaginary part of a complex scalar a

$\angle\{a\}$ argument of a complex number in $[0, 2\pi]$

$\hat{a}$ estimate for the parameter a

$\tilde{a}$ trial value for a

$\boldsymbol{a}$ vector

$\boldsymbol{a}^*$ complex conjugate of the vector $\boldsymbol{a}$

$\boldsymbol{a}^T$ transpose of the vector $\boldsymbol{a}$

$\boldsymbol{a}^H$ Hermitian of the vector $\boldsymbol{a}$

$\boldsymbol{A}$ matrix

$[\boldsymbol{A}]_{(m,l)}$ (m,l)-th entry of the matrix $\boldsymbol{A}$

$\boldsymbol{A}^T$ transpose of the matrix $\boldsymbol{A}$

$\boldsymbol{A}^H$ Hermitian of the matrix $\boldsymbol{A}$

$\boldsymbol{A}^{-1}$ inverse of the matrix $\boldsymbol{A}$

$\det\{\boldsymbol{A}\}$ determinant of the matrix $\boldsymbol{A}$

$\boldsymbol{I}_n$ $n \times n$ identity matrix

$\boldsymbol{O}_{n\times m}$ $n \times m$ null matrix

$\mathbf{1}_n$ n-dimensional column vector of all ones

$x(t)$ time continuous signal

$x(n)$ time discrete signal

$E[\cdot]$ statistical expectation

$\mathfrak{F}[\cdot]$ Fourier transform

$\mathrm{diag}\{\cdot\}$ diagonal matrix

$\mathrm{Tr}\{\cdot\}$ trace operator

$\otimes$ Kronecker product

$(f*g)(m) \stackrel{\triangle}{=} \sum_n f(n)g(m-n)$ convolution product of the time discrete functions $f(\cdot)$ and $g(\cdot)$

$\lceil\cdot\rceil$ rounds its argument to the nearest integer towards infinity

$\lfloor\cdot\rfloor$ rounds its argument to the nearest integer towards minus infinity

$\mathrm{u}(m)$ unit step function

$\delta[m]$ Kronecker delta

$$\delta(t) \stackrel{\triangle}{=} \begin{cases} 1 & t = 0\,, \\ 0 & \text{otherwise} \end{cases}$$

$$\Pi\,(t/T) \stackrel{\triangle}{=} \begin{cases} 1 & |t| \leq T\,, \\ 0 & \text{otherwise} \end{cases}$$

$\mathrm{sinc}(t) \triangleq \dfrac{\sin(\pi t)}{(\pi t)}$

$\mathrm{rep}_T[\cdot]$ replication of period T

N number of subcarriers

L_c cyclic prefix

$M = N + L_c$ total length of OFDM symbol

N_m delay spread

L number of identical parts of training symbol

$P = N/L$

T symbol interval

T_c sampling interval

f_c sampling frequency

θ symbol timing

ϕ carrier phase

ϵ carrier frequency offset normalized to the intercarrier spacing

$\tau_1 \triangleq \{0, \ldots, N-1\}$

$\tau_2 \triangleq \{-L_c, \ldots, N-1\}$

Glossary

ADC	Analogous Digital Converter
AWGN	Additive White Gaussian Noise
BER	Bit Error Rate
BLU	Best Linear Unbiased
BPSK	Binary Phase Shift Keying
C	Circular
CFO	Carrier Frequency Offset
CGRV	Complex Gaussian Random Vector
CP	Cyclic Prefix
CRB	Cramèr Rao Bound
DFT	Discrete Fourier Transform
DMT	Discrete Multi Tone
DAC	Digital to Analogous Converter
FDM	Frequency Division Multiplexing
GCRB	Gaussian Cramèr-Rao Bound
GSC	Generalized Schmidl and Cox
ICI	Inter Carrier Interference
ISI	Inter Symbol Interference

IDFT	Inverse Discrete Fourier Transform
LLF	Log Likelihood Function
MBL	Minn Bhargava Letaief
MCL0	Maximum Correlation for $L_c = 0$
MCL0R	Maximum Correlation for $L_c = 0$ Refined
MMLC	Modified Maximum Likelihood Circular
ML	Maximum Likelihood
MLC	Maximum Likelihood Circular
MLS	Maximum Length Sequence
MSE	Mean Squared Error
NC	Noncircular
NC-BLU	Noncircular Best Linear Unbiased
NCR	Noncircular Refined
OFDM	Orthogonal Frequency Division Multiplexing
PDF	Probability Density Function
PSD	Power Spectral Density
QPSK	Quadrature Phase Shift Keying
RHS	Right Hand Side
SER	Symbol Error Rate
SNR	Signal to Noise Ratio
SS	Serpedin Shi

Chapter 1

Introduction

Although the principles of Orthogonal Frequency Division Multiplexing (OFDM) modulation [1, 2] have been in existence since 1960, in the last years OFDM modulation is emerged as a key modulation technique of commercial high speed communication systems. The principal reason of this increasing interest is due to its capability to provide high-speed data rate transmissions with low complexity and to counteract the intersymbol interference (ISI) introduced by dispersive channels. For this reason OFDM modulation has been adopted by several digital wireline and wireless communication standards, such as the European digital audio and video broadcasting standards, as well as local area networks.

On the other hand, the use of OFDM systems with a high number of subcarriers has some drawbacks. The major drawback is its high sensitivity to synchronization non idealities between the transmitter and receiver oscillators [3]-[8]. Specifically, incorrect timing synchronization can cause interference between successive symbols and, if not perfectly compensated before the equalization process, can lead to a severe performance degradation. In addition, a carrier-frequency offset (CFO) induces an amplitude reduction of the useful signal and provokes interference between adjacent subcarriers (ICI).

Several studies have been focused on parameter estimation for OFDM systems based on data-aided and non data-aided (or blind) techniques. In the first case it is in demand the transmission of known sequences or the use of a training symbol with a known structure while blind estimation algorithms use exclusively the statistic properties of transmitted signal. For example, ef-

ficient blind techniques that take advantage of temporal redundancy induced by the cyclic prefix (CP) has been exploited in [9] to obtain a low complexity estimator. In particular, J.J. van de Beek *et al.* in [9] derive the joint symbol timing and CFO maximum likelihood (ML) estimator under the assumption of a non dispersive channel and by modeling the OFDM signal vector as a circular complex Gaussian random vector (C-CGRV) [10]. The Gaussian assumption is reasonable when the number of subcarriers is sufficiently large. However, if a noncircular (NC) (or improper [11]) signal constellation is adopted the received signal vector becomes an NC-CGRV [12]. Hence, in this case the estimators derived in [9], termed MLC estimators, are not ML estimators.

In this thesis the problem of CFO and symbol timing synchronization in OFDM systems is examined and, moreover, new blind estimation techniques for OFDM systems with NC transmissions are proposed (see [13], [14] and [15]). Specifically, unlike zero-mean C-CGRVs, completely described by their covariance matrix, the statistical properties of zero-mean NC-CGRVs are also characterized by the relation matrix [16], defined as the statistical expectation of the product between the vector and its transpose. By exploiting the joint information of covariance and relation matrices a performance improvement with respect to estimation methods that rely only on circular statistics can be expected. However, unlike estimators based only on circular statistics, since the relation matrix preserves phase information, it is necessary to consider joint symbol timing, CFO and carrier phase estimation to obtain symbol timing and CFO estimators robust with respect to a residual carrier phase offset in the received signal. Specifically, by exploiting the generalized probability density function (PDF) of NC-CGRVs, we derive the unconditional ML algorithm for joint symbol timing and CFO estimation. The derived estimators can be also used in absence of CP, turning into those proposed in [9] in the case of circular transmissions.

The derived ML synchronization algorithm results particularly efficient since it does not use training sequences, besides, it assures optimal performances in AWGN furnishing estimates unbiased with a mean squared error very close to the corresponding Gaussian Cramèr-Rao Bound (GCRB). In presence of dispersive channel, however, there is a drawback because an accurate synchronization needs an averaging over different OFDM symbols. For high-rate packet transmission, the synchronization time needs to be as short

as possible, preferably a few OFDM symbols only. To achieve this, special OFDM training symbols can be used to obtain synchronization. In particular, in [17] Schmidl and Cox consider a timing and CFO synchronization scheme that exploits the redundancy associated with a training symbol composed by two identical halves. However, the considered timing metric reaches a plateau that produces large variance for the timing estimates. The training symbol proposed in [18], with four identical parts and a sign inversion, provides a timing metric with steeper rolloff. Nevertheless, the sign inversion in the transmitted training symbol introduces, in dispersive channels, some interference in the frequency estimation process causing severe performance degradation. This drawback is investigated by Bhargava et al. in [19] where a more general synchronization algorithm based on a structured training sequence is proposed and, moreover, channel estimation is also incorporated in order to obtain fine timing and CFO estimates. This refinement step reduces the interference introduced in the coarse CFO acquisition process but at the cost of some increase in computational load.

To overcome these limitations we develop in this thesis a reduced complexity synchronization scheme for data-aided symbol timing and CFO recovery with robust acquisition properties in dispersive channels ([20]-[23]). Specifically, this algorithm exploits the known structure of a training symbol made up of L identical parts obtained by transmitting BPSK data symbols on the subcarriers whose indexes are multiple of L and setting zero on the remaining subcarriers. In this case, if the number of subcarriers is sufficiently large, the training symbol can be modeled as an NC-CGRV. Therefore, by exploiting the joint PDF for improper CGRV's in this work is derived the joint ML estimator for the parameters of interest in an AWGN channel. The proposed method, as illustrated by numerical simulations, assures, in multipath channels, attractive properties for symbol timing acquisition and offers sufficiently accurate CFO estimates outperforming the estimators prosed in [18] and [19].

1.1 Outline

The organization of this thesis is as follows.

- **Chapter 2** provides an introduction to OFDM in general. After a brief history on origin of multicarrier modulation, this chapter describes what

OFDM is, and how it can be generated and received illustrating OFDM digital implementation scheme by using the discrete Fourier Transform (DFT) and its counterpart, the inverse discrete Fourier Transform (IDFT). Moreover, it is explained the concept of CP necessary to avoid ISI in dispersive channels. It also analyzes the robustness of the OFDM modulation scheme and some of its advantages over single carrier modulation schemes.

- **Chapter 3** analyzes detrimental effects of symbol timing and CFO synchronization errors on OFDM system performance. Moreover, it provides an outline on principal synchronization techniques proposed in literature.

- **Chapter 4** looks at blind estimation techniques for OFDM systems. In particular, by considering the generalized PDF for NC-CGRVs the joint symbol timing and CFO ML estimator for AWGN channel is obtained. The derived ML estimator can also be used in absence of CP and it is equal to the algorithm proposed in [9] in the case of circular transmissions. Moreover, the joint GCRB of CFO and carrier phase estimation for both circular and NC transmissions is presented. Finally, to combat dispersive effects of multipath channels in this chapter we develop blind refined symbol timing estimators that do not require channel-parameters knowledge at the receiver.

- **Chapter 5** provides a treatment of OFDM synchronization techniques using a training symbol. Precisely, the chapter includes new ML-based estimation techniques using a training symbol made up of L identical parts, obtained by transmitting BPSK data symbols on the subcarriers whose indexes are multiple of L and setting zero on the remaining subcarriers. Moreover, due to computational complexity of ML estimator a feasible method for CFO estimation is proposed. Finally, a refined symbol timing estimator, apt to counteract the degrading effects of channel dispersion, is considered.

- **Chapter 6** contains numerical evaluations of the performance of proposed blind and data-aided estimators in presence of AWGN and dispersive channel providing comparison with some of estimators previously

proposed in literature.

- In **Chapter 7** conclusions are provided, which summarize the major results obtained in this thesis and outline possible future work in this field.

Chapter 2

OFDM Basics

In this chapter, after a brief introduction on basic principles of OFDM modulation technique and an overview on its actual and future applications, we start by describing its basic architecture. Then, we illustrate OFDM digital implementation scheme by means IDFT/DFT and finally we explain how the insertion of the CP avoids interference between successive symbols in presence of dispersive channels.

2.1 Introduction

In the last years OFDM (see [1], [2] and references therein) has been object of increasing interest, in relationship to different applications, since it assures high data rate transmissions immune to channel dispersion. It is well know that if the channel impulse response is much longer than the symbol duration, the received signal will be distorted in time. Nevertheless, for modern multimedia applications operating with very high data rate communications the required signal bandwidth can result much greater than the channel coherence bandwidth so that distortion effects are severe. To contain such distortion it is necessary to use equalization systems, whose structure results more and more complex as the ratio among the channel delay spread and the symbol period increases. The OFDM modulation scheme offers an alternative solution to deal this problem. This modulation technique is a particular application of more general frequency division multiplexing (FDM) technique (also called

multicarrier or multitone modulation). Specifically, in an FDM system a single high-rate bit stream is divided into many lower-rate substreams transmitted over parallel subchannels (or subcarriers). If N is the number of such substreams, the rate on each subchannel decreases as a function of the number of subcarriers. Therefore, for a sufficiently large value of N, each subchannel can present a bandwidth less than the channel coherence bandwidth, and then, it will appear flat fading. This implies that in the receiver a very simple equalization system can be used to compensate, for every subchannel, the attenuation and the phase offset induced by the channel.

The multicarrier modulation technique is not new, in fact its origin goes back to the end-1950, when multicarrier modulation has been used in military context to realize high speed communication systems, we cite as examples "Kineplex", "Adeft" and "Kathryn" systems. Nevertheless, at that time, it didn't have a particular success because of the high implementation complexity due to the use of analogical devices. Almost 10 years later, in the 1971, Weinstein and Ebert overcame the problem, publishing their pioneering paper [24] about how to implement a multicarrier system with IDFT/DFT. Subsequently, the principle of the multicarrier modulation became the foundation of most current industry standards and in the coming broadband communication era, especially in wireless communication systems through two principal implementation schemes:

- **DMT (Discrete MulTitone)** developed for broadband wired applications has been used as modulation technique for high-bit-rate digital subscriber lines (HDSL) [25], asynchronous digital subscriber lines (ADSL) [26] and the most recent very-high-speed digital subscriber lines (VDSL) [27].

- **OFDM** has been exploited in the European digital audio/video broadcasting (DAB [28], DVB [29]) standards and it has been chosen for wireless local area network (WLAN) applications [30] (such as asynchronous transfer mode (ATM) network and IEEE, ETSI and MMAC WLAN standards). OFDM is under investigation for the fourth generation mobile communication systems and for data transmissions with power lines. There are also a number of emerging new uses for multicarrier techniques, including fixed and mobile wireless broadband services, ul-

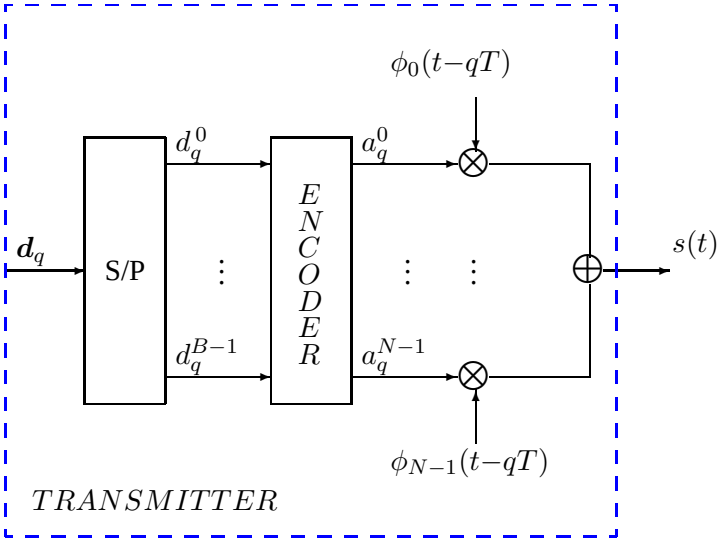

Figure 2.1: Scheme of the OFDM transmitter.

trawideband radios, multiple access systems (Orthogonal Frequency Division Multiple Access (OFDMA)) and in association with other modulation technique, see [1].

2.2 OFDM System

2.2.1 Basic Architecture

Let us consider a binary information source with rate $R_b = \frac{1}{T_b}$. With reference to Fig.2.1 and indicated with T the symbol period of considered multicarrier system, through a serial/parallel buffer in the q-th OFDM symbol interval $B = R_bT$ bits are stacked, obtaining the vector

$$\boldsymbol{d}_q \triangleq [d_q^0, d_q^1, \ldots, d_q^{B-1}]^T ,$$

where $d_q^i \stackrel{\triangle}{=} d(i + qB)$ is the i-th bit transmitted in the qth OFDM symbol period. Subsequently, the bit vector $\boldsymbol{d}_q$ is mapped into a the new vector

$$\boldsymbol{a}_q \stackrel{\triangle}{=} [a_q^0, a_q^1, \ldots, a_q^{N-1}]^T ,$$

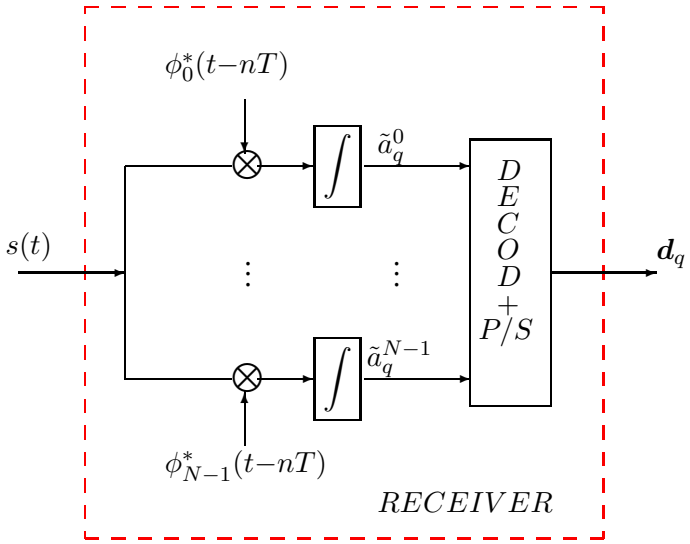

Figure 2.2: Scheme of the OFDM receiver.

composed by N complex symbols modulating different subcarriers $\{\phi_i(t)\}_{i=0}^{N-1}$. The baseband signal transmitted in the q-th symbol interval $[qT,(q+1)T]$ is given by the sum of the signals conveyed through the N parallel subchannels

$$f_q(t) = \sum_{i=0}^{N-1} a_q^i \phi_i(t-qT)\,, \tag{2.1}$$

therefore, the OFDM signal emitted in consecutive symbol intervals can be written as

$$s(t) = \sum_{q=-\infty}^{\infty} f_q(t) = \sum_{q=-\infty}^{\infty} \sum_{i=0}^{N-1} a_q^i \phi_i(t-qT)\,. \tag{2.2}$$

Under the hypothesis of a non dispersive channel and in the absence of noise, at the receiver, (see Fig.2.2) to obtain the i-th symbol transmitted in the q-th interval it is necessary to consider the correlation with the signal $\phi_i^*(t-$

$qT)$

$$\tilde{a}_q^i = \int_{-\infty}^{\infty} s(t)\phi_i^*(t-qT)\mathrm{d}t = \sum_{p=-\infty}^{\infty}\sum_{k=0}^{N-1} a_p^k \int_{-\infty}^{\infty} \phi_k(t-pT)\phi_i^*(t-qT)\mathrm{d}t\,. \tag{2.3}$$

From (2.3) we can note that the signal $\tilde{a}_q^i$ depends on the contribution of the symbols a_q^k transmitted in the same interval but modulating different subcarriers (ICI) and on the terms a_p^k transmitted in a different symbol interval (ISI). To eliminate both the ISI and the ICI it is necessary to consider a set of functions $\phi_i(t)$ that verify the following *biorthonormality* condition

$$\langle \phi_k(t-qT)\phi_i^*(t-pT)\rangle = \delta[k-i]\delta[p-q]\,. \tag{2.4}$$

In this way, at least in principle, it is possible to perfectly recover the desired symbol from the received OFDM signal. To such end, we consider the set of orthogonal functions

$$\phi_i(t) = \frac{1}{\sqrt{T}}\Pi\left(\frac{t-T/2}{T}\right)e^{j2\pi f_i t} \triangleq \mathrm{R}_T(t)e^{j2\pi f_i t},\quad i\in\tau_1 \triangleq \{0,\ldots N-1\}. \tag{2.5}$$

with reference to (2.4) we obtain

$$\begin{aligned}
&\langle \phi_k(t-qT)\phi_i^*(t-pT)\rangle = \\
&= \int_{-\infty}^{\infty} \underbrace{\mathrm{R}_T(t-qT)\mathrm{R}_T(t-pT)}_{\frac{1}{T}\mathrm{R}_T(t-qT)\delta[q-p]} e^{j2\pi f_k(t-qT)}e^{-j2\pi f_i(t-pT)}\mathrm{d}t \\
&= \frac{1}{T}\int_{qT}^{(q+1)T} e^{j2\pi(f_k-f_i)(t-qT)}\mathrm{d}t \\
&= \frac{e^{j2\pi\Delta fT}-1}{j2\pi\Delta fT} = \begin{cases} 1 & \Delta fT = 0\,, \\ 0 & \Delta fT = \alpha\,,\quad \alpha\in\mathbb{Z}\,. \end{cases}
\end{aligned}$$

Therefore, the choice of a rectangular pulse allows to select the desired symbol annulling ISI. On the other hand, considering an intercarrier spacing Δf equal to a multiple of $1/T$ the interference among the different subchannels is absent and therefore the biorthonormality condition (2.4) is verified. In particular,

choosing the minimum intercarrier spacing $\Delta f = \frac{1}{T}$ we obtain the maximum spectral efficiency. This is the value selected for the OFDM system, for which the pulse $\phi_i(t)$ results to be

$$\phi_i(t) = \mathrm{R}_T(t) e^{j\frac{2\pi}{T}it}, \quad i \in \tau_1 \,. \tag{2.6}$$

Moreover, with the previous choice the transmitted OFDM signal is given by

$$s(t) = \sum_{q=-\infty}^{\infty} \sum_{i=0}^{N-1} a_q^i \mathrm{R}_T(t-qT) e^{j\frac{2\pi}{T}i(t-qT)} = \sum_{q=-\infty}^{\infty} \mathrm{R}_T(t-qT) \sum_{i=0}^{N-1} a_q^i e^{j\frac{2\pi}{T}it}. \tag{2.7}$$

2.2.2 Spectral Analysis

In this section we evaluate the power spectral density (PSD) of the multicarrier signal described in the subsection § 2.2.1.

Let us observe, preliminarily, that under the hypothesis that the data bits $\left\{d_p^i\right\}_{p=-\infty}^{\infty}$ for $i \in \tau_1$ can be modeled as independent and identically distributed (i.i.d.) random variables, we have:

1) the symbols a_q^i and a_p^k, with $i \neq k$ and $q{=}p$, transmitted in the same OFDM interval but on different subcarriers, result to be i.i.d. random variables since they are obtained from different bits of the same block $\boldsymbol{d}_q$;

2) the symbols a_q^i and a_p^k, with $q \neq p$ e $\forall\ i,k \in \tau_1$, transmitted in different OFDM intervals, result to be random variables i.i.d. since they are obtained from bits of different blocks $\boldsymbol{d}_p$ and $\boldsymbol{d}_q$.

Therefore, under the hypothesis of data symbols $\left\{a_q^i\right\}_{q=-\infty}^{\infty}$ with zero mean and variance $E[|a_q^i|^2] = \sigma_i^2$, it follows that:

$$E[a_q^i (a_p^k)^*] = \sigma_i^2 \delta[i-k]\delta[q-p] \,.$$

From this relation and with reference to the model (2.2), the autocorrelation

function of the transmitted OFDM signal is given by:

$$\begin{aligned} r_s(t,\tau) &\stackrel{\triangle}{=} E[s(t)s(t-\tau)^*] \\ &= \sum_{p,q=-\infty}^{\infty} \sum_{i,k=0}^{N-1} \underbrace{E[a_q^i (a_p^k)^*]}_{\sigma_i^2 \delta[i-k]\delta[q-p]} \phi_i(t-qT)\phi_k^*(t-\tau-pT) \\ &= \sum_{i=0}^{N-1} \sigma_i^2 \sum_{q=-\infty}^{\infty} \phi_i(t-qT)\phi_i^*(t-\tau-qT) \\ &= \sum_{i=0}^{N-1} \sigma_i^2 \mathrm{rep}_T \left[\phi_i(t)\phi_i^*(t-\tau)\right] \ . \end{aligned}$$

Because of $r_s(t,\tau)$ is a periodic function of period T with respect to the variable t, the autocorrelation function $r_s(\tau)$ is given by

$$\begin{aligned} r_s(\tau) &\stackrel{\triangle}{=} \langle r(t,\tau) \rangle = \frac{1}{T} \sum_{i=0}^{N-1} \sigma_i^2 \int_0^T \mathrm{rep}_T \left[\phi_i(t)\phi_i^*(t-\tau)\right] \mathrm{d}t \\ &= \frac{1}{T} \sum_{i=0}^{N-1} \sigma_i^2 r_{\phi_i}(\tau) \end{aligned}$$

where $r_{\phi_i}(\tau) \stackrel{\triangle}{=} \int_{-\infty}^{\infty} \phi_i(\lambda)\phi_i^*(\lambda-\tau)\mathrm{d}\lambda$ is the autocorrelation function of the pulse $\phi_i(t)$.
Then, by the theorem of Wiener-Kintchine, considering the Fourier transform of the autocorrelation function $r_s(\tau)$, the PSD $P_s(f)$ of the signal $s(t)$ is given by

$$P_s(f) = \frac{1}{T} \sum_{i=0}^{N-1} \sigma_i^2 P_{\phi_i}(f) = \frac{1}{T} \sum_{i=0}^{N-1} \sigma_i^2 |\Phi_i(f)|^2 \ , \tag{2.8}$$

where $\Phi_i(f) \stackrel{\triangle}{=} \mathfrak{F}\left[\phi_i(t)\right]$.

Now, particularizing the expression (2.8) to the case of the pulse (2.6), for

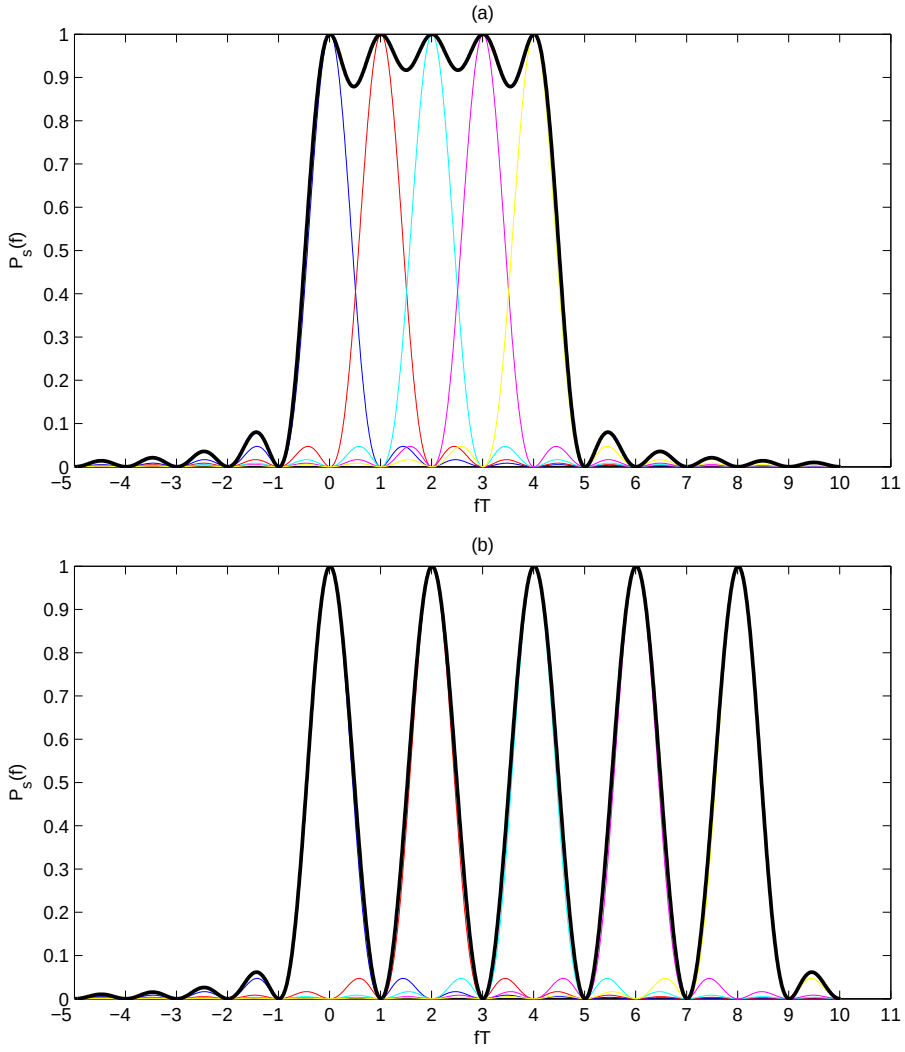

Figure 2.3: PSD into the case of an OFDM signal with an intercarrier spacing $1/T$ (a) and for an FDM signal with an intercarrier spacing $2/T$ (b).

$i \in \tau_1$, we obtain

$$\begin{aligned}\mathfrak{F}\left[\mathrm{R}_T(t)e^{j\frac{2\pi it}{T}}\right] = & \ \mathfrak{F}\left[\tfrac{1}{\sqrt{T}}\Pi\left(\tfrac{t-T/2}{T}\right)e^{j\frac{2\pi}{T}it}\right] \\ & = \sqrt{T}\mathrm{sinc}\left[\left(f-\tfrac{i}{T}\right)T\right]e^{-j\pi\left[\left(f-\frac{i}{T}\right)T\right]},\end{aligned}$$

and then

$$P_s(f) = \sum_{i=0}^{N-1}\sigma_i^2\mathrm{sinc}^2\left[\left(f-\frac{i}{T}\right)T\right].$$

The PSD of the OFDM signal has been plotted in Fig.2.3 (a) as a function of the normalized frequency fT and for a system with $N = 5$ subcarriers modulated by symbols with unit variance. We can note that the spectra of different subchannels are partially overlapped with a total bandwidth

$$W_{OFDM} \simeq \frac{2}{T} + \frac{N-1}{T} \simeq \frac{N}{T}.$$

Instead, into the case of a multicarrier system with an intercarrier spacing $\Delta f = 2/T$, as we can observe in Fig. 2.3 (b), the total bandwidth of transmitted signal is given by

$$W_{FDM} \simeq \frac{2N}{T},$$

with a 50% reduction in the spectral efficiency.

2.3 Digital Implementation

The idea behind the analog implementation of the OFDM system can be extended to the digital domain by means IDFT/DFT. Let us consider the PSD of the analogous OFDM signal plotted in Fig.2.4 for a number of subcarriers fixed to $N = 8$ and $N = 64$. We can note that the sum of different subchannels gives rise to a resulting spectrum approximatively flat for $|f| \leq \frac{N}{T}$ and decaying rapidity to zero for $|f| > \frac{N}{T}$, and this characteristic is more evident for a large number of subcarriers. Therefore, although the analogous OFDM signal is not perfectly bandlimited, for $N \gg 1$ we can assume that the bandwidth of the OFDM signal is $W_{OFDM} \simeq \frac{N}{T}$. Thus, the continuous-time OFDM signal $s(t)$ can be reconstructed from its samples $s(n)$ by considering a sampling interval $T_c = 1/W_{OFDM} = T/N$. Specifically, let us consider the

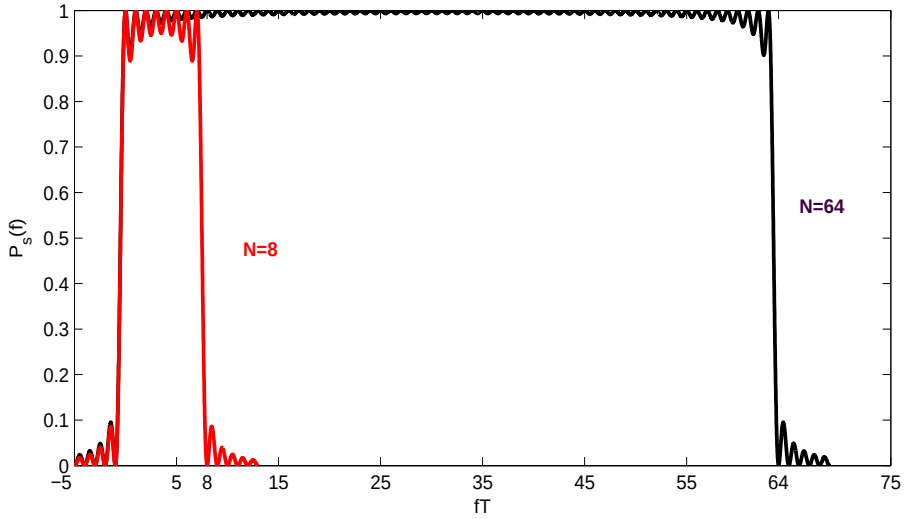

Figure 2.4: PSD of the OFDM signal for a multicarrier system with $N = 8$ and $N = 64$ subcarriers.

baseband discrete-time OFDM signal transmitted in the q-th OFDM interval and sampled with a rate $f_c = N/T$

$$\begin{aligned} f(qT + kT_c) = & \frac{1}{\sqrt{T}} \sum_{i=0}^{N-1} a_q^i e^{j\frac{2\pi}{T} i\left(qT + k\frac{T}{N}\right)} \\ = & \frac{1}{\sqrt{T}} \sum_{i=0}^{N-1} a_q^i e^{j\frac{2\pi}{N} ik} = \frac{N}{\sqrt{T}} s_q(k) \,, \end{aligned} \tag{2.9}$$

where

$$s_q(k) \stackrel{\triangle}{=} \frac{1}{N} \sum_{i=0}^{N-1} a_q^i e^{j\frac{2\pi}{N} ik} \quad \forall k \in \tau_1 \tag{2.10}$$

is the IDFT of size N of the sequence $\boldsymbol{a}_q$. Then, from (2.9), it follows that the IDFT of the sequence $\boldsymbol{a}_q$ is, unless a multiplicative constant, a sampled version of the analogous signal $f_q(t)$, transmitted in the q-th OFDM interval. This observation suggests a more efficient ways to implement an OFDM system. An entirely discrete time model of the multicarrier system is displayed in Fig. 2.5, compared to the continuous time model, shown in Figures 2.1 and 2.2, the demodulation and the modulation schemes are replaced by IDFT and DFT. Precisely, in transmission, after a serial/parallel buffer and an encoder, the scheme presents an IDFT elaboration implemented through the efficient IFFT algorithm. In this ways we obtain the sampling sequence $\boldsymbol{s}_q$ transmitted in the q-th OFDM interval

$$\boldsymbol{s}_q = [s_q(0), \ldots, s_q(N-1)]^T \,,$$

successively, elaborated by a digital to analog converter (DAC) with a sampling frequency f_c. Then, considering the transmission of successive frames, the transmitted OFDM signal is given by

$$s(t) = \frac{N}{\sqrt{T}} \sum_{q=-\infty}^{\infty} \sum_{k=0}^{N-1} s_q(k) h_{DA}(t - qT - kT_c) \,. \tag{2.11}$$

We can consider an alternative expression for (2.11). Let us define the resulting signal after parallel-to-serial conversion

$$s(qN + k) = s_q(k), \qquad \forall k \in \tau_1 \,,$$

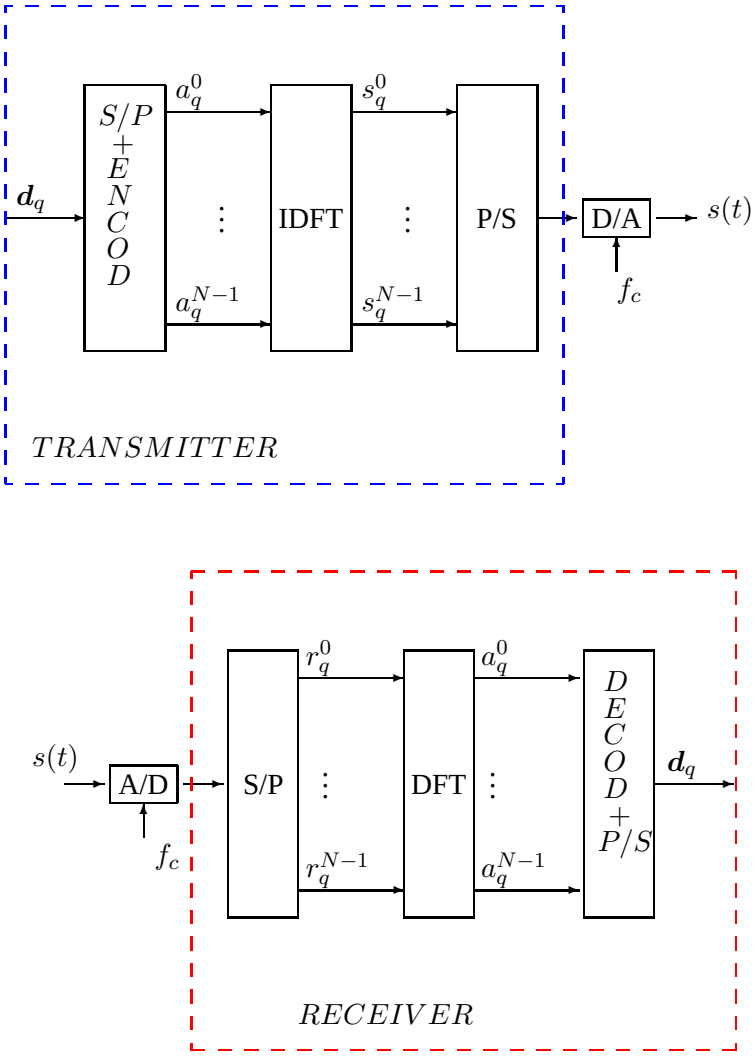

Figure 2.5: Scheme of the multicarrier system based on IDFT/DFT.

then, in this case the DAC output can be expressed as

$$\begin{aligned} s(t) &= \frac{N}{\sqrt{T}} \sum_{q=-\infty}^{\infty} \sum_{k=0}^{N-1} s(qN+k) h_{DA}(t - qT - kT_c) \\ &= \frac{N}{\sqrt{T}} \sum_{p=-\infty}^{\infty} s(p) h_{DA}(t - pT_c) = \frac{N}{\sqrt{T}} s_\delta(t) \otimes h_{DA}(t) \end{aligned} \tag{2.12}$$

where $s_\delta(t) \stackrel{\triangle}{=} \sum_{p=-\infty}^{\infty} s(p)\delta(t - pT_c)$.
In the absence of noise and indicating with $h_{AD}(t)$ the impulse response of the analog to digital converter (ADC), at the receiving side, the received baseband signal is given by

$$r(t) = \frac{N}{\sqrt{T}} s_\delta(t) \otimes h_{DA}(t) \otimes h_{AD}(t) \, . \tag{2.13}$$

Moreover, let us assume that the impulsive response of DAC and of ADC filters are equal to

$$h_{DA}(t) = \text{sinc}\left(\frac{t}{T_c}\right) \tag{2.14}$$

and

$$h_{AD}(t) = \frac{1}{\sqrt{T}} \text{sinc}\left(\frac{t}{T_c}\right) \tag{2.15}$$

then, from (2.13) the received OFDM signal can be written as

$$r(t) = s_\delta(t) \otimes \text{sinc}\left(\frac{t}{T_c}\right) = \sum_{p=-\infty}^{\infty} s(p) \text{sinc}\left(\frac{t - pT_c}{T_c}\right) \, . \tag{2.16}$$

The received signal is sampled with rate $R_c = 1/T_c$ at time instants $t_k = kT_c + qT$, with $k \in \tau_1$, yielding the discrete time sequence

$$\begin{aligned} r_q(k) &\stackrel{\triangle}{=} r(kT_c + qT) = \sum_{p=-\infty}^{\infty} s(p) \text{sinc}\left(\frac{kT_c + qT - pT_c}{T_c}\right) \\ &= \sum_{p=-\infty}^{\infty} s(p)\delta\left[k + qN - p\right] = s(qN+k) = s_q(k) \, . \end{aligned} \tag{2.17}$$

Therefore, into the case where the filters given by (2.14) and (2.15) are adopted, there is not interference between successive symbols or between successive subcarriers and, then, it is possible to extract perfectly the different subchannels. Besides, it follows that

$$\begin{aligned}\tilde{a}_q^i &= \{DFT[\boldsymbol{r}_q]\}_i = \sum_{k=0}^{N-1} r_q(k) e^{-j\frac{2\pi}{N}ki} \\ &= \sum_{k=0}^{N-1} \left[\frac{1}{N} \sum_{h=0}^{N-1} a_q^h e^{j\frac{2\pi}{N}hk} \right] e^{-j\frac{2\pi}{N}ki} = a_q^i.\end{aligned} \tag{2.18}$$

Then, by considering the DFT of the N-sequence $\boldsymbol{r}_q$ it is possible to recover the sequence of bit transmitted.

2.4 Cyclic Prefix

Two difficulties arise when the OFDM signal is transmitted over a dispersive channel. One difficulty is that channel dispersion destroys the orthogonality between subcarriers and causes ICI. In addition, a dispersive channel causes ISI between successive OFDM symbols. The insertion of a silent guard period between successive OFDM symbols would avoid ISI in a dispersive environment but it does not avoid the loss of the subcarrier orthogonality. Peled and Ruiz in [31] solved this problem with the introduction of a CP. This CP preserves the orthogonality of the subcarriers and prevents ISI between successive OFDM symbols. Therefore, equalization at the receiver is very simple. This often motivates the use of OFDM in wireless systems. The cyclic extension, illustrated in Fig.2.6, works as follows. Between consecutive OFDM signals a guard period is inserted that contains a cyclic extension of the OFDM symbol. The OFDM signal is extended over a period of length $M = N + L_c$ so that

$$s_q(n) = \begin{cases} \dfrac{1}{N} \displaystyle\sum_{k=0}^{N-1} a_q^k e^{j\frac{2\pi}{N}k(N+n)}, & n \in \{-L_c, \ldots, -1\}, \\ \dfrac{1}{N} \displaystyle\sum_{k=0}^{N-1} a_q^k e^{j\frac{2\pi}{N}kn}, & n \in \{0, \ldots, N-1\}. \end{cases} \tag{2.19}$$

Let us note that $e^{j2\pi k} = 1 \; \forall \; k \in \mathbb{Z}$, therefore (2.19) can be rewritten as

$$s_q(n) = \frac{1}{N} \sum_{k=0}^{N-1} a_q^k e^{j\frac{2\pi}{N}kn}, \qquad n \in \tau_2 \stackrel{\triangle}{=} \{-L_c, \ldots, N-1\} \, . \tag{2.20}$$

Then, based on (2.11), the transmitted signal in presence of CP is given by

$$\begin{aligned} s(t) \; &= \frac{N}{\sqrt{T}} \sum_{p=-\infty}^{\infty} \sum_{n=0}^{M-1} s(qM+n) h_{DA}(t - qT - nT_c) \\ &= \frac{N}{\sqrt{T}} \sum_{m=-\infty}^{\infty} s(m) h_{DA}(t - mT_c) = \frac{N}{\sqrt{T}} s_\delta(t) \otimes h_{DA}(t) \end{aligned} \tag{2.21}$$

where $T_c \stackrel{\triangle}{=} T/M$ and, moreover, T is the OFDM symbol interval. In presence of a linear time invariant channel with impulsive response $h(t)$ and with additive noise, after the reconstruction filter, we obtain

$$r(t) = \underbrace{\frac{N}{\sqrt{T}} s_\delta(t) \otimes h_{DA}(t) \otimes h(t) \otimes h_{AD}(t)}_{y(t)} + n(t) \otimes h_{AD}(t) \, .$$

If we disregard the presence of additive noise and consider DAC and ADC filters (2.14) and (2.15), respectively, we have

$$\begin{aligned} y(t) \; &= \frac{N}{\sqrt{T}} s_\delta(t) \otimes \underbrace{h_{DA}(t) \otimes h_{AD}(t)}_{\frac{T_c}{\sqrt{T}} \mathrm{sinc}\left(\frac{t}{T_c}\right)} \otimes h(t) = \frac{N}{M} s_\delta(t) \otimes \underbrace{\mathrm{sinc}\left(\frac{t}{T_c}\right) \otimes h(t)}_{h_{eq}(t)} \\ &= \frac{N}{M} s_\delta(t) \otimes h_{eq}(t) = \frac{N}{M} \sum_{m=-\infty}^{\infty} s(m) \delta(t - mT_c) \otimes h_{eq}(t) \\ &= \frac{N}{M} \sum_{m=-\infty}^{\infty} s(m) h_{eq}(t - mT_c) \, . \end{aligned} \tag{2.22}$$

Then, the received signal sampled at time instant $t_n = nT_c + qT$, with $n \in \tau_2$, is equal to

$$y_q(n) \stackrel{\triangle}{=} y(qT + nT_c) = \frac{N}{M} \sum_{m=-\infty}^{\infty} s(m) h_{eq}(qT + nT_c - mT_c) \tag{2.23}$$

and, putting $h_{eq}(mT_c) \stackrel{\triangle}{=} h_{eq}(m)$, we have

$$\begin{aligned} y_q(n) &= \frac{N}{M} \sum_{m=-\infty}^{\infty} s(m) h_{eq}(qM+n-m) \\ &= \frac{N}{M} \sum_{m=-\infty}^{\infty} s(qM+n-m) h_{eq}(m) \\ &= \frac{N}{M} \sum_{m=0}^{N_m-1} s(qM+n-m) h_{eq}(m) \,, \end{aligned} \tag{2.24}$$

where N_m is the the length of the discrete time channel impulsive response. Let us rewrite (2.24) as

$$y_q(n) = \frac{N}{M} \sum_{l=0}^{p} s(qM+n-l) h_{eq}(l) + \frac{N}{M} \sum_{l=p+1}^{N_m-1} s(qM+n-l) h_{eq}(l) \,, \tag{2.25}$$

we can see that the first term contains the contribution of the q-th useful symbol, while the second term includes the interference of the $(q-1)$-th symbol (ISI). To avoid ISI it is necessary to discard the CP samples considering the vector

$$\boldsymbol{y}_q \stackrel{\triangle}{=} [y_q(0), y_q(1), \ldots, y_q(N-1)]^T \,,$$

moreover, if $L_c \geq N_m - 1$, the ISI term is zero and then

$$y_q(n) = \frac{N}{M} \sum_{l=0}^{p} s(qM+n-l) h_{eq}(l) = \frac{N}{M} \sum_{l=0}^{p} s_q(n-l) h_{eq}(l). \tag{2.26}$$

From (2.19) it results that

$$y_q(n) = \frac{1}{M} \sum_{k=0}^{N-1} a_q^k e^{j\frac{2\pi}{N}kn} \sum_{l=0}^{p} h_{eq}(l) e^{-j\frac{2\pi}{N}lk} \,, \tag{2.27}$$

and since $p \geq L_c \geq N_m - 1$, we have

$$\sum_{l=0}^{p} h_{eq}(l) e^{-j\frac{2\pi}{N}lk} = \sum_{l=0}^{N_m-1} h_{eq}(l) e^{-j\frac{2\pi}{N}lk} = \{DFT[\boldsymbol{h}_{eq}]\}_k \stackrel{\triangle}{=} H_{eq}(k), \tag{2.28}$$

where the vector N-dimensional $\boldsymbol{h}_{eq}$ is defined as $\boldsymbol{h}_{eq} \stackrel{\triangle}{=} [h_{eq}(0), h_{eq}(1), ..., h_{eq}(N_m - 1), 0, ..., 0]^T$. Moreover, from (2.27) it follows that

$$y_q(n) = \frac{1}{M} \sum_{k=0}^{N-1} a_p^k e^{j\frac{2\pi}{N}kn} H_{eq}(k) = \frac{N}{M} \{IDFT[\boldsymbol{g}_q]\}_n, \tag{2.29}$$

where $\boldsymbol{g}_q \stackrel{\triangle}{=} \left[a_q^0 H_{eq}(0), a_q^1 H_{eq}(1), ..., a_q^{N-1} H_{eq}(N-1)\right]^T$. Computing the DFT of the vector $\boldsymbol{y}_q$ yields

$$\tilde{a}_q^i = \{DFT[\boldsymbol{y}_q]\}_i = \frac{N}{M} \{DFT[IDFT[\boldsymbol{g}_q]]\}_i = \frac{N}{M} a_q^i H_{eq}(i)\,. \tag{2.30}$$

Thus, each subchannel is characterized by a complex gain. In this case the transmitted information is completely recovered by multiplying the received data symbols by the channel coefficients $H_{eq}^{-1}(i)$. Moreover, including Gaussian noise in the signal model, the equation (2.30) yields

$$\tilde{a}_q^i = \frac{N}{M} a_q^i H_{eq}(i) + \eta_q(i)\,, \tag{2.31}$$

where $\eta_q(i)$ is the DFT of the sampled noise terms $n_q(iT_c)$. If the received noise is modeled as a white complex Gaussian random process, it follows that the noise contributions of different subchannels $\eta_q(i)$ are statistically independent. Therefore, an ML detector is equivalent to an independent detector on each subchannel output.

Finally, we can note that the price to pay for eliminating ISI through the cyclic extension is extra power. In fact, the cyclic extension means that an additional $(L_c - 1)$ units of average power are carried by the cyclically extended symbols determining an SNR loss equal to $SNR = (M-1)/NdB$.

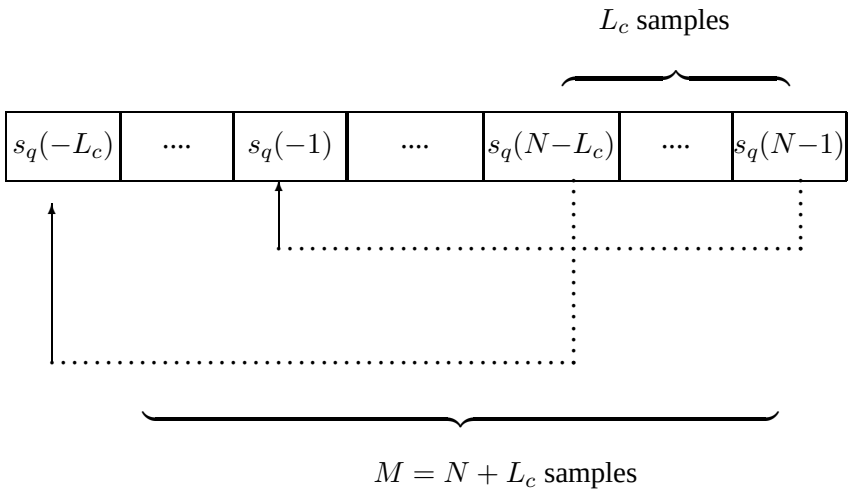

Figure 2.6: Insertion of CP.

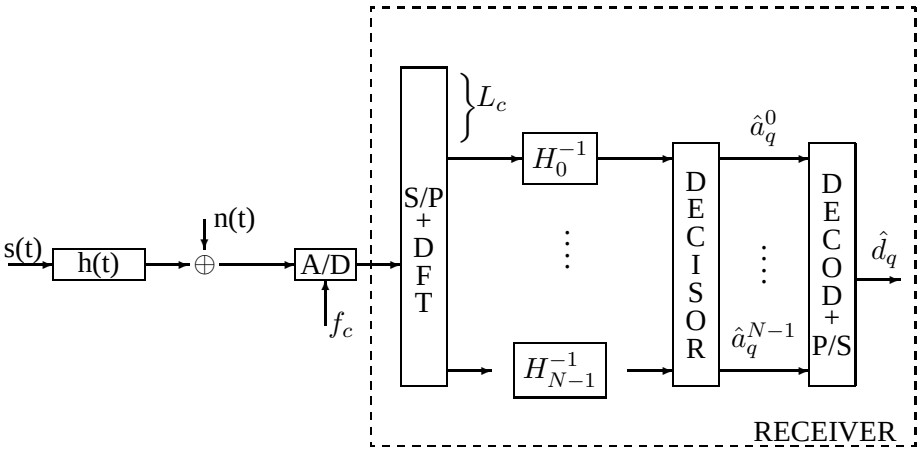

Figure 2.7: Scheme of the OFDM receiver in presence of dispersive channel and additive noise.

Chapter 3

Synchronization Problem in OFDM Systems

Demodulation and detection of OFDM signals require accurate synchronization. For example, symbol timing and CFO estimation errors may cause ISI and ICI and can lead to a severe performance degradation. Therefore, after the description of the adopted model, we separately consider their effects on the system performance and, then, we present an overview on useful synchronization schemes.

3.1 Model of Synchronization Errors

As previously stated one of the drawbacks of multicarrier systems is their high sensitivity to synchronization errors. In fact, symbol timing and CFO estimation errors can significantly deteriorate the performance of OFDM systems. Specifically, incorrect timing synchronization can cause interference between successive symbols and, if not perfectly compensated before the equalization process, can lead to a severe performance degradation, [3]-[5]. In addition, a CFO induces an amplitude reduction of the useful signal and provokes interference between adjacent subcarriers, see, for example, [6]-[8].
To investigate the effects of synchronization errors on the performance of OFDM systems let us consider the received signal in presence of a delay τ and a frequency offset $\triangle f$. In this case, under the hypothesis of ideal DAC e

ADC filters and in the absence of noise, it follows that

$$r(t) = \frac{N}{M} \sum_{i=-\infty}^{\infty} s(i) \mathrm{sinc}\left(\frac{t - \tau - iT_c}{T_c}\right) e^{j2\pi \triangle f t}. \tag{3.1}$$

Let us suppose, moreover, without loss of generality, that the delay τ is the integer part, with respect to the sampling period, of the propagation delay $\tau = \theta T_c$. If we denote with $\hat{\theta}$ a timing estimate, we obtain

$$\begin{aligned} r_q(k+\hat{\theta}) &= \sum_{i=-\infty}^{\infty} s(i) e^{j2\pi \triangle f[(k+\hat{\theta})T_c + qT]} \delta[k + qM + \hat{\theta} - \theta - i] \\ &= s_q(k + \triangle\theta) e^{j\left(\frac{2\pi}{N}\epsilon k + \phi\right)} \end{aligned} \tag{3.2}$$

where $\epsilon \stackrel{\triangle}{=} \triangle f T_c N$ is the frequency offset normalized to the intercarrier spacing, $\triangle\theta \stackrel{\triangle}{=} \hat{\theta} - \theta$ is the error in the delay estimation, $\phi \stackrel{\triangle}{=} 2\pi\epsilon \left[q + \frac{(qL_c + \hat{\theta})}{N}\right]$ and, moreover, $r_q(k) \stackrel{\triangle}{=} \frac{M}{N} r_q(k)$. In the following we consider separately the sensitivity to CFO ($\triangle f \neq 0$ and $\triangle\theta = 0$) and to symbol timing errors ($\triangle f = 0$ and $\triangle\theta \neq 0$).

3.2 Effect of Symbol Timing Errors

Let us put $\triangle f = 0$ in (3.2), then in presence of noise the received signal is given by

$$r_q(k + \hat{\theta}) = s_q(k + \triangle\theta) + w_q(k + \hat{\theta}) \, . \tag{3.3}$$

Then, removing the CP and after the DFT, we have

$$\tilde{a}_q^l = \sum_{k=0}^{N-1} r_q(k + \hat{\theta}) e^{-j\frac{2\pi}{N}kl} = \sum_{k=0}^{N-1} \left[s_q(k + \triangle\theta) + w_q(k + \hat{\theta})\right] e^{-j\frac{2\pi}{N}kl} \, . \tag{3.4}$$

From the last expression it results that if the timing error satisfies the condition $-L_c \leq \triangle\theta \leq 0$, the vector $\boldsymbol{s}_q \stackrel{\triangle}{=} [s_q(\triangle\theta), \ldots, s_q(N - 1 + \triangle\theta)]^T$ contains all

samples of the q-th OFDM symbol and then based on (2.19) we can write

$$\begin{aligned}\tilde{a}_q^l &= \sum_{k=0}^{N-1}\left[\frac{1}{N}\sum_{h=0}^{N-1} a_q^h e^{j\frac{2\pi}{N}h(k+\triangle\theta)} + w_q(k+\hat{\theta})\right] e^{-j\frac{2\pi}{N}kl} \\ &= a_q^l e^{j\frac{2\pi}{N}l\triangle\theta} + \eta(l)\end{aligned}$$

with $\eta(l) \stackrel{\triangle}{=} \sum_{k=0}^{N-1} w_q(k+\hat{\theta})e^{-j\frac{2\pi}{N}kl}$.

Therefore, a symbol timing error $\triangle\theta \in \{-L_c,\ldots,0\}$ only introduces a phase offset, that must be compensated in a coherent receiver. Instead, for $\triangle\theta \notin \{-L_c,\ldots,0\}$ it exists interference between successive OFDM symbols. In particular, let us assume that $\triangle\theta \in \{-M,\ldots,-L_c\}$ so that there is interference between the q-th and the $(q-1)$-th OFDM symbol, moreover in this case (3.4) can be rewritten as

$$\begin{aligned}\tilde{a}_q^l = \; & \frac{M+\triangle\theta}{N} a_q^l e^{j\frac{2\pi}{N}l\triangle\theta} \\ & \underbrace{+\frac{1}{N}\sum_{k=-\triangle\theta-L_c}^{N-1} e^{-j\frac{2\pi}{N}kl} \sum_{\substack{h=0 \\ h\neq l}}^{N-1} a_q^h e^{j\frac{2\pi}{N}h(k+\triangle\theta)}}_{ICI} \\ & \underbrace{+\frac{1}{N}\sum_{k=0}^{-\triangle\theta-L_c} e^{-j\frac{2\pi}{N}kl} \sum_{h=0}^{N-1} a_{q-1}^h e^{j\frac{2\pi}{N}h(k+\triangle\theta)}}_{ISI} + \eta(l)\,.\end{aligned}$$

The demodulated signal now consists of a useful portion and disturbances caused by ISI, ICI and AWGN. Concerning the useful portion, as in the case $\triangle\theta \in \{-L_c,\ldots,0\}$, the transmitted symbols a_q^l are attenuated and rotated by a phasor whose phase is proportional to the subcarrier index and the symbol timing. In addition to this effect the demodulated signals suffer from the disturbances caused by adjacent subcarriers and from the interference from the previous OFDM symbol.

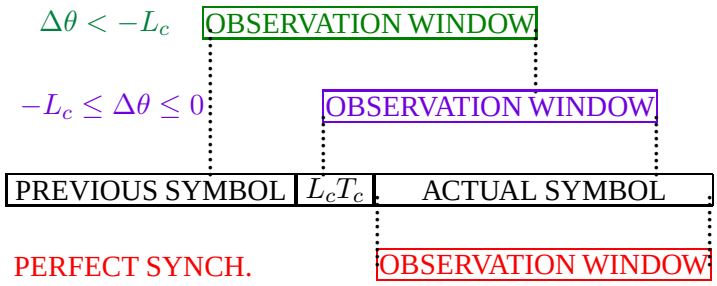

Figure 3.1: Symbol timing errors

In presence of a multipath channel, basically the same analysis applies. In particular, in this case let us consider the expression received signal

$$r_q(n) = \sum_{l=0}^{N_m} h(l) s_q(k - l - \theta) + w_q(n) \tag{3.5}$$

where $\{h(l)\}_{l=0}^{N_m}$ is the channel impulsive response with a maximum delay spread N_m. The post-DFT signal is described by

$$\tilde{a}_q^l = \alpha(\theta) a_q^l H(l) e^{-j\frac{2\pi}{N} l\theta} + \xi(l) + \eta(l)\,, \tag{3.6}$$

where ISI and ICI disturbance are modeled as additional noise $\xi(l)$ while $\alpha(\theta)$ is the resulting attenuation of the symbol. In this case it is necessary synchronize the receiver to the first arriving multipath component. Therefore, as shown in Fig.3.2, the range of symbol timing errors for which does not exist ISI is given by

$$-L_c + N_m \leq \triangle\theta \leq 0\,.$$

In such a *lock-in region*, the orthogonality among the subcarriers is preserved, resulting only in phase rotation and attenuation at the output of the DFT processor which is easily corrected.

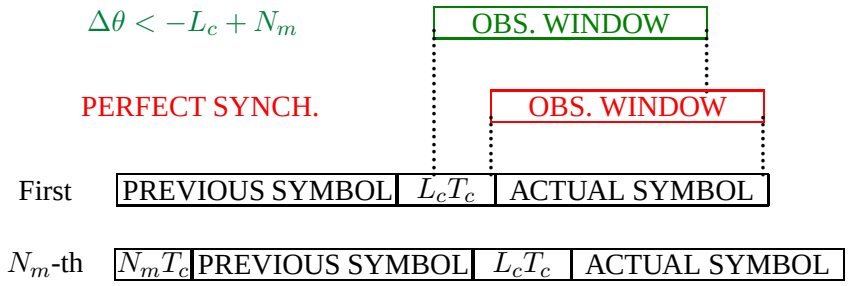

Figure 3.2: Symbol timing errors in multipath channel

3.3 Effect of CFO

Let us put $\Delta\theta = 0$ in (3.2) and let us consider the expression of the received signal in presence of AWGN channel

$$r_q(n) = s_q(n)e^{j\left(\frac{2\pi}{N}\epsilon k+\phi\right)} + w_q(n) \tag{3.7}$$

where $\phi \triangleq \dfrac{2\pi}{N}\epsilon qM$.
Let us observe that a synchronization error ϵ equal to an integer multiple of the intercarrier spacing provokes a common rotation of different subcarriers that will be still mutually orthogonal. Instead, a CFO ϵ equal to a fraction of the intercarrier space can cause ICI and attenuation in the transmitted signal. In particular, to evaluate analytically this effect let us consider the expression of received signal at the output of the OFDM demodulator

$$\tilde{a}_q^l = \sum_{k=0}^{N-1}\left[s_q(k)e^{j\left[\frac{2\pi}{N}\epsilon k+\phi\right]} + w_q(k)\right]e^{-j\frac{2\pi}{N}kl}.$$

Then, accounting for the expression of transmitted signal we have

$$\begin{aligned}
\tilde{a}_q^l &= \sum_{k=0}^{N-1}\left[\frac{e^{j(\frac{2\pi}{N}\epsilon k+\phi)}}{N}\sum_{h=0}^{N-1}a_q^h e^{j\frac{2\pi}{N}hk}+w_q(k)\right]e^{-j\frac{2\pi}{N}kl} \\
&= e^{j\left[\pi\epsilon\left(\frac{N-1}{N}\right)+\phi\right]}\frac{\sin(\pi\epsilon)}{N\sin\left(\frac{\pi\epsilon}{N}\right)}a_q^l \\
&\quad \underbrace{+\frac{e^{j\phi}}{N}\sum_{\substack{h=0\\h\neq l}}^{N-1}a_q^h\sum_{k=0}^{N-1}e^{j\frac{2\pi}{N}k(h-l+\epsilon)}}_{ICI}+\eta(l) \qquad (3.8)\\
&= \frac{e^{j\phi}}{N}a_q^l I_0(\epsilon)+\underbrace{\frac{e^{j\phi}}{N}\sum_{\substack{h=0\\h\neq l}}^{N-1}a_q^h I_{h-l}(\epsilon)}_{ICI}+\eta(l)
\end{aligned}$$

where

$$I_p(\epsilon)\triangleq\sum_{k=0}^{N-1}e^{j\frac{2\pi}{N}k(\epsilon+p)}=\frac{\sin\left[\pi\left(\epsilon+p\right)\right]}{\sin\left[\frac{\pi}{N}\left(\epsilon+p\right)\right]}e^{j\left[\pi\left(\frac{N-1}{N}\right)(\epsilon+p)\right]}. \qquad (3.9)$$

From (3.8) we can observe that the received signal is given by the sum of three different terms: the additive noise $\eta(l)$, the useful term a_q^l that presents attenuation and phase rotation and the ICI term. The effect of CFO synchronization errors is presented in Fig. 3.3, where it is shown the PSD of the OFDM signal in absence of synchronization errors (solid lines) and in presence of a CFO $\epsilon = 0.2$ (dashed lines). As we can see the presence of a CFO provokes a reduction in signal amplitude and ICI.

In [6], Pollet *e*t al., analytically evaluate the degradation of the bit error rate (BER) caused by the presence of CFO for an AWGN channel. It is found that a multicarrier system is much more sensitive than single-carrier system and, in particular, the degradation in SNR (in dB) can be approximated by

$$D(dB)\triangleq\frac{SNR}{SNR_e(\epsilon)}\simeq\frac{10(\pi\epsilon)^2SNR}{3\ln 10}=\frac{10(\pi\Delta f T_c N)^2SNR}{3\ln 10}, \qquad (3.10)$$

From (3.10) we can note that the degradation (in dB) increases with the square of the number of subcarriers, if ϵ and T_c are fixed.
With a similar reasoning we can demonstrate that in presence of dispersive channel the received OFDM signal after demodulation can be written as

$$\tilde{a}_q^l = \frac{e^{j\phi}}{N} I_0(\epsilon) a_q^l H(l) + \underbrace{\frac{e^{j\phi}}{N} \sum_{\substack{h=0 \\ h \neq l}}^{N-1} a_q^h H(h) I_{h-l}(\epsilon)}_{ICI} + \eta(l) \, ,$$

that is, a dispersive channel leads to an attenuation and a constant carrier offset that are added to those introduced by CFO synchronization errors. In regard to the degradation due to the presence of ICI, Moose in [7], has estimated analytically the incidence of such disturbance deriving the relation between the effective SNR $SNR_e(\epsilon)$ in presence of additive noise and ICI and that of a perfectly synchronized system SNR. In particular, the lower bound for the $SNR_e(\epsilon)$ at the output of the DFT derived in [7] is

$$SNR_e(\epsilon) \geq \frac{SNR}{1 + 0.5947 SNR \sin^2(\pi\epsilon)} \left(\frac{\sin(\pi\epsilon)}{\pi\epsilon} \right)^2 . \tag{3.11}$$

Therefore, the degradation in dB induced by the presence of CFO synchronization errors is limited by

$$D(\epsilon) \stackrel{\triangle}{=} \frac{SNR}{SNR_e(\epsilon)} \leq 10 \log_{10} \left[\frac{1 + 0.5947 SNR \sin^2(\pi\epsilon)}{\mathrm{sinc}^2(\epsilon)} \right] . \tag{3.12}$$

In Fig.3.4 is plotted the degradation (3.10) in AWGN (dashed lines) and for dispersive channel (3.12) (solid lines) as a function of the normalized carrier frequency offset ϵ, for different values of signal to noise ratio SNR. In particular we can observe that in presence of a signal to noise ratio equal to 30 dB to have a degradation lower than 10% it is necessary that $|\epsilon| < 10^{-2}$.

3.4 Synchronization Schemes

Several CFO and symbol timing synchronization scheme have been suggested in literature. In particular they can be divided into two categories:

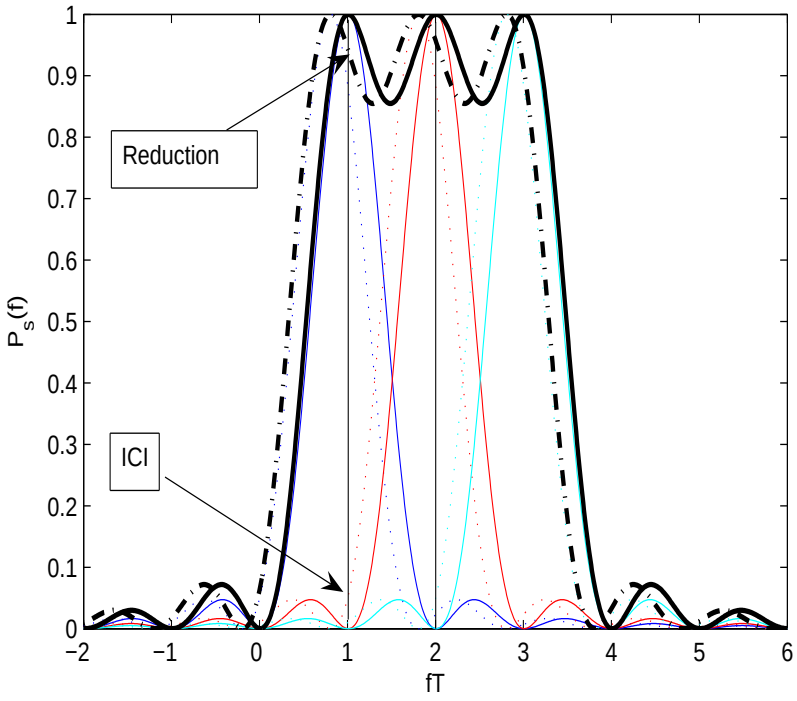

Figure 3.3: PSD of the OFDM signal for a multicarrier system with $N = 3$ subcarriers in presence (dashed lines) and in absence (solid lines) of CFO.

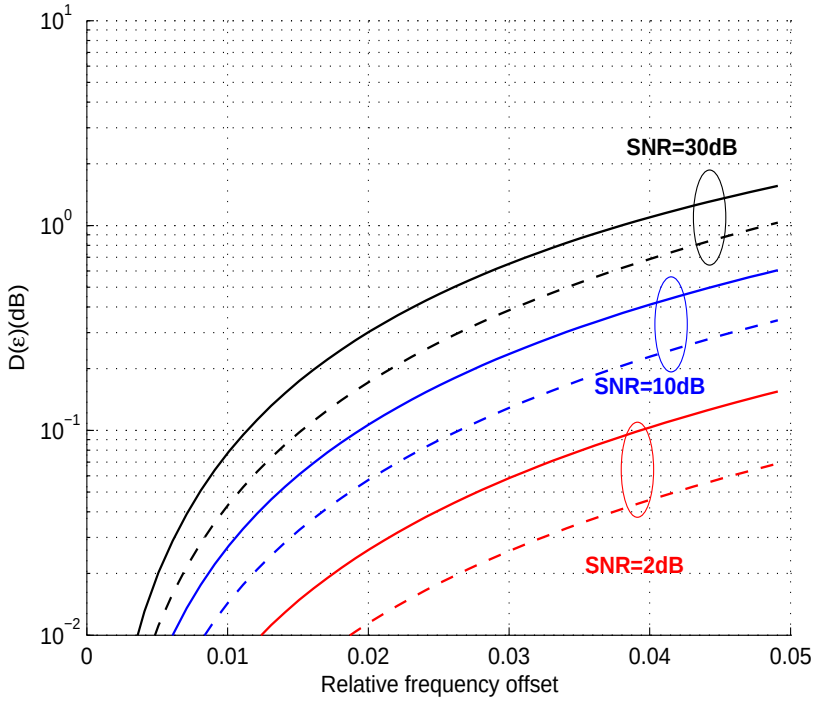

Figure 3.4: Degradation in SNR due to a frequency offset (normalized to the subcarrier spacing). Analytical expression for AWGN (dashed lines) and fading channel (solid lines).

***Data-aided* algorithms** : algorithms based on known sequences or with a known structure.

***Non data-aided* o *blind* algorithms** : non data-aided (or blind) algorithms exploiting only the statistical properties of the useful signal.

3.4.1 Blind and Semiblind Synchronization Schemes

Non data-aided synchronization techniques result to be particularly interesting since they do not require the transmission of training symbols. Specifically, Van de Beek *e*t al. propose in [9] an ML method for joint symbol timing and CFO estimation in flat fading channel that exploits the signal redundancy induced by the CP. The algorithm performance is influenced by the CP length and the SNR value. Moreover, the algorithm performs very well in AWGN, but exhibits a floor error in presence of a multipath channel since the CP contains interference from the previous symbol. A solution that mitigates this problem is considered in [5] where a modified ML estimator exploiting only ISI-free samples of the CP is proposed to counteract the degrading effects of dispersive channels.

Efficient blind techniques that take advantage of transmission of virtual subcarriers have also been considered in [32]. If the transmit and receive oscillators are perfectly synchronized, the modulated carriers in the received signal and virtual carriers are orthogonal. The degree to which these two sets of subcarriers are orthogonal then is a measure of how far out of synchronization the receiver oscillator is. Orthogonality between the modulated and virtual carriers over an interference free window of the received signal is used to develop an algorithm for estimating the CFO and detecting the symbol timing.

Landström et al. propose in [33] an improved ML timing estimator using both CP and training pilots. Two log-likelihood functions of the time delay are constructed by also considering the contribution of the training symbols. One log-likelihood function gives the position of the CP, thus giving an unambiguous but coarse timing estimate. Another log-likelihood function is a matched filter to the training symbols and this has many distinct correlation peaks that give an ambiguous estimate of the time delay. The weighted criterion combining the two functions yields an unambiguous and distinct peak of the log-likelihood function. The frequency offset causes an increase in the time delay

estimator variance due to a random phase in the correlation sums. In order to avoid this problem, the absolute value is taken in the log-likelihood function thus preserving the constructive contributions of the peaks in the weighted log-likelihood function.

Finally in [34] Bölcskei proposes a blind method for synchronization in a pulse-shaped OFDM. The method exploits the cyclostationarity introduced by the pulse-shaping operation to blindly identify both the symbol timing and the frequency offset. The pulse shaped OFDM is preferable for high data rate services since it reduces out-of-band emission and it has a reduced sensitivity to frequency offsets. Different ways of inducing cyclostationarity in the OFDM signal are discussed, including the carrier weighting (transmitting different sub-carriers with different powers). If no pulse-shaping and carrier weighting is performed, the OFDM signal is stationary and the blind synchronization cannot be performed based on the second order statistics. The proposed blind method does not need any CP to perform the synchronization.

3.4.2 Data-Aided Synchronization Schemes

For high-rate packet transmission, the synchronization time needs to be as short as possible, preferably a few OFDM symbols only. To achieve this, special OFDM training symbols can be used to achieve synchronization. For example current WLAN standards, like IEEE 802.11a or HiperLAN/2 [35], include a preamble in the start of the packet composed by identical parts in the time domain. The length and the contents of the preamble have been carefully designed to provide enough information for good synchronization performance. In [17] Schmidl and Cox consider a timing and frequency offset synchronization scheme that exploits the redundancy associated with a training symbol composed by two identical halves generated by transmitting a pseudo-random sequence on even frequencies and zeroes on the odd frequencies. However, the considered timing metric reaches a plateau, whose length is equal to the CP length minus the length of the channel impulse response, that produces large variance for the timing estimates.

The training symbol proposed in [18], with four identical parts and a sign inversion, provides a timing metric with steeper rolloff. Nevertheless, the sign inversion in the transmitted training symbol introduces, in dispersive channels,

some interference in the frequency estimation process causing severe performance degradation. This drawback is investigated by Bhargava et al. in [19] where a more general synchronization algorithm based on a structured training sequence is proposed and, moreover, channel estimation is also incorporated in order to obtain fine timing and CFO estimates. This refinement step reduces the interference introduced in the coarse CFO acquisition process but at the cost of some increase in computational load.

In the following chapters we will explore some of these issues in more detail. Moreover, we will present and analyze new data-aided and blind methods to estimate symbol timing and CFO.

Chapter 4

Blind Synchronization

ML estimators of symbol timing and CFO have been derived under the assumption of non dispersive channel and by modeling the OFDM signal vector as a CGRV. However, when NC constellations are adopted the OFDM signal results to be an NC (or improper) process. This chapter deals with the problem of blind joint symbol timing and CFO estimation in OFDM systems with NC transmissions. Since the implementation complexity of derived ML estimator is high, feasible computational algorithms are considered. Finally, refined symbol timing estimators, apt to counteract the degrading effects of ISI in dispersive channels, are suggested.

4.1 Problem Statement and Assumptions

With reference to the discrete time signal model (2.20), let us consider the m-th sample of the q-th transmitted OFDM symbol

$$s_q(m) \stackrel{\triangle}{=} s(m+qM) = \frac{\sigma_s}{\sqrt{N}} \sum_{l=0}^{N-1} a_q^l e^{j\frac{2\pi}{N}lm},\ m \in \tau_2, \tag{4.1}$$

where the set τ_2 has been defined in (2.20) and $\sigma_s^2 \stackrel{\triangle}{=} E[|s_q(m)|^2]$. Throughout this chapter the following assumptions are made:

(AS1) The data symbols $\{a_q^l\}_{q=-\infty}^{\infty}$, $l \in \tau_1$, are i.i.d. random variables with zero-mean and unit variance.

(AS2) The number of subcarriers N is sufficiently large so that the OFDM signal $s_q(m)$ can be modeled as a complex Gaussian process.

(AS3) The data symbols $\{a_q^l\}_{q=-\infty}^{\infty}$, $l \in \tau_1$, belong to a constellation with $E[(a_q^l)^2] = b \neq 0$.

The assumption (AS3) imposes that the transmitted symbols belong to an NC constellation [12]. Typical examples of NC constellations are those with real symbols (e.g. BPSK, m-ASK, DBPSK), that present a noncircularity rate $|b| = 1$ and are commonly used in the telecommunication context to assure low BER at the expense of reduction in the data throughput. For example, in the WLAN standard HIPERLAN2 BPSK constellations are adopted for the broadcast channel, the frame channel, the access frame channel, the random access channel and the physical layer channels 1 and 2 (see [36] and [35]). Moreover, new NC constellations have been also proposed in [37].

Let us observe that from assumption (AS1) and in virtue of the redundancy introduced by the CP, we can easily derive the following result:

Result 1 In each OFDM symbol the samples in the CP and their copies are mutually correlated, thus the correlation function of the transmitted OFDM signal is equal to

$$E\left[s_p(k)s_q^*(m)\right] = \begin{cases} \sigma_s^2\delta[p-q], & m-k \in \{-N, 0, N\}, \\ & \forall m,k \in \tau_2, \\ 0, & \text{otherwise.} \end{cases} \tag{4.2}$$

Moreover, by the assumption (AS3) of NC transmissions it follows that

Result 2 For $N \geq 2$ and $N > 2L_c$, the relation (or conjugate correlation) function is given by[1]

$$E\left[s_p(k)s_q(m)\right] = \begin{cases} b\sigma_s^2\delta[p-q], & m+k \in \{0, N\}, \\ & \forall m, k \in \tau_2, \\ 0, & \text{otherwise.} \end{cases} \tag{4.3}$$

By reconsidering the signal model (4.1), we suppose that the OFDM signal is transmitted through an AWGN channel. Therefore, in presence of a CFO (normalized to the intercarrier spacing) ϵ, a phase offset ϕ and a delay θ, assumed to be a multiple of the sampling period, the discrete-time received signal can be modeled as

$$r_q(k) = s_q(k-\theta)e^{j\left[\frac{2\pi}{N}\epsilon(k+qM)+\phi\right]} + n_q(k)\,. \tag{4.4}$$

Let us introduce the vector $\boldsymbol{s}_q \stackrel{\triangle}{=} [s_q(-L_c), \ldots, s_q(N-1)]^T$ indicating the qth transmitted OFDM symbol, then, using a vectorial notation, we can write

$$\boldsymbol{r}_q = \boldsymbol{\Psi}_q \boldsymbol{s}_q + \boldsymbol{n}_q \tag{4.5}$$

where

$$\boldsymbol{\Psi}_q \stackrel{\triangle}{=} e^{j\left[\frac{2\pi}{N}\epsilon(qM+\theta)+\phi\right]}\text{diag}\left\{e^{-j\frac{2\pi}{N}\epsilon L_c}, \ldots, e^{j\frac{2\pi}{N}\epsilon(N-1)}\right\}$$

is an $M \times M$ diagonal matrix and the noise vectors $\boldsymbol{n}_q \stackrel{\triangle}{=} [n_q(-L_c + \theta), \ldots, n_q(N-1+\theta)]^T$ are modeled as a zero-mean C-CGRVs with $E[\boldsymbol{n}_q\boldsymbol{n}_p^H] = \delta[p-q]\sigma_n^2\boldsymbol{I}_M$ and statistically independent of the useful signal vectors $\boldsymbol{s}_q$. Finally, $\boldsymbol{r}_q \stackrel{\triangle}{=} [r_q(-L_c+\theta), \ldots, r_q(N-1+\theta)]^T$ is the vector of the received signal assumed to be a zero-mean NC-CGRV characterized by the matrix $\bar{\boldsymbol{C}}_{\boldsymbol{r}_q} \in \mathbb{C}^{2M\times 2M}$ [16]

$$\bar{\boldsymbol{C}}_{\boldsymbol{r}_q} \stackrel{\triangle}{=} E\left\{\begin{bmatrix} \boldsymbol{r}_q \\ \boldsymbol{r}_q^* \end{bmatrix}[\boldsymbol{r}_q^H, \boldsymbol{r}_q^T]\right\} = \begin{bmatrix} \boldsymbol{C}_{\boldsymbol{r}_q} & \boldsymbol{R}_{\boldsymbol{r}_q} \\ \boldsymbol{R}_{\boldsymbol{r}_q}^* & \boldsymbol{C}_{\boldsymbol{r}_q}^* \end{bmatrix} \tag{4.6}$$

[1]The condition $N \geq 2$ assures the presence of the conjugate correlation (4.3) for $m+k \in \{0, N\}$ while for $N < 2$ only $m+k = 0$ should be considered in (4.3). Moreover, the assumption $N > 2L_c$ allows to exclude the condition $m+k = -N$ in (4.3). In fact, for $N \leq 2L_c$ it follows that $E\left[s_p(k)s_q(m)\right] = b\sigma_s^2\delta[p-q]$ also for $m+k = -N$. However, the much more complex analysis with $m+k \in \{-N, 0, N\}$ in (4.3) turns out to be of little interest since the condition $N > 2L_c$ is always satisfied in practice.

where

$$\begin{aligned} \boldsymbol{C}_{\boldsymbol{r}_q} \stackrel{\triangle}{=} E[\boldsymbol{r}_q \boldsymbol{r}_q^H] = & \quad \boldsymbol{\Psi}_q \underbrace{E[\boldsymbol{s}_q \boldsymbol{s}_q^H]}_{\boldsymbol{C}_{\boldsymbol{s}_q}} \boldsymbol{\Psi}_q^* + \sigma_n^2 \boldsymbol{I}_M \\ = & \quad \boldsymbol{\Psi}_q \left[\boldsymbol{C}_{\boldsymbol{s}_q} + \sigma_n^2 \boldsymbol{I}_M\right] \boldsymbol{\Psi}_q^* \end{aligned} \tag{4.7}$$

is the covariance matrix of the vector $\boldsymbol{r}_q$, while

$$\boldsymbol{R}_{\boldsymbol{r}_q} \stackrel{\triangle}{=} E[\boldsymbol{r}_q \boldsymbol{r}_q^T] = \boldsymbol{\Psi}_q \underbrace{E[\boldsymbol{s}_q \boldsymbol{s}_q^T]}_{\boldsymbol{R}_{\boldsymbol{s}_q}} \boldsymbol{\Psi}_q \tag{4.8}$$

is the so-called relation matrix.

Note that accounting for the assumptions (AS1) and (AS3), and according to result 1, the covariance matrix $\boldsymbol{C}_{\boldsymbol{s}_q}$, whose (i,l)th entry is $\left[\boldsymbol{C}_{\boldsymbol{s}_q}\right]_{(i,l)} \stackrel{\triangle}{=} E[s_q(-L_c{+}i)s_q^*(-L_c{+}l)], \forall i,l \in \{0,\ldots,M-1\}$, results to be a real symmetric Toeplitz matrix and its first row is equal to

$$\left[\boldsymbol{C}_{\boldsymbol{s}_q}\right]_{(0,:)} = \sigma_s^2[1, \boldsymbol{O}_{1\times(N-1)}, 1, \boldsymbol{O}_{1\times(L_c-1)}]\,. \tag{4.9}$$

Moreover, in virtue of result 2, the (i,l)th entry of $\boldsymbol{R}_{\boldsymbol{s}_q}$, the relation matrix of the vector $\boldsymbol{s}_q$, is given by

$$\begin{aligned} \left[\boldsymbol{R}_{\boldsymbol{s}_q}\right]_{(i,l)} & \stackrel{\triangle}{=} E[s_q(-L_c{+}i)s_q(-L_c{+}l)] \\ & = \begin{cases} b\sigma_s^2, & i{+}l{=}2L_c \text{ or } i{+}l{=}2L_c{+}N, \\ & \quad \forall i,l \in \{0,\ldots,M-1\}\,, \\ 0, & \text{otherwise.} \end{cases} \end{aligned} \tag{4.10}$$

4.2 Stochastic ML Estimators

In this section ML-based symbol timing and CFO estimators for OFDM systems with NC transmissions (NC-OFDM systems) are derived by maximizing the log-likelihood function (LLF) for the vector of unknown parameters $\boldsymbol{\lambda} \stackrel{\triangle}{=} [\theta, \epsilon, \phi]^T$. Then, the resulting estimators are particularized to the case of OFDM systems exploiting circular constellations (C-OFDM systems) and for NC-OFDM systems with a null CP.

4.2.1 ML Estimator for NC-OFDM Systems

Let us consider the observation vector of total length $W = N/2 + (2+\eta)M$

$$\boldsymbol{r} \stackrel{\triangle}{=} [\underbrace{(\boldsymbol{G}_1\boldsymbol{r}_{q-1})^T}_{\check{\boldsymbol{r}}_{q-1}^T}, \boldsymbol{r}_q^T, \ldots, \boldsymbol{r}_{q+\eta}^T, \underbrace{(\boldsymbol{G}_2\boldsymbol{r}_{q+\eta+1})^T}_{\check{\boldsymbol{r}}_{q+\eta+1}^T}]^T$$

where the matrices $\boldsymbol{G}_1$ and $\boldsymbol{G}_2$, defined as

$$\boldsymbol{G}_1 \stackrel{\triangle}{=} [\boldsymbol{O}_{(N/2+L_c+\theta)\times(N/2-\theta)} \;\; \boldsymbol{I}_{N/2+L_c+\theta}] \tag{4.11}$$

and

$$\boldsymbol{G}_2 \stackrel{\triangle}{=} [\boldsymbol{I}_{N-\theta} \;\; \boldsymbol{O}_{(N-\theta)\times(L_c+\theta)}] \,, \tag{4.12}$$

are real matrices with $\boldsymbol{G}_1\boldsymbol{G}_1^T = \boldsymbol{I}_{N/2+\theta+L_c}$, $\boldsymbol{G}_2\boldsymbol{G}_2^T = \boldsymbol{I}_{N-\theta}$, $\boldsymbol{G}_1^T\boldsymbol{G}_1 = [\boldsymbol{O}_{M\times(N/2-\theta)} \;\; \boldsymbol{G}_1^T]$ and $\boldsymbol{G}_2^T\boldsymbol{G}_2 = [\boldsymbol{G}_2^T \;\; \boldsymbol{O}_{M\times(L_c+\theta)}]$. Note that the vector $\boldsymbol{r}$ contains the last $\theta + N/2 + L_c$ samples of the $(q-1)$th OFDM symbol through the subvector $\check{\boldsymbol{r}}_{q-1}$, the first $N-\theta$ samples of the $(q+\eta+1)$th OFDM symbol through $\check{\boldsymbol{r}}_{q+\eta+1}$ and moreover, the subvector $[\boldsymbol{r}_q^T, \ldots, \boldsymbol{r}_{q+\eta}^T]^T$ contains $\eta+1$ whole OFDM symbols. This particular choice for the observation window allows us to maximize, for $\theta \in \tau_1$ and $\eta = 0$, the number of samples having a nonzero conjugate correlation (see (4.3)) with respect to those exhibiting the correlation property (4.2).

The W-dimensional NC-CGRV $\boldsymbol{r}$ is characterized by the joint PDF [16]

$$f(\boldsymbol{r}, \boldsymbol{r}^*; \boldsymbol{\lambda}) = \frac{1}{\pi^W \sqrt{\det\{\bar{\boldsymbol{C}}_{\boldsymbol{r}}\}}} \exp\left\langle -\frac{1}{2}[\boldsymbol{r}^H \boldsymbol{r}^T]\, \bar{\boldsymbol{C}}_{\boldsymbol{r}}^{-1} \begin{bmatrix} \boldsymbol{r} \\ \boldsymbol{r}^* \end{bmatrix} \right\rangle \tag{4.13}$$

where $\bar{\boldsymbol{C}}_{\boldsymbol{r}}$ is the covariance matrix of the vector $[\boldsymbol{r}^T, \boldsymbol{r}^H]^T$ depending on the second-order circular and NC statistical properties of the useful signal and of the noise. In [9] the matrix $\bar{\boldsymbol{C}}_{\boldsymbol{r}}$ has been particularized to the case of C-OFDM systems. In the following we will consider the situation appearing when the circularity assumption is not valid.

In order to simplify the mathematical treatment, let us consider an appropriate permutation matrix $\boldsymbol{P} \in \mathbb{R}^{2W\times 2W}$ such that the vector $[\boldsymbol{r}^T, \boldsymbol{r}^H]^T$ can be rearranged as

$$\bar{\boldsymbol{r}} = \boldsymbol{P}[\boldsymbol{r}^T, \boldsymbol{r}^H]^T = [\check{\boldsymbol{r}}_{q-1}^T, \check{\boldsymbol{r}}_{q-1}^H \boldsymbol{r}_q^T, \boldsymbol{r}_q^H, \ldots, \check{\boldsymbol{r}}_{q+\eta+1}^T, \check{\boldsymbol{r}}_{q+\eta+1}^H]^T \,. \tag{4.14}$$

In the following we assume that the symbol timing belongs to the interval $0 \leq \theta \leq N/2 - L_c - 1$, then the covariance matrix of vector $\bar{\boldsymbol{r}}$ in (4.14) can be written as

$$\bar{\boldsymbol{C}}_{\bar{\boldsymbol{r}}} = \mathrm{diag}\left\{\bar{\boldsymbol{C}}_{\check{\boldsymbol{r}}_{q-1}}, \ldots, \bar{\boldsymbol{C}}_{\check{\boldsymbol{r}}_{q+\eta+1}}\right\} = \boldsymbol{\Psi}\bar{\boldsymbol{C}}\boldsymbol{\Psi}^* \,, \tag{4.15}$$

where

$$\boldsymbol{\Psi}=\mathrm{diag}\big\{\boldsymbol{G}_1\boldsymbol{\Psi}_{q-1}\boldsymbol{G}_1^T, \boldsymbol{G}_1\boldsymbol{\Psi}_{q-1}^*\boldsymbol{G}_1^T, \boldsymbol{\Psi}_q, \ldots, \boldsymbol{G}_2\boldsymbol{\Psi}_{q+\eta+1}^*\boldsymbol{G}_2^T\big\}. \tag{4.16}$$

Moreover, accounting for (4.6)-(4.8) and since $\boldsymbol{R}_{\boldsymbol{s}_{q+i}} = \boldsymbol{R}_{\boldsymbol{s}} \;\; \forall \; i \in \{-1, \ldots, \eta+1\}$ and $\boldsymbol{C}_{\boldsymbol{s}_{q+i}} = \boldsymbol{C}_{\boldsymbol{s}} \;\; \forall \, i \in \{0, \ldots, \eta\}$, the matrix $\bar{\boldsymbol{C}}$ in (4.15) can be written as

$$\begin{aligned}\bar{\boldsymbol{C}}=\mathrm{diag}\Bigg\{\Bigg[& \begin{array}{ll} (\sigma_s^2+\sigma_n^2)\boldsymbol{I}_{N/2+L_c+\theta} & \boldsymbol{G}_1\boldsymbol{R}_{\boldsymbol{s}}\boldsymbol{G}_1^T \\ \boldsymbol{G}_1\boldsymbol{R}_{\boldsymbol{s}}^*\boldsymbol{G}_1^T & (\sigma_s^2+\sigma_n^2)\boldsymbol{I}_{N/2+L_c+\theta} \end{array} \Bigg], \\ & \Bigg[\begin{array}{ll} \boldsymbol{C}_{\boldsymbol{s}}+\sigma_n^2\boldsymbol{I}_M & \boldsymbol{R}_{\boldsymbol{s}} \\ \boldsymbol{R}_{\boldsymbol{s}}^* & \boldsymbol{C}_{\boldsymbol{s}}+\sigma_n^2\boldsymbol{I}_M \end{array} \Bigg] \otimes \boldsymbol{I}_{\eta+1}, \\ & \Bigg[\begin{array}{ll} (\sigma_s^2+\sigma_n^2)\boldsymbol{I}_{N-\theta} & \boldsymbol{G}_2\boldsymbol{R}_{\boldsymbol{s}}\boldsymbol{G}_2^T \\ \boldsymbol{G}_2\boldsymbol{R}_{\boldsymbol{s}}^*\boldsymbol{G}_2^T & (\sigma_s^2+\sigma_n^2)\boldsymbol{I}_{N-\theta} \end{array} \Bigg] \Bigg\} \,, \end{aligned} \tag{4.17}$$

where the relation $\boldsymbol{C}_{\boldsymbol{s}}^* = \boldsymbol{C}_{\boldsymbol{s}}$, deriving from (4.9), has been exploited.

Then, taking into accounting (4.13)-(4.15) and the properties of permutation matrices, and dropping a positive constant independent of the parameters to estimate, we obtain the classic expression of the LLF for θ, ϵ and ϕ given the observation vector $\bar{\boldsymbol{r}}$

$$\Lambda(\boldsymbol{\lambda}) = \log\{f(\bar{\boldsymbol{r}};\boldsymbol{\lambda})\} = -\frac{1}{2}\mathrm{Tr}\left\{\boldsymbol{\Psi}\bar{\boldsymbol{C}}^{-1}\boldsymbol{\Psi}^*\bar{\boldsymbol{r}}\bar{\boldsymbol{r}}^H\right\}. \tag{4.18}$$

This quadratic form by following the lines of Appendix A and putting, for the sake of simplicity, $q = 0$ can be rewritten as

$$\begin{aligned}\Lambda(\boldsymbol{\lambda})=T(\theta)+\Re\Bigg\{ & e^{-j2\pi\epsilon}\sum_{i=0}^{\eta} U_i(\theta) \\ & +\gamma^*\sum_{i=-1}^{\eta+1}\left[V_i(\theta)e^{-j\frac{4\pi}{N}\epsilon iM}+Z_i(\theta)e^{-j\frac{2\pi}{N}\epsilon(2iM+N)}\right]\Bigg\},\end{aligned} \tag{4.19}$$

where

$$\gamma \stackrel{\triangle}{=} e^{j\left[\frac{4\pi}{N}\epsilon\theta+2\phi\right]} \tag{4.20}$$

while the terms $T(\theta)$, $U_i(\theta)$, $i \in \{0,\ldots,\eta\}$, $V_i(\theta)$ and $Z_i(\theta)$, $i \in \{-1,\ldots,\eta+1\}$, are defined, in (A.2)-(A.5) in Appendix A, respectively.

As indicated in [38] the unconditional ML estimator is obtained by searching the value of the vector $\boldsymbol{\lambda}$ that maximizes the LLF. To proceed we keep the vector $[\theta,\epsilon]$ fixed and let ϕ vary. In these conditions the function $\Lambda(\boldsymbol{\lambda})$ in (4.19) achieves a maximum for

$$\hat{\phi}_{ML}(\theta,\epsilon)=\frac{1}{2}\angle\left\{e^{-j\frac{4\pi}{N}\epsilon\theta}\sum_{i=-1}^{\eta+1}e^{-j\frac{4\pi}{N}\epsilon iM}\left[V_i(\theta)+Z_i(\theta)e^{-j2\pi\epsilon}\right]\right\}. \tag{4.21}$$

Moreover, substituting (4.21) in (4.19), the joint ML symbol timing and CFO estimator is given by

$$\begin{aligned}(\hat{\theta}_{ML},\hat{\epsilon}_{ML})=\arg\max_{(\tilde{\theta},\tilde{\epsilon})}\Bigg\langle & T(\tilde{\theta})+\Re\left\{e^{-j2\pi\tilde{\epsilon}}\sum_{i=0}^{\eta}U_i(\tilde{\theta})\right\}\\ & +\left|\sum_{i=-1}^{\eta+1}e^{-j\frac{4\pi}{N}\tilde{\epsilon}iM}\Big[V_i(\tilde{\theta})+Z_i(\tilde{\theta})e^{-j2\pi\tilde{\epsilon}}\Big]\right|\Bigg\rangle,\end{aligned} \tag{4.22}$$

where $\tilde{\theta}$ and $\tilde{\epsilon}$ are trial values for symbol timing and frequency offset, respectively. Unfortunately, the solution of this two-dimensional maximization problem can be found only by numerical methods. Therefore, due to the computational complexity of the joint ML estimator, we consider a more feasible synchronization scheme that requires two one-dimensional maximization procedures. Specifically, we can note that the terms $U_i(m)$ (for $i \in \{0,\ldots,\eta\}$), $V_i(m)$ and $Z_i(m)$ (for $i \in \{-1,0,\ldots,\eta+1\}$), defined in (A.3)-(A.5), take into account the correlation and relation (conjugate correlation) (see (4.2) and (4.3)) between the samples of each OFDM symbol. Moreover, their magnitude exhibits a maximum when m is equal to the actual value of the symbol timing, since in this case mutually correlated samples are perfectly aligned in the summation windows. Thus, we propose the NC symbol timing estimator

$$\hat{\theta}_{NC}=\arg\max_{\tilde{\theta}}\left\{T(\tilde{\theta})+\sum_{i=0}^{\eta}|U_i(\tilde{\theta})|+\sum_{i=-1}^{\eta+1}\Big[|V_i(\tilde{\theta})|+|Z_i(\tilde{\theta})|\Big]\right\}. \tag{4.23}$$

Moreover, according to (4.22) and (4.21), we consider the NC CFO and carrier phase estimators

$$\begin{aligned}\hat{\epsilon}_{NC}= \quad & \arg\max_{\tilde{\epsilon}} \left\langle \Re\left\{ e^{-j2\pi\tilde{\epsilon}} \sum_{i=0}^{\eta} U_i(\hat{\theta}_{NC}) \right\} \right. \\ & \left. + \left| \sum_{i=-1}^{\eta+1} e^{-j\frac{4\pi}{N}\tilde{\epsilon} i M} \left[V_i(\hat{\theta}_{NC}) + Z_i(\hat{\theta}_{NC}) e^{-j2\pi\tilde{\epsilon}} \right] \right| \right\rangle \end{aligned} \tag{4.24}$$

and

$$\hat{\phi}_{NC} = \hat{\phi}_{ML}(\hat{\theta}_{NC}, \hat{\epsilon}_{NC}) \, . \tag{4.25}$$

Note that accounting for (4.21) it follows that the carrier phase estimator $\hat{\phi}_{NC}$ gives unambiguous estimates if $\mid \phi \mid \leq \frac{\pi}{2}$. Moreover, it can be easily shown that the function to be maximized with respect to ϵ in the right hand side (RHS) of (4.24) is a periodic function whose period Q is the minimum integer-value in the set

$$\left\{ \frac{\kappa}{2(\alpha+1)}, \;\; \kappa \in \mathbb{N} \right\}$$

with $\alpha \stackrel{\triangle}{=} L_c/N$. Therefore, the CFO estimator $\hat{\epsilon}_{NC}$ gives ambiguous estimates unless $\mid \epsilon \mid \leq Q/2$. In particular, with a suitable choice of the parameter α the CFO acquisition range can be enlarged or reduced. For example, for an OFDM system with $N = 512$ subcarriers and a CP length $L_c = 12$ the period is equal to $Q = 64$.

4.2.2 ML Estimator for C-OFDM Systems

In the case of circular transmissions ($E[(a_q^l)^2] = b = 0$) the matrix $\boldsymbol{R_s}$ is identically zero. Therefore, accounting for (A.2)-(A.5) and for the definition (A.9) in Appendix A, the LLF (4.19) becomes

$$\begin{aligned}\Lambda_C(\theta,\epsilon)= \; & -\frac{\rho}{2} \sum_{l=0}^{\eta} \sum_{k=\theta-L_c}^{\theta-1} \left[|r_l(k)|^2 + |r_l(k+N)|^2 \right] \\ & + \Re\left\{ e^{-j2\pi\epsilon} \sum_{l=0}^{\eta} \sum_{k=\theta-L_c}^{\theta-1} r_l^*(k) r_l(k+N) \right\} \, , \end{aligned} \tag{4.26}$$

which is the LLF calculated in [39] for $\eta+1$ consecutive OFDM symbols.

Let us observe that the LLF (4.26) does not depend on the carrier phase, thus, in this case, only the symbol timing and the CFO can be estimated. Moreover, the solution of the corresponding maximization problem is (see [9] and [39])

$$\hat{\theta}_{MLC}= \arg\max_{\tilde{\theta}} \left\{ -\frac{\rho}{2} \sum_{l=0}^{\eta} \sum_{k=\tilde{\theta}-L_c}^{\tilde{\theta}-1} \left[|r_l(k)|^2 + |r_l(k+N)|^2 \right] + \left| \sum_{l=0}^{\eta} \sum_{k=\tilde{\theta}-L_c}^{\tilde{\theta}-1} r_l^*(k) r_l(k+N) \right| \right\} \tag{4.27}$$

and

$$\hat{\epsilon}_{MLC} = \frac{1}{2\pi} \angle \left[\sum_{l=0}^{\eta} \sum_{k=\hat{\theta}_{MLC}-L_c}^{\hat{\theta}_{MLC}-1} r_l^*(k) r_l(k+N) \right] \tag{4.28}$$

that gives ambiguous estimates unless $\mid \epsilon \mid \leq 0.5$.

Note that the MLC symbol timing statistic (4.27), for high SNR values ($\rho \rightarrow 1$, see (A.9)), becomes the minimum mean-squared error symbol timing statistic in AWGN channel proposed in [5]. On the other hand, for low SNR values ($\rho \rightarrow 0$), it reduces to the maximum correlation timing estimator considered in [40].

4.2.3 ML Estimator for NC-OFDM Systems with $L_c = 0$

In the case of NC-OFDM systems with a null CP we can refer to the model (4.5) by putting $L_c = 0$. In this situation, accounting for result 1, $\boldsymbol{C_s} = \sigma_s^2 \boldsymbol{I}_N$, while the (i,l)th entry of the matrix $\boldsymbol{R_s} \in \mathbb{C}^{N \times N}$ is given by

$$[\boldsymbol{R_s}]_{(i,l)} = \begin{cases} b\sigma_s^2, & i+l=0 \text{ or } i+l=N, \\ & \forall\ i,l \in \{0,\ldots,N-1\}, \\ 0, & \text{otherwise.} \end{cases} \tag{4.29}$$

Table 4.1: Error probability $P(\hat{\theta} \neq \theta)$

θ	NC	MLC	MCL0
0	0.0000	0.0759	0.0016
20	0.0000	0.1594	0.0005
40	0.0000	0.1458	0.0000
60	0.0000	0.1505	0.0000
65	0.0000	0.1995	0.0000
69	0.0000	0.5752	0.0001
71	0.0002	0.6459	0.0003
73	0.0006	0.8205	0.0014
75	0.0012	0.9693	0.0031

Therefore, in this case the LLF for the vector of unknown parameters $\boldsymbol{\lambda}$ takes the simpler form

$$\begin{aligned}\Lambda_{L0}(\boldsymbol{\lambda}) = & -\rho|b|^2 T_{L0}(\theta) \\ & + \Re\left\{ b^* \gamma^* \sum_{i=-1}^{\eta+1} e^{-j4\pi\epsilon i} \left[V_{i_{L0}}(\theta) + Z_{i_{L0}}(\theta) e^{-j2\pi\epsilon} \right] \right\},\end{aligned} \tag{4.30}$$

where the parameters ρ and γ are defined in (A.9) and (4.20), respectively, while

$$\begin{aligned}T_{L0}(\theta) \triangleq & \sum_{i=0}^{\eta} \sum_{k=0}^{N-1} |r_i(k+\theta)|^2 + \sum_{k=0}^{2\theta} |r_{-1}(k+N/2)|^2 \\ & + |r_{\eta+1}(\theta)|^2 + \sum_{k=\theta+1}^{N-\theta-1} |r_{\eta+1}(k+\theta)|^2\end{aligned} \tag{4.31}$$

$$V_{i_{L0}}(\theta) \triangleq \begin{cases} 0, & i = -1, \\ r_i^2(\theta), & i = 0, \ldots, \eta+1, \end{cases} \tag{4.32}$$

and

$$Z_{i_{L0}}(\theta)\stackrel{\triangle}{=}\begin{cases}\displaystyle\sum_{k=0}^{2\theta} r_i(k+N/2)r_i(N/2+2\theta-k), & i=-1,\\ \displaystyle\sum_{k=1}^{N-1} r_i(k+\theta)r_i(N+\theta-k), & i=0,\ldots,\eta,\\ \displaystyle\sum_{k=\theta+1}^{N-\theta-1} r_i(k+\theta)r_i(N+\theta-k), & i=\eta+1.\end{cases} \tag{4.33}$$

Let us observe that, unlike the circular case developed in the previous subsection, for an NC-OFDM system with $L_c = 0$ the corresponding LLF (4.30) depends also on the phase offset ϕ. Specifically, accounting for (4.30), the ML carrier phase estimator is given by

$$\hat{\phi}(\theta,\epsilon)=\frac{1}{2}\angle\left\{b^* e^{-j\frac{4\pi}{N}\epsilon\theta}\sum_{i=-1}^{\eta+1} e^{-j4\pi\epsilon i}\left[V_{i_{L0}}(\theta)+Z_{i_{L0}}(\theta)e^{-j2\pi\epsilon}\right]\right\} \tag{4.34}$$

and provides unambiguous estimates for $\mid \phi \mid \leq \pi/2$. Moreover, by replacing (4.34) in (4.30), the ensuing LLF for the parameters $[\theta,\epsilon]^T$ is equivalent to

$$\begin{aligned}\Lambda_{L0}(\theta,\epsilon,\hat{\phi}(\theta,\epsilon))= &-\rho|b|T_{L0}(\theta)\\ &+\left|\sum_{i=-1}^{\eta+1} e^{-j4\pi\epsilon i}\left[V_{i_{L0}}(\theta)+Z_{i_{L0}}(\theta)e^{-j2\pi\epsilon}\right]\right|.\end{aligned} \tag{4.35}$$

Due to the complexity of the joint ML symbol timing and CFO estimator, by following the same considerations applied to derive the NC algorithm, we can consider the decoupled timing metric

$$\hat{\theta}=\arg\max_{\tilde{\theta}}\left\{-\rho|b|T_{L0}(\tilde{\theta})+\sum_{i=-1}^{\eta+1}\left|Z_{i_{L0}}(\tilde{\theta})\right|\right\}, \tag{4.36}$$

where in virtue of assumption (AS2) ($N \gg 1$) and accounting for the definitions (4.31)-(4.33) we omit $V_{i_{L0}}(m)$ terms. Moreover, with a further simplification, (4.36) can be approximated with its expression for low SNR ($\rho \to 0$)

$$\hat{\theta}_{MCL0}=\arg\max_{\tilde{\theta}}\left\{\sum_{i=-1}^{\eta+1}\left|Z_{i_{L0}}(\tilde{\theta})\right|\right\}. \tag{4.37}$$

Since the estimate of the symbol timing is obtained by considering the maximum correlation of the metric $Z_{i_{L0}}(m)$, the estimator (4.37) will be referred in the following to as maximum correlation for $L_c = 0$ (MCL0) algorithm. Notice that the MCL0 symbol timing estimator does not require the knowledge of the parameter ρ (that is, accounting for (A.9), it is independent of the SNR value) and of the noncircularity rate $|b|$. Moreover, accounting for (4.35) we propose the closed form CFO estimator

$$\hat{\epsilon}_{MCL0} = \frac{1}{4\pi} \angle \left\{ \sum_{i=0}^{\eta} \frac{Z_{i+1_{L0}}(\hat{\theta}_{MCL0})}{Z_{i_{L0}}(\hat{\theta}_{MCL0})} \right\} , \tag{4.38}$$

that provides an unambiguous estimate for $\mid \epsilon \mid \leq 1/4$.

To obtain some insights about the acquisition range of the considered symbol timing estimators Table 4.1 shows the error probability $P(\hat{\theta} \neq \theta)$ of NC, MLC and MCL0 algorithms in AWGN channel with $SNR = 10dB$ and for an OFDM system with $N = 64$ BPSK subcarriers and $L_c = 12$. By investigating these results, obtained by performing 10^4 runs, we can deduce that the acquisition range of NC and MCL0 estimators is $0 \leq \theta \leq M - 1$ while the MLC estimator provides anomalous estimates in the interval $N \leq \theta \leq M - 1$.

Moreover, with a slight adjustment the estimators (4.37) and (4.38) could also be exploited in OFDM systems with a CP different from zero or in OFDM systems with zero-padding, that is for OFDM systems in which the CP is replaced by a null prefix.

4.3 Performance Bounds

In this section we evaluate the CRB on CFO and carrier phase estimation for NC-OFDM systems in the case of known symbol timing and for the observed data vector $\bar{\boldsymbol{r}}$ in (4.14). Note that since a Gaussianity assumption is imposed on the useful OFDM signal vector, the derived CRB is the Gaussian [41] (or stochastic [42]) CRB. Let $\boldsymbol{\nu} \stackrel{\triangle}{=} [\epsilon, \phi]^T$ the vector of the parameters of interest, the (i, l)th entry of the Fisher information matrix (FIM) under the assumptions (AS1)-(AS3) can be expressed as follows (see [42] and [41])

$$[\boldsymbol{F}]_{(i,l)} = \frac{1}{2} \mathrm{Tr} \left[\frac{\partial \bar{\boldsymbol{C}}_{\bar{\boldsymbol{r}}}}{\partial [\boldsymbol{\nu}]_i} \bar{\boldsymbol{C}}_{\bar{\boldsymbol{r}}}^{-1} \frac{\partial \bar{\boldsymbol{C}}_{\bar{\boldsymbol{r}}}}{\partial [\boldsymbol{\nu}]_l} \bar{\boldsymbol{C}}_{\bar{\boldsymbol{r}}}^{-1} \right] , \ \forall i, l \in \{0, 1\} \tag{4.39}$$

where the covariance matrix $\bar{\boldsymbol{C}}_{\bar{\boldsymbol{r}}}$ is defined in (4.15). Substituting (4.15) into (4.39) we obtain the 2×2 FIM,

$$\boldsymbol{F}=\begin{bmatrix} \left(\frac{2\pi}{N}\right)^2 \mathrm{Tr}\left[\bar{\boldsymbol{C}}^{-1}\boldsymbol{D}_\epsilon\bar{\boldsymbol{C}}\boldsymbol{D}_\epsilon-\boldsymbol{D}_\epsilon^2\right] & \frac{2\pi}{N}\mathrm{Tr}\left[\bar{\boldsymbol{C}}^{-1}\boldsymbol{D}_\epsilon\bar{\boldsymbol{C}}\boldsymbol{D}_\phi-\boldsymbol{D}_\epsilon\boldsymbol{D}_\phi\right] \\ \frac{2\pi}{N}\mathrm{Tr}\left[\bar{\boldsymbol{C}}^{-1}\boldsymbol{D}_\epsilon\bar{\boldsymbol{C}}\boldsymbol{D}_\phi-\boldsymbol{D}_\epsilon\boldsymbol{D}_\phi\right] & \mathrm{Tr}\left[\bar{\boldsymbol{C}}^{-1}\boldsymbol{D}_\phi\bar{\boldsymbol{C}}\boldsymbol{D}_\phi-\boldsymbol{I}_{2W}\right] \end{bmatrix}$$

where the matrix $\bar{\boldsymbol{C}}$ is defined in (4.17) and $\forall i \in \{0,1\}$

$$\begin{aligned}\boldsymbol{D}_{[\boldsymbol{\nu}]_i}=\mathrm{diag}\Big\{&\boldsymbol{G}_1\boldsymbol{\Delta}_{-1}^{[\boldsymbol{\nu}]_i}\boldsymbol{G}_1^T,-\boldsymbol{G}_1\boldsymbol{\Delta}_{-1}^{[\boldsymbol{\nu}]_i}\boldsymbol{G}_1^T,\boldsymbol{\Delta}_0^{[\boldsymbol{\nu}]_i},\ldots,\\ &-\boldsymbol{\Delta}_\eta^{[\boldsymbol{\nu}]_i},\boldsymbol{G}_2\boldsymbol{\Delta}_{\eta+1}^{[\boldsymbol{\nu}]_i}\boldsymbol{G}_2^T,-\boldsymbol{G}_2\boldsymbol{\Delta}_{\eta+1}^{[\boldsymbol{\nu}]_i}\boldsymbol{G}_2^T\Big\}\end{aligned}$$

with $\boldsymbol{\Delta}_m^{[\boldsymbol{\nu}]_0} \triangleq \mathrm{diag}\left\{-L_c+\theta+mM,\ldots,N-1+\theta+mM\right\}$ and $\boldsymbol{\Delta}_m^{[\boldsymbol{\nu}]_1} \triangleq \boldsymbol{I}_M$, $\forall m \in \{-1,\ldots,\eta+1\}$. The CRB for ϵ and ϕ is given by the corresponding inverse FIM diagonal element, that is

$$\begin{aligned}CRB_\epsilon^{NC}=&\frac{N^2}{4\pi^2}\Big\{\mathrm{Tr}\Big[\bar{\boldsymbol{C}}^{-1}\boldsymbol{D}_\epsilon\bar{\boldsymbol{C}}\boldsymbol{D}_\epsilon-\boldsymbol{D}_\epsilon^2\Big]\\ &-\mathrm{Tr}\Big[\bar{\boldsymbol{C}}^{-1}\boldsymbol{D}_\epsilon\bar{\boldsymbol{C}}\boldsymbol{D}_\phi-\boldsymbol{D}_\epsilon\boldsymbol{D}_\phi\Big]^2\mathrm{Tr}\Big[\bar{\boldsymbol{C}}^{-1}\boldsymbol{D}_\phi\bar{\boldsymbol{C}}\boldsymbol{D}_\phi-\boldsymbol{I}_{2W}\Big]^{-1}\Big\}^{-1}\end{aligned} \tag{4.40}$$

and

$$\begin{aligned}CRB_\phi^{NC}=&\Big\{\mathrm{Tr}\Big[\bar{\boldsymbol{C}}^{-1}\boldsymbol{D}_\phi\bar{\boldsymbol{C}}\boldsymbol{D}_\phi-\boldsymbol{I}_{2W}\Big]\\ &-\mathrm{Tr}\Big[\bar{\boldsymbol{C}}^{-1}\boldsymbol{D}_\epsilon\bar{\boldsymbol{C}}\boldsymbol{D}_\phi-\boldsymbol{D}_\epsilon\boldsymbol{D}_\phi\Big]^2\mathrm{Tr}\Big[\bar{\boldsymbol{C}}^{-1}\boldsymbol{D}_\epsilon\bar{\boldsymbol{C}}\boldsymbol{D}_\epsilon-\boldsymbol{D}_\epsilon^2\Big]^{-1}\Big\}^{-1}\end{aligned} \tag{4.41}$$

Thanks to the above expressions for the CRBs, we make the following comments:

1. In the case of C-OFDM systems the covariance matrix $\bar{\boldsymbol{C}}_{\bar{\boldsymbol{r}}}$ is independent of the carrier phase (see subsection 4.2.2). Thus, the CRB on the CFO estimate is easily obtained as

$$\begin{aligned}CRB_\epsilon^{C}=&\frac{N^2}{4\pi^2}\left\{\mathrm{Tr}\Big[\bar{\boldsymbol{C}}^{-1}\boldsymbol{D}_\epsilon\bar{\boldsymbol{C}}\boldsymbol{D}_\epsilon-\boldsymbol{D}_\epsilon^2\Big]\right\}^{-1}\\ =&\frac{1-\rho^2}{8\pi^2\rho^2\left(\eta+1\right)L_c}=\frac{2SNR+1}{8\pi^2L_cSNR^2(\eta+1)}\,.\end{aligned} \tag{4.42}$$

   This expression for $\eta = 0$ is coincident with that reported in [43].

2. In Fig.4.1 we report the ratio $CRB_{\epsilon}^{NC}/CRB_{\epsilon}^{C}$ as a function of the non-circularity rate $|b|$ for different values of SNR and by choosing $N = 512$, $L_c = 12$ and $\theta = 0$. The results, according to [42] (where the CRB on direction-of-arrival estimation for NC sources has been derived), show that the CRB_{ϵ}^{NC} is upper bounded by the associated CRB_{ϵ}^{C} and, in the examined case, the difference between them is more prominent for low SNR values and, for a fixed SNR value, when the length of the observation window increases.

3. Figures 4.2 and 4.3 present CRB_{ϵ}^{NC} and CRB_{ϕ}^{NC}, respectively, versus the number of subcarriers N for different values of the parameter $|b|$ and $SNR = 10$dB. The results show that both the CRB_{ϵ}^{NC} and CRB_{ϕ}^{NC} decrease at the rate $1/N$ when the noncircularity rate is different from zero. Thus, according to [41], in the case of NC transmissions ($b \neq 0$) the convergence rate of the phase and the CFO $\triangle F = \epsilon/N$ (remember that ϵ is the CFO normalized to the intercarrier spacing) are $1/N$ and $1/N^3$, respectively.

4. For $W = M$ and $L_c \neq 0$ the CRB_{ϵ}^{NC} in (4.40) takes the form (see [14])

$$CRB_{\epsilon}^{NC} = \overbrace{\left[\frac{1-\rho^2}{8\pi^2\rho^2\, L_c}\right]}^{CRB_{\epsilon}^{C}} \times \left\{\frac{(1+\rho-2\rho^2|b|^2)}{(1+\rho)\left[1-|b|^2\rho+|b|^2(1-\rho)\dfrac{k_1k_2}{(k_1+k_2)}\right]}\right\},$$

where

$$k_1 = 1 + \frac{(1+\rho-2\rho^2|b|^2)}{2\, L_c\, (1-\rho^2|b|^2)} \tag{4.43}$$

and

$$k_2 = 1 + \frac{(1+\rho-2\rho^2|b|^2)}{2\, L_c\, (1-\rho^2|b|^2)}(N-2L_c-1). \tag{4.44}$$

Let us observe that for $N \gg 2(L_c+1)$, $\dfrac{k_1k_2}{(k_1+k_2)} \simeq k_1 > 1$, and, then the

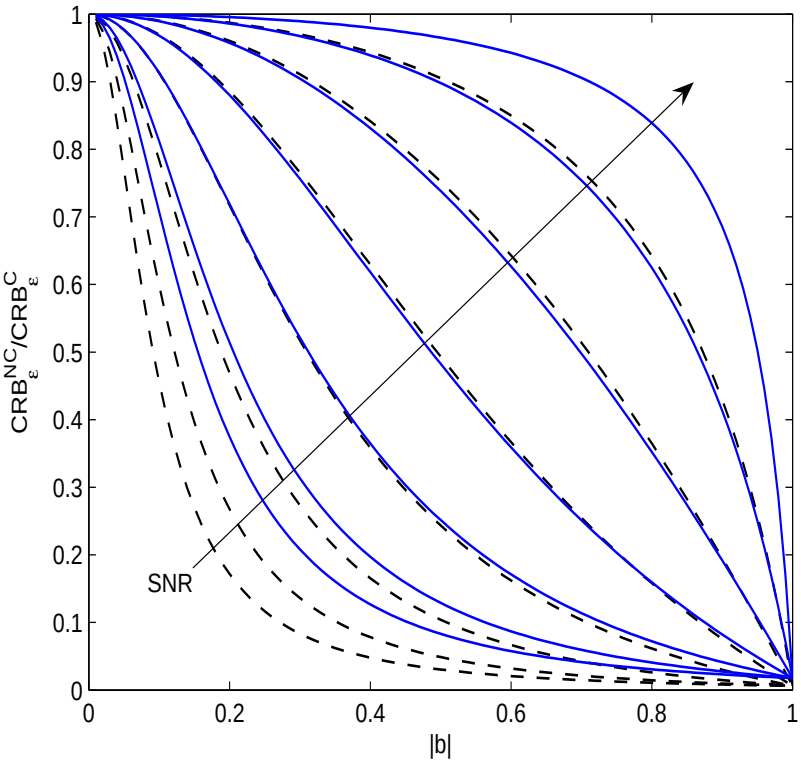

Figure 4.1: Ratio $CRB_\epsilon^{NC}/CRB_\epsilon^{C}$ versus the noncircularity rate $|b|$ for $SNR\in\{0,5,10,15,20,25,30\}$ dB and for an observation window of length $W{=}2M{+}N/2$ (solid lines) and $W{=}4M{+}N/2$ (dashed lines).

CRB_{ϵ}^{NC} can be approximated as

$$CRB_{\epsilon}^{NC} \simeq CRB_{\epsilon}^{C} \left\{ \frac{1}{1+|b|^2(1-\rho)\left[\frac{k_1(1+\rho)-\rho}{1+\rho-2\rho^2|b|^2}\right]} \right\}. \tag{4.45}$$

Equivalently, it can shown that

$$CRB_{\phi}^{NC} \simeq \frac{(1+\rho-2\rho^2|b|^2)}{8\rho^2 L_c |b|^2 \left[k_1 + \frac{1-\rho|b|^2}{(1-\rho)|b|^2}\right]}. \tag{4.46}$$

From (4.45) we can easily deduce that the CRB_{ϵ}^{NC} decreases monotonically by increasing the noncircularity rate $|b|$ of the adopted NC constellation. In particular it attains its maximum CRB_{ϵ}^{C} for $|b| = 0$ (circular case) and the minimum $CRB_{\epsilon}^{NCb1} = \frac{(1-\rho)(1+2\rho)}{8\pi^2\rho^2\, L_c(1+k_1)}$ for $|b| = 1$ (e.g., real constellations).

Note also that the CRB_{ϵ}^{NC} in (4.45), obtained for $N \gg 2(L_c+1)$, does not depend on the number of subcarriers N. This implies that the convergence rate of the CFO $\triangle F = \epsilon/N$ is $1/N^2$, i.e., one order of magnitude less than the convergence rate obtained in the previously considered case of a sample size $W > M$. This is due to the fact that when the joint CFO and carrier phase estimation is considered and only one OFDM symbol is exploited, that is the length of the observation window is $W = M$, there exists a strong correlation between the CFO estimate and the carrier phase estimate whose CRB presents a floor (see (4.46)). To corroborate this statement we note that, when $W = M$ and the phase offset is assumed to be known, the resulting CRB, $CRB_{\epsilon}^{NC-k\phi}$, is given by

$$CRB_{\epsilon}^{NC-k\phi} = CRB_{\epsilon}^{C} \left\{ \frac{(1+\rho-2\rho^2|b|^2)}{(1+\rho)[1-|b|^2\rho+|b|^2(1-\rho)k_3]} \right\}, \tag{4.47}$$

where $k_3 = k_1 \left(\frac{2L_c}{N}\right)^2 + k_2 \left(\frac{2L_c}{N}+1\right)^2$, and, for $N \gg 2L_c$, we obtain

$$CRB_{\epsilon}^{NC-k\phi} \simeq CRB_{\epsilon}^{C} \left\{ \frac{(1+\rho-2\rho^2|b|^2)}{(1+\rho)[1-|b|^2\rho+|b|^2(1-\rho)k_2]} \right\}.$$

Thus, accounting for (4.44), it follows that, when $W = M$ and the phase offset is assumed to be known, the CRB on the CFO estimate $CRB_{\epsilon}^{NC-k\phi}$ decreases at the rate $1/N$, and, then, the convergence rate of the CFO $\triangle F = \epsilon/N$ is again $1/N^3$ as in the case 3).

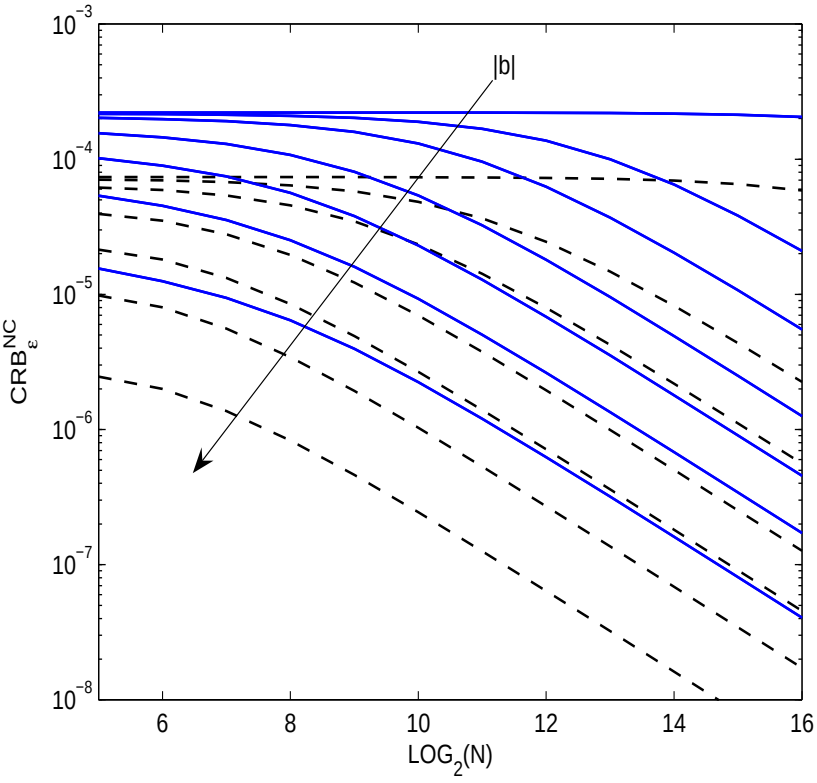

Figure 4.2: Behavior of CRB_ϵ^{NC} as a function of $\log_2 N$ for SNR=10 dB, $|b| \in \{10^{-3}, 0.1, 0.2, 0.4, 0.6, 0.8, 1\}$, and for an observation window of length $W=2M+N/2$ (solid lines) and $W=4M+N/2$ (dashed lines).

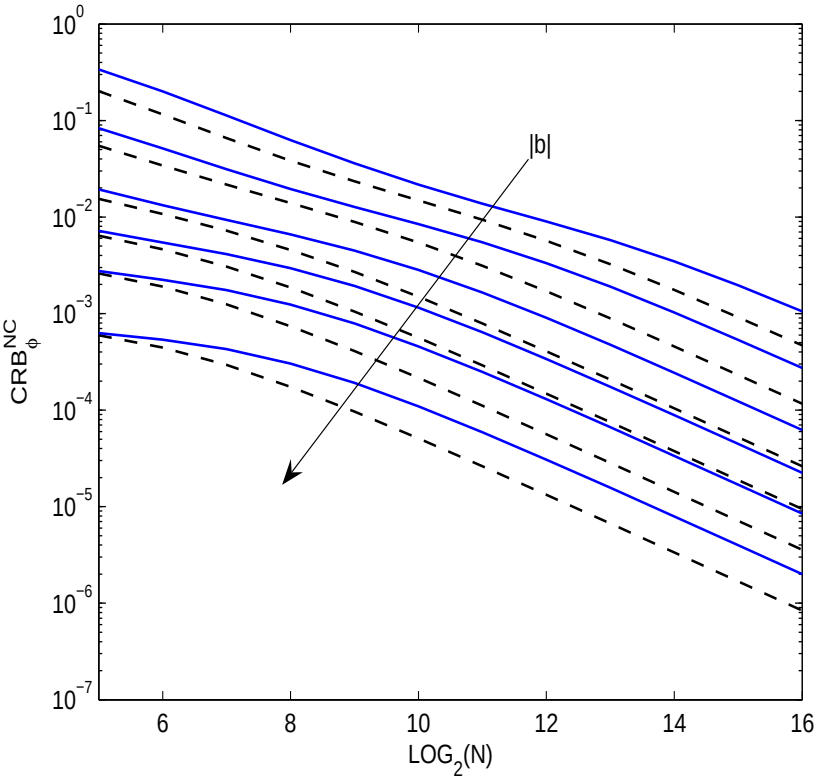

Figure 4.3: Behavior of CRB_{ϕ}^{NC} as a function of $\log_2 N$ for $SNR = 10$ dB, $|b| \in \{0.1, 0.2, 0.4, 0.6, 0.8, 1\}$, and for an observation window of length $W{=}2M{+}N/2$ (solid lines) and $W{=}4M{+}N/2$ (dashed lines).

4.4 Estimators in Multipath Channel

One of the main advantages of the OFDM system is its intrinsic robustness to multipath propagation that involves a significant reduction in the complexity of equalizers at the receiver. However, in presence of dispersive channels the statistics $\hat{\theta}_{NC}$ and $\hat{\theta}_{MCL0}$, in (4.23) and (4.37), respectively, derived for ISI-free channels, could not provide satisfactory performance. Thus, in this case, it is necessary to refine these estimates.

Let us consider a multipath channel, then the discrete-time received signal can be rewritten as

$$r_q(k) = \sum_{l=0}^{N_m} h(l) s_q(k-l-\theta) e^{j\frac{2\pi}{N}\epsilon(k+qM)} + n_q(k)\,, \tag{4.48}$$

where N_m is the maximum delay spread. Moreover, for $N \gg 1$ and under the hypothesis that the channel impulse response is constant in the observation window it follows that (see Appendix B)

$$\begin{aligned} &\frac{1}{N}\left\{ T(\theta+\beta)+\sum_{i=0}^{\eta} |U_i(\theta+\beta)| + \sum_{i=-1}^{\eta+1} [|V_i(\theta+\beta)| + |Z_i(\theta+\beta)|] \right\} \\ &\simeq \begin{cases} \mu_1 |(h*h)(2\beta)| - \mu_2, & \beta \in \{0,\ldots,N_m\}, \\ -\mu_2, & \text{otherwise}, \end{cases} \end{aligned} \tag{4.49}$$

where μ_1 and μ_2 are positive constants defined in Appendix B. Therefore, because of the channel dispersion, the statistic $\hat{\theta}_{NC}$ in (4.23) provides a coarse estimate of the arrival time of the first multipath component that, with high probability, differs from its actual value θ by a quantity $\beta \in \{0,\ldots,N_m\}$. Thus, a refined estimate $\hat{\theta}_{NCR}$ of the symbol timing is given by

$$\hat{\theta}_{NCR} = \hat{\theta}_{NC} - \hat{\beta}. \tag{4.50}$$

In particular, an estimate $\hat{\beta}$ of the parameter β can be obtained (see [44]) by

observing that, for $\beta \in \{0,\dots,N_m\}$ and for $N \gg 1$

$$\chi(u,\theta+\beta) \stackrel{\triangle}{=} \frac{1}{N-1}\sum_{l=0}^{\eta}\left|\sum_{k=1}^{N-1} r_l(\theta+\beta+k)r_l(N+\theta+\beta-k-u)\right|$$

$$\simeq \begin{cases} |b|\sigma_s^2(\eta+1)\,|\,(h*h)(2\beta-u)\,|, & 2\beta-u\in\{0,\dots,2N_m\}, \\ 0, & \text{otherwise.} \end{cases}$$

Hence, for

$$u = 2\beta + 1 \tag{4.51}$$

$\chi(u,\theta+\beta)$ drops to a value nearly equal to zero. An estimate $\hat{u}$ of the point u where $\chi(u,\theta+\beta)$ takes this value is given by

$$\hat{u} = \arg\min_{\tilde{u}} \left\{ \left(\chi(\tilde{u},\hat{\theta}_{NC}) / \chi(\tilde{u}-1,\hat{\theta}_{NC}) \right)^2 \right\}. \tag{4.52}$$

Then, accounting for (4.50), (4.51) and (4.52), the proposed estimator results to be

$$\hat{\theta}_{NCR} = \hat{\theta}_{NC} - \left\lceil \frac{1}{2}\,(\hat{u}-1) \right\rceil\,, \tag{4.53}$$

where $\lceil\cdot\rceil$ represents the operator that rounds its argument to the nearest integer towards infinity.

Moreover, following the lines of Appendix B it can be shown that

$$\frac{1}{N}\sum_{i=-1}^{\eta+1} |Z_{i_{L0}}(\theta+\beta)| \simeq \begin{cases} (\eta+2)\sigma_s^2|b(h*h)(2\beta)|, & \beta\in\{0,\dots,N_m\}, \\ 0, & \text{otherwise.} \end{cases} \tag{4.54}$$

Thus, the coarse estimate $\hat{\theta}_{MCL0}$ in (4.37) can be refined by following the same procedure exploited for the statistic $\hat{\theta}_{NC}$ (see (4.49) and (4.54)). Specifically, the refined symbol timing estimator MCL0R is given by

$$\hat{\theta}_{MCL0R} = \hat{\theta}_{MCL0} - \left\lceil \frac{1}{2}\,(\hat{u}-1) \right\rceil\,. \tag{4.55}$$

It should be noted that accounting for (4.51) the trial parameter $\tilde{u}$ belongs to the set $\{1, \ldots, 2N_m + 1\}$ whose size depends on the channel dispersion N_m. Thus, to obtain an algorithm independent of this channel parameter knowledge, we can assume that the channel dispersion does not exceed the CP length, that is $N_m \leq L_c$, so that the search of the minimum of the function in the RHS of (4.52) is done in the set $\tilde{u} \in \{1, \ldots, 2L_c + 1\}$.

Finally, let us observe that NC and MCL0 CFO estimators in (4.24) and (4.38), respectively, can be used in presence of dispersive channel provided that the channel impulse response is constant during the whole observation interval. Moreover, for $N \gg N_m + 1$, $\theta = 0$ and high SNR values, the mean squared error of the MCL0 CFO estimator, evaluated at $\hat{\theta} = \beta$, can be approximated by (see Appendix C)

$$E[(\hat{\epsilon}_{MCL0} - \epsilon)^2] \simeq \frac{\sum_{l=0}^{N_m} |h(l)|^2}{4\pi^2 SNR |b|^2 (\eta+1)^2 |(h * h)(2\beta)|^2 N}. \tag{4.56}$$

Thus for fixed SNR, η, $|b|$ and N, the value of β maximizing the term $|(h * h)(2\beta)|^2$ minimizes (4.56). Since, the coarse MCL0 symbol timing estimate maximizes the term $|(h * h)(2\beta)|$ (see (4.37) and (4.54)), it follows that in presence of a dispersive channel the MCL0 CFO synchronization algorithm provides estimates with a lower mean squared error when the coarse MCL0 symbol timing estimate is exploited. Moreover, simulation results have shown that also the NC algorithm assures in dispersive channel more accurate CFO estimates when the coarse NC symbol timing estimate is used. Therefore, in the following the performance of the proposed CFO estimators is assessed by substituting in (4.24) and (4.38) the corresponding coarse timing estimates.

Chapter 5

Synchronization with Training

This chapter deals with the problem of data-aided symbol timing and CFO estimation in OFDM systems. A synchronization scheme based on a training symbol made up of L identical parts, obtained by transmitting BPSK data symbols on the subcarriers whose indexes are multiple of L and setting zero on the remaining subcarriers, is proposed. In this case, if the number of subcarriers is sufficiently large, the training symbol can be modeled as an NC-CGRV. By exploiting the joint PDF for NC-CGRVs, the joint ML estimator for the parameters of interest is derived. Since its implementation complexity is significant, a lower complexity algorithm is proposed. Finally, a refined symbol timing estimator, apt to counteract the degrading effects of channel dispersion, is considered.

5.1 Training Symbol

With reference to the signal model (4.1) let us assume that the training symbol ($q = 0$) is made up (excluding the CP) of L identical parts with a possible sign inversion, that is, it has the form

$$\left[\ p(0)\boldsymbol{x}^T,\ p(1)\boldsymbol{x}^T,\ p(2)\boldsymbol{x}^T,\ \ldots,\ p(L-1)\boldsymbol{x}^T\ \right]\ , \tag{5.1}$$

where $\boldsymbol{x} \stackrel{\triangle}{=} [s(0), \ldots, s(P-1)]^T$ is a column vector of length $P = N/L$ and $p(l)$ represents the l-th entry of the vector $\boldsymbol{p} \in \{1, -1\}^{L\times 1}$ denoting the training symbol pattern, that is, the sign of each block $\boldsymbol{x}^T$ in (5.1). The structure of

the training symbol has been shown in Fig 5.1 into the case of $L = 2$.

In the following we consider the assumptions (AS1) and (AS2) stated in the previous chapter and moreover we suppose that

(AS3) The training symbol in (5.1) (except for the sign of each block) is given by transmitting a BPSK sequence with mean squared value L on the subcarriers whose indexes are multiple of L and setting zero on the remaining subcarriers.

(AS4) Except for the training symbol, the subcarrier symbols belong to a circular constellation (i.e., $E[(a_q^l)^2] = 0$ for $q \neq 0$).

From the previous assumptions, we can easily derive the following results:
Result 1 The (k, m)-th of the covariance matrix of the vector in (5.1) is equal to

$$E\left[s(k)s^*(m)\right] = \begin{cases} \sigma_s^2 p\left(\lfloor \frac{k}{P} \rfloor\right) p\left(\lfloor \frac{m}{P} \rfloor\right), & k-m{=}lP, \\ & \forall m, k \in \tau_1, \\ 0, & \text{otherwise}, \end{cases} \tag{5.2}$$

where, the set τ_1 is defined in (2.5). Moreover, since the training symbol is made up by transmitting, on the different subcarriers, BPSK data symbols, for $N \geq 4L$ it follows that
Result 2 The (k, m)-th of the relation matrix of the vector in (5.1) is given

$$E\left[s(k)s(m)\right] = \begin{cases} b\sigma_s^2 p(\lfloor \frac{k}{P} \rfloor) p(\lfloor \frac{m}{P} \rfloor), & k{+}m{=}lP, \\ & \forall m, k \in \tau_1, \\ 0, & \text{otherwise}. \end{cases} \tag{5.3}$$

Let us note that the **Result 1** particularized to the case of $L = 4$ and a possible sign inversion has been used in [18] and [19] to derive a joint CFO and timing estimator.

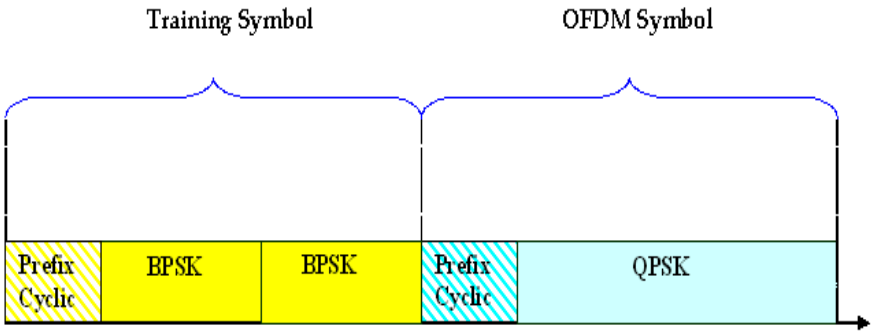

Figure 5.1: Scheme of training symbol with $L = 2$ identical parts.

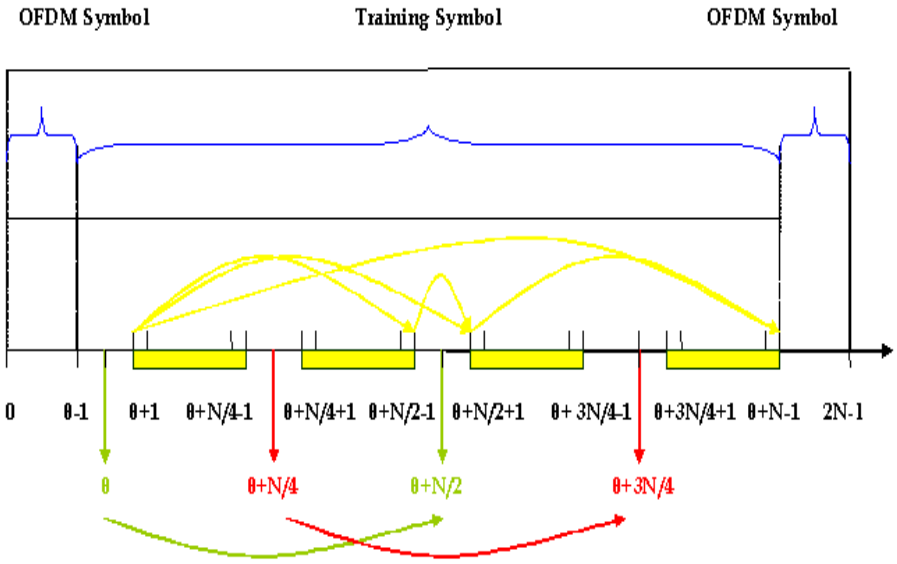

Figure 5.2: Scheme of correlation sets for a training symbol with $L = 2$ identical parts.

5.2 Stochastic ML Estimators

In this section ML-based symbol timing and CFO estimators for OFDM systems supported by a training symbol obtained by transmitting on the subcarriers whose indexes are multiple of L, symbols belonging to an NC constellation. Specifically, they are derived by maximizing the LLF for the vector of unknown parameters $\boldsymbol{\lambda} \stackrel{\triangle}{=} [\theta, \epsilon, \phi]^T$. Successively, the obtained estimators are particularized to the case of circular transmissions on the different subcarriers.

5.2.1 Estimators Based on an NC Training Symbol

Let us consider the $2N \times 1$ vector

$$\bar{\boldsymbol{r}} \stackrel{\triangle}{=} [r(-L_c), \ldots, r(\theta - L_c - 1), r(\theta), \ldots, r(2N-1)]^T , \qquad (5.4)$$

obtained by discarding the samples in the CP $r(\theta - L_c), \ldots, r(\theta - 1)$ and let us suppose that the unknown delay θ satisfies the condition $0 \leq \theta \leq N$, so that $\bar{\boldsymbol{r}}$ contains the entire training symbol. Using the vectorial model defined in chapter §4 the considered observation vector can be rewritten as

$$\bar{\boldsymbol{r}} \stackrel{\triangle}{=} [\underbrace{(\boldsymbol{G}_1 \boldsymbol{r}_{-1})^T}_{\check{\boldsymbol{r}}_{-1}^T}, \boldsymbol{r}_0^T, \underbrace{(\boldsymbol{G}_2 \boldsymbol{r}_1)^T}_{\check{\boldsymbol{r}}_1^T}]^T$$

where the matrices $\boldsymbol{G}_1$ and $\boldsymbol{G}_2$, defined as

$$\boldsymbol{G}_1 \stackrel{\triangle}{=} [\boldsymbol{O}_{\theta \times (N-\theta)} \;\; \boldsymbol{I}_\theta] \qquad (5.5)$$

and

$$\boldsymbol{G}_2 \stackrel{\triangle}{=} [\boldsymbol{I}_{N-\theta} \;\; \boldsymbol{O}_{(N-\theta)\times\theta}] , \qquad (5.6)$$

are real matrices with $\boldsymbol{G}_1 \boldsymbol{G}_1^T = \boldsymbol{I}_\theta$, $\boldsymbol{G}_2 \boldsymbol{G}_2^T = \boldsymbol{I}_{N-\theta}$, $\boldsymbol{G}_1^T \boldsymbol{G}_1 = [\boldsymbol{O}_{N\times(N-\theta)} \; \boldsymbol{G}_1^T]$ and $\boldsymbol{G}_2^T \boldsymbol{G}_2 = [\boldsymbol{G}_2 \; \boldsymbol{O}_{\theta\times N}]$. Note that the vector $\bar{\boldsymbol{r}}$ contains the last θ samples of the (-1)th OFDM symbol through the subvector $\check{\boldsymbol{r}}_{-1}$, the first $N - \theta$ samples of the OFDM symbol $\check{\boldsymbol{r}}_1$ and moreover, the subvector $\boldsymbol{r}_0^T$ contains, except for the CP, the training symbol.

The $2N$-dimensional NC-CGRV $\bar{\boldsymbol{r}}$ is characterized by the joint PDF [16]

$$f(\bar{\boldsymbol{r}}, \bar{\boldsymbol{r}}^*; \boldsymbol{\lambda}) = \frac{1}{\pi^{2N} \sqrt{\det\{\bar{\boldsymbol{C}}_{\bar{\boldsymbol{r}}}\}}} \exp\left\langle -\frac{1}{2} [\bar{\boldsymbol{r}}^H \bar{\boldsymbol{r}}^T] \, \bar{\boldsymbol{C}}_{\bar{\boldsymbol{r}}}^{-1} \begin{bmatrix} \bar{\boldsymbol{r}} \\ \bar{\boldsymbol{r}}^* \end{bmatrix} \right\rangle \qquad (5.7)$$

where $\bar{\boldsymbol{C}}_{\bar{\boldsymbol{r}}}$ is the covariance matrix of the vector $[\bar{\boldsymbol{r}}^T, \bar{\boldsymbol{r}}^H]^T$. Moreover, since the vectors $\check{\boldsymbol{r}}_{-1}$, $\boldsymbol{r}_0^T$ and $\check{\boldsymbol{r}}_1$ are statistically independent CGRVs, the joint PDF (5.7) can be rewritten as

$$\begin{aligned} f(\bar{\boldsymbol{r}}, \bar{\boldsymbol{r}}^*; \boldsymbol{\lambda}) \quad &= f(\check{\boldsymbol{r}}_{-1}, \check{\boldsymbol{r}}_{-1}^*; \boldsymbol{\lambda}) f(\boldsymbol{r}_0, \boldsymbol{r}_0^*; \boldsymbol{\lambda}) f(\check{\boldsymbol{r}}_1, \check{\boldsymbol{r}}_1^*; \boldsymbol{\lambda}) \\ &= \frac{1}{\pi^{\theta}\sqrt{\det\left\{\bar{\boldsymbol{C}}_{\check{\boldsymbol{r}}_{-1}}\right\}}} \exp\left\langle -\frac{1}{2}\left[\check{\boldsymbol{r}}_{-1}^H \check{\boldsymbol{r}}_{-1}^T\right] \bar{\boldsymbol{C}}_{\check{\boldsymbol{r}}_{-1}}^{-1} \begin{bmatrix} \check{\boldsymbol{r}}_{-1} \\ \check{\boldsymbol{r}}_{-1}^* \end{bmatrix} \right\rangle \\ &\times \frac{1}{\pi^{N}\sqrt{\det\left\{\bar{\boldsymbol{C}}_{\boldsymbol{r}_0}\right\}}} \exp\left\langle -\frac{1}{2}[\boldsymbol{r}_0^H \boldsymbol{r}_0^T] \bar{\boldsymbol{C}}_{\boldsymbol{r}_0}^{-1} \begin{bmatrix} \boldsymbol{r}_0 \\ \boldsymbol{r}_0^* \end{bmatrix} \right\rangle \\ &\times \frac{1}{\pi^{N-\theta}\sqrt{\det\left\{\bar{\boldsymbol{C}}_{\check{\boldsymbol{r}}_1}\right\}}} \exp\left\langle -\frac{1}{2}[\check{\boldsymbol{r}}_1^H \check{\boldsymbol{r}}_1^T] \bar{\boldsymbol{C}}_{\check{\boldsymbol{r}}_1}^{-1} \begin{bmatrix} \check{\boldsymbol{r}}_1 \\ \check{\boldsymbol{r}}_1^* \end{bmatrix} \right\rangle , \end{aligned} \tag{5.8}$$

where the matrices $\bar{\boldsymbol{C}}_{\check{\boldsymbol{r}}_{-1}}$, $\bar{\boldsymbol{C}}_{\boldsymbol{r}_0}$ and $\bar{\boldsymbol{C}}_{\check{\boldsymbol{r}}_1}$ are given by

$$\bar{\boldsymbol{C}}_{\check{\boldsymbol{r}}_{-1}} = \begin{bmatrix} (\sigma_s^2+\sigma_n^2)\boldsymbol{I}_{\theta} & \boldsymbol{O}_{\theta} \\ \boldsymbol{O}_{\theta} & (\sigma_s^2+\sigma_n^2)\boldsymbol{I}_{\theta} \end{bmatrix} , \tag{5.9}$$

$$\bar{\boldsymbol{C}}_{\boldsymbol{r}_0} = \begin{bmatrix} \boldsymbol{\Psi}(\boldsymbol{\lambda})\left[\boldsymbol{C}_{\boldsymbol{s}}+\sigma_n^2\boldsymbol{I}_M\right]\boldsymbol{\Psi}^*(\boldsymbol{\lambda}) & \boldsymbol{\Psi}(\boldsymbol{\lambda})\boldsymbol{R}_{\boldsymbol{s}}\boldsymbol{\Psi}(\boldsymbol{\lambda}) \\ \boldsymbol{\Psi}^*(\boldsymbol{\lambda})\boldsymbol{R}_{\boldsymbol{s}}^*\boldsymbol{\Psi}^*(\boldsymbol{\lambda}) & \boldsymbol{\Psi}^*(\boldsymbol{\lambda})\left[\boldsymbol{C}_{\boldsymbol{s}}^*+\sigma_n^2\boldsymbol{I}_M\right]\boldsymbol{\Psi}(\boldsymbol{\lambda}) \end{bmatrix} \tag{5.10}$$

and

$$\bar{\boldsymbol{C}}_{\check{\boldsymbol{r}}_1} = \begin{bmatrix} (\sigma_s^2+\sigma_n^2)\boldsymbol{I}_{N-\theta} & \boldsymbol{O}_{N-\theta} \\ \boldsymbol{O}_{N-\theta} & (\sigma_s^2+\sigma_n^2)\boldsymbol{I}_{N-\theta} \end{bmatrix} , \tag{5.11}$$

with

$$\boldsymbol{\Psi}(\boldsymbol{\lambda}) \stackrel{\triangle}{=} e^{j\left[\frac{2\pi}{N}\epsilon\theta+\phi\right]}\mathrm{diag}\left\{1, \ldots, e^{j\frac{2\pi}{N}\epsilon(N-1)}\right\}$$

$N \times N$ diagonal matrix while $\boldsymbol{R}_{\boldsymbol{s}}$ and $\boldsymbol{C}_{\boldsymbol{s}}$ are the relation and the correlation matrices of the transmitted training symbol $\boldsymbol{s} \stackrel{\triangle}{=} [s(0), \ldots, s(N-1)]^T$.

Thus, accounting for (5.8)-(5.11) and the results (5.2) and (5.3), after some algebraic manipulation, the LLF takes the form

$$\begin{aligned}\Lambda(\boldsymbol{\lambda}) =&\kappa_1\Bigg\{-c_1\rho P(\theta)+\sum_{l=0}^{L-2}\Re\left[Q_l(\theta)e^{-j\frac{2\pi(l+1)}{L}\epsilon}\right.\\ &\left.+\gamma^*\sum_{n=1}^{L}\sum_{l=n}^{L}\left(S_{l,n}(\theta)+T_{l,n}(\theta)e^{j\frac{2\pi\epsilon}{L}}\right)e^{-j\frac{2\pi(2l-n)}{L}\epsilon}\right]\Bigg\}\ ,\end{aligned} \tag{5.12}$$

where

$$P(\theta)\stackrel{\triangle}{=}\sum_{k=0}^{N-1}|\bar{r}(k+\theta)|^2,$$

$$Q_l(\theta)\stackrel{\triangle}{=}\sum_{n=1}^{L-(l+1)}2p(n-1)p(n+l)\sum_{k=0}^{P-1}\bar{r}^*(k+(n-1)P+\theta)\bar{r}(k+(n+l)P+\theta)\ ,$$

$$S_{l,n}(\theta)\stackrel{\triangle}{=}\sum_{h=l-n}^{l-1}p(2l-n-h-1)p(h)\sum_{k=1}^{P-1}\bar{r}(k+hP+\theta)\bar{r}((2l-n-h)P+\theta-k)$$

and

$$T_{l,n}(\theta)\stackrel{\triangle}{=}\sum_{h=l-n}^{l-1}p(2l-n-h-1)p(h)\bar{r}(hP+\theta)\bar{r}((2l-n-h-1)P+\theta)\ .$$

Moreover, γ and ρ are defined in (4.20) and (A.9), respectively, while

$$\kappa_1\stackrel{\triangle}{=}\frac{\rho}{(\sigma_s^2+\sigma_n^2)(c_1\rho+1)(1-\rho)}\ , \tag{5.13}$$

and

$$c_1\stackrel{\triangle}{=}\frac{(L+1)(L+2)}{6}+L-1\ . \tag{5.14}$$

To derive the joint ML frequency offset and symbol timing estimator we initially keep the vector $[\theta,\epsilon]^T$ fixed and let ϕ vary. In these circumstances the LLF (5.12) achieves a maximum for

$$\hat{\phi}_{ML}(\theta,\epsilon)=\frac{1}{2}\arg\left[\sum_{n=1}^{L}\sum_{l=n}^{L}\left(S_{l,n}(\theta)+T_{l,n}(\theta)e^{j\frac{2\pi\epsilon}{L}}\right)e^{-j2\pi\epsilon\left[\frac{(2l-n)}{L}+\frac{2\theta}{N}\right]}\right]\ . \tag{5.15}$$

Then, substituting (5.15) in (5.12) and accounting for the fact that κ_1 is a positive constant, we obtain

$$\begin{aligned}(\hat{\theta}_{ML},\hat{\epsilon}_{ML}) &= \arg\max_{(\tilde{\theta},\tilde{\epsilon})} \Lambda\Big(\tilde{\theta},\tilde{\epsilon},\hat{\phi}_{ML}(\tilde{\theta},\tilde{\epsilon})\Big) \\ &= \arg\max_{(\tilde{\theta},\tilde{\epsilon})} \left\{ -c_1\rho P(\tilde{\theta}) + \sum_{l=0}^{L-2} \Re\left[Q_l(\tilde{\theta})e^{-j\frac{2\pi(l+1)}{L}\tilde{\epsilon}}\right] \right. \\ &\quad \left. + \left| \sum_{n=1}^{L}\sum_{l=n}^{L} \left(S_{l,n}(\tilde{\theta}) + T_{l,n}(\tilde{\theta})e^{j\frac{2\pi\tilde{\epsilon}}{L}}\right) e^{-j\frac{2\pi(2l-n)}{L}\tilde{\epsilon}} \right| \right\}. \end{aligned} \tag{5.16}$$

Unfortunately, the solution of this problem requires a two-dimensional search. To reduce the computational complexity of the joint ML estimator, we consider a simpler synchronization scheme. Specifically, in virtue of results 1 and 2, the magnitude of each term $Q_\iota(\alpha)$, $S_{\iota,\eta}(\alpha)$ and $T_{\iota,\eta}(\alpha)$ in (5.16) can present a peak when α is the actual symbol timing. Thus we consider the decoupled symbol timing metric

$$\hat{\theta} = \arg\max_{\tilde{\theta}} \left\{ -c_1\rho P(\tilde{\theta}) + \sum_{l=0}^{L-2} |Q_l(\tilde{\theta})| + \sum_{n=1}^{L}\sum_{l=n}^{L} \Big(|S_{l,n}(\tilde{\theta})| + |T_{l,n}(\tilde{\theta})|\Big) \right\}. \tag{5.17}$$

This estimator provides high false probability detection when the useful signal is absent, therefore it can be used with difficulty for a burst transmission mode (see [19]). To obtain a timing metric with low false detection probability we propose the NC symbol timing estimator

$$\hat{\theta}_{NC} = \arg\max_{\tilde{\theta}} \left\{ \left[\frac{\sum_{l=0}^{L-2} \Big|Q_l(\tilde{\theta})\Big| + \sum_{n=1}^{L}\sum_{l=n}^{L} \Big(\Big|S_{l,n}(\tilde{\theta})\Big| + \Big|T_{l,n}(\tilde{\theta})\Big|\Big)}{c_1 P(\tilde{\theta})} \right]^2 \right\}. \tag{5.18}$$

Moreover, accounting for (5.15) and (5.16), we propose the NC frequency

offset and carrier phase estimators

$$\hat{\epsilon}_{NC} = \arg\max_{\tilde{\epsilon}} \left\{ \sum_{l=0}^{L-2} \Re\Big[Q_l(\hat{\theta}_{NC}) e^{-j\frac{2\pi(l+1)}{L}\tilde{\epsilon}} \Big] + \left| \sum_{n=1}^{L} \sum_{l=n}^{L} \Big[S_{l,n}(\hat{\theta}_{NC}) + T_{l,n}(\hat{\theta}_{NC}) e^{j\frac{2\pi\tilde{\epsilon}}{L}} \Big] e^{-j\frac{2\pi(2l-n)}{L}\tilde{\epsilon}} \right| \right\} \tag{5.19}$$

and

$$\hat{\phi}_{NC} = \hat{\phi}_{ML}(\hat{\epsilon}_{NC}, \hat{\theta}_{NC}) \, . \tag{5.20}$$

Note that the estimator $\hat{\phi}_{NC}$ in (5.20), accounting for (5.15), provides a closed form estimate for the carrier phase and gives an unambiguous estimate if $\mid \phi \mid \leq \pi/2$. Moreover, since the function to be maximized in the RHS of (5.19) is a periodic function of period L, it follows that the CFO estimator $\hat{\epsilon}_{NC}$ gives ambiguous estimates unless $\mid \epsilon \mid \leq L/2$.

5.2.2 Estimators Based on a Circular Training Symbol

In the case where the training symbol (with L identical parts) is made up by transmitting subcarrier symbols belonging to a circular constellation (that is, $E[(a_q^l)^2] = 0$ for $q = 0$), the relation matrix of the training symbol $\boldsymbol{R_s}$ is identically zero. Therefore, accounting for (5.8)-(5.11), the LLF (5.12) becomes

$$\Lambda_c(\theta, \epsilon) = \kappa_2 \left\{ \Re \left[\sum_{l=0}^{L-2} e^{-j\frac{2\pi(l+1)}{L}\epsilon} Q_l(\theta) \right] - c_2 \rho P(\theta) \right\} \tag{5.21}$$

where $\kappa_2 \stackrel{\triangle}{=} \dfrac{\rho}{(\sigma_s^2 + \sigma_n^2)(c_2\rho + 1)(1-\rho)}$ and $c_2 \stackrel{\triangle}{=} L - 1$. Exploiting the approach followed before, accounting for (5.21) and for the fact that κ_2 is a positive constant, we obtain the symbol timing and CFO estimators

$$\hat{\theta}_{GSC} = \arg\max_{\tilde{\theta}} \left\{ \left(\sum_{l=0}^{L-2} \frac{\Big| Q_l(\tilde{\theta}) \Big|}{c_2 P(\tilde{\theta})} \right)^2 \right\} \tag{5.22}$$

and

$$\hat{\epsilon}_{GSC} = \arg\max_{\tilde{\epsilon}} \left\{ \sum_{l=0}^{L-2} \Re \left[Q_l(\hat{\theta}_{GSC}) e^{-j\frac{2\pi(l+1)}{L}\tilde{\epsilon}} \right] \right\} , \tag{5.23}$$

that give ambiguous estimates unless $\mid \epsilon \mid \leq L/2$ and $0 \leq \theta \leq N$. It is of interest to observe that in the case of a training symbol with two identical halves and without a sign inversion estimators (5.22) and (5.23) take a form similar to the symbol timing and CFO estimators proposed by Schmidl and Cox in [17]. Therefore, since estimators (5.22) and (5.23) can be considered a generalization of those obtained in [17] to the case where the training symbol has more than two identical parts, they are referred to as generalized Schmidl and Cox (GSC) estimators.
The symbol timing statistic (5.22) in the case where $L = 4$ and the training symbol pattern $\boldsymbol{p} = [1, 1, -1, 1]^T$ is exploited, reduces to the coarse estimator proposed in [18] by Shi and Serpedin that will be referred to as SS estimator. Moreover, to limit the computational cost, the following simplified coarse CFO estimator has been proposed in [18] in place of (5.23)

$$\hat{\epsilon}_{SS} = \frac{L}{2\pi} \arg[Q_0(\hat{\theta}_{SS})] \, . \tag{5.24}$$

By minimizing the squared average distance between L succeeding parts of the received training symbol, Minn, Bhargava and Letaief proposed in [19] the coarse symbol timing metric

$$\hat{\theta}_{MBL} = \arg \max_{\tilde{\theta}} \left\{ \left(\frac{L|Q_0(\tilde{\theta})|}{c_2 P(\tilde{\theta})} \right)^2 \right\} \, . \tag{5.25}$$

In the case where $L = 2$ the MBL timing estimator (5.25) and the GSC estimator (5.22) are coincident. Nevertheless, when the number of repeated parts increases, the simpler expression (5.25) does not account for the correlation between not adjacent parts of the training symbol. Thus, in this case a performance loss with respect to the GSC estimator (5.22) could occur. Moreover, the coarse frequency-offset estimator proposed in [19] is a slight modification of the CFO estimator proposed in [45].

5.3 Practical Estimator

The frequency offset estimators (5.19) and (5.23) require a maximization procedure with respect to the continuous parameter $\tilde{\epsilon}$. They can be obtained, as

pointed out in [46], exploiting a two step procedure. In the first step is performed a coarse search followed, in the second step, by a fine search. Specifically, in this paper the dichotomous fine search, described in detail in [47], is considered. However, this is a time-consuming procedure.
To overcome this problem, in this section we propose a lower complexity synchronization algorithm viable for practical implementation. Specifically, we propose a best linear unbiased (BLU) estimator that provides a closed form expression for the frequency shift estimate. Let us consider the terms

$$R(m) = \frac{1}{N-mP} \sum_{k=0}^{N-mP-1} \bar{r}(k+\theta)^* \bar{r}(k+mP+\theta)\, b_{k,k+mP} \tag{5.26}$$

and

$$\begin{aligned} C(m) \quad =& \frac{1}{N-mP} \sum_{k=1}^{N-mP-1} [\bar{r}(k+mP+\theta)\bar{r}(N-k+\theta) b_{N-k,k+mP} \\ & + \bar{r}(mP+\theta)\bar{r}(\theta) b_{0,mP}], \end{aligned} \tag{5.27}$$

with $0 \leq m \leq L-1$ and

$$b_{m,l} \stackrel{\triangle}{=} p\left(\left\lfloor \frac{m}{P} \right\rfloor\right) p\left(\left\lfloor \frac{l}{P} \right\rfloor\right) , \tag{5.28}$$

where $p(l)$ is the l-th entry of the vector $\boldsymbol{p}$ denoting the training symbol pattern except for the CP (see Section § 5.1).
We observe preliminarily that, in virtue of the repetitive structure of the training symbol and since it is obtained by transmitting on the different subcarriers data symbols belonging to a real constellation, it results that

$$s(0) = s(0)^* , \tag{5.29}$$

$$p\left(\left\lfloor \frac{k}{P} \right\rfloor\right) s(k) = p\left(\left\lfloor \frac{k+mP}{P} \right\rfloor\right) s(k+mP) , \tag{5.30}$$

$\forall k, k+mP \in \tau_2 \cup \{0\}$,

$$p\left(\left\lfloor \frac{N-k}{P} \right\rfloor\right) s(N-k) = p\left(\left\lfloor \frac{k+mP}{P} \right\rfloor\right) s(k+mP)^* . \tag{5.31}$$

$\forall k, k+mP \in \tau_2$,

Thus, by substituting the received signal (see (4.4)) in (5.26) and (5.27), accounting for (5.29)-(5.31) and neglecting noise×noise terms, we have

$$R(m)= \quad \sigma_s^2 e^{j\frac{2\pi m\epsilon}{L}}$$

$$\times\left[1+\frac{1}{\sigma_s^2(N-mP)}\sum_{k=0}^{N-mP-1}\left[s(k)^* w(k+mP+\theta)+w(k+\theta)^* s(k+mP)\right] b_{k,k+mP}\right] \tag{5.32}$$

and

$$C(m)= \quad \sigma_s^2 e^{j\left[\frac{2\pi\epsilon(mP+N+2\theta)}{N}+2\phi\right]}$$

$$\times\left[1+\frac{2}{\sigma_s^2(N-mP)}\sum_{k=0}^{N-mP-1} s(k)^* w(k+mP+\theta) b_{k,k+mP}\right], \tag{5.33}$$

where $w(k) \triangleq n(k)e^{-j\left[\frac{2\pi\epsilon k}{N}+\phi\right]}$.
Let us now consider the vector $\boldsymbol{y} \in \mathbb{R}^{(L-1)\times 1}$ whose elements are defined as

$$y(m) \triangleq \arg\left[R(m)R(m-1)^* + C(m)C(m-1)^*\right], \qquad m \in [1,...,L-1]. \tag{5.34}$$

At high SNR values and for $|\epsilon| \leq L/2$, $y(m)$ can be approximated by a linear expression in the unknown parameter ϵ

$$y(m) \simeq \frac{2\pi\epsilon}{L} + \frac{\Im[\eta(m)+\eta(m-1)^*]}{2\sigma_s^2}, \tag{5.35}$$

with

$$\eta(m) \triangleq \frac{1}{N-mP}\sum_{k=0}^{N-mP-1}\left[s(k+mP)w(k+\theta)^* + 3s(k)^* w(k+mP+\theta)\right] b_{k,k+mP}. \tag{5.36}$$

Thus, the estimation problem can be reduced to a linear model and by exploiting the Gauss-Markov theorem we can consider (see [38]) the BLU CFO estimator

$$\hat{\epsilon} = \frac{L}{2\pi}\left[\frac{\boldsymbol{y}^T \boldsymbol{C}_y^{-1}\mathbf{1}}{\mathbf{1}^T \boldsymbol{C}_y^{-1}\mathbf{1}}\right] \tag{5.37}$$

where the (m,l)-th entry of the covariance matrix $\boldsymbol{C}_y \in \mathbb{R}^{L-1\times L-1}$ is given by

$$[\mathbf{C}_y](m,l) \quad \stackrel{\triangle}{=} E[y(m)y(l)^*] = \frac{1}{4P\,SNR(L-(l-1))} \times \left[\frac{5\delta[m-l]}{(L-l)} + \frac{3L\,\mathrm{u}(L-m-l)}{(L-l)(L-m)(L-(m-1))} - \frac{3\delta[m+l-L-1]}{(L-(m-1))}\right]. \tag{5.38}$$

Note that this approach generalizes that proposed by Mengali and Morelli in [45] to the case where the training symbol with L identical parts is obtained by transmitting, on the different subcarriers, data symbols belonging to a noncircular constellation. Specifically, in this case, in addition to the correlation term (5.26) considered in [45], the term (5.27) is exploited. It is worth pointing out that, accounting for (5.37) and (5.38), the NC-BLU estimator does not require the knowledge of the SNR value and of the channel. Moreover, the acquisition range of the proposed NC-BLU frequency offset estimator is coincident with that of estimators in (5.19) and (5.23).

5.4 Data-Aided Estimators in Multipath Channel

Since the statistic $\hat{\theta}_{NC}$ in (5.18) is derived for ISI-free channels, in presence of dispersive channels it could not provide satisfactory performance. Thus, in this case, it is necessary to refine the symbol timing estimate. Specifically, by exploiting the periodic structure of the training symbol, basically the same analysis considered for blind symbol timing estimator in the section § 4.4 can be applied.

Let us consider the received signal model in multipath channel (4.48). Let us observe that for $N \gg N_m$, following the lines of appendix B, we can easily

demonstrate tha following approximation

$$\frac{\sum_{l=0}^{L-2}|Q_l(\theta+\beta)|+\sum_{n=1}^{L}\sum_{l=n}^{L}(|S_{l,n}(\theta+\beta)|+|T_{l,n}(\theta+\beta)|)}{c_1P(\theta+\beta)}$$

$$\simeq\begin{cases}\dfrac{\sigma_s^2\,|(h\otimes h)(2\beta)\,|}{\sigma_s^2\sum_{l=0}^{N_m}|\,h(l)\,|^2+\sigma_n^2}, & \beta\in\{0,\ldots,N_m\}\\ \\ 0, & \text{otherwise}\,.\end{cases}$$

Therefore, as in the case of blind symbol timing estimators, because of the channel dispersion, the statistic $\hat{\theta}_{NC}$ in (5.18) provides a coarse estimate of the arrival time of the first multipath component that, with high probability, differs from its actual value θ by a quantity $\beta\in\{0,\ldots,N_m\}$. Thus, by following the lines of subsection 4.4, a refined estimate $\hat{\theta}_{NCR}$ of the symbol timing is given by

$$\hat{\theta}_{NCR}=\hat{\theta}_{NC}-\left\lceil\frac{1}{2}\,(\hat{u}-1)\right\rceil\,. \tag{5.39}$$

The estimate $\hat{u}$ can be obtained considering the estimator (4.52) and in this case the function $\chi(u,\theta+\beta)$ is defined as

$$\begin{aligned}\chi(u,\theta+\lambda)\;&\stackrel{\triangle}{=}\frac{1}{N-1}\sum_{n=1}^{L}\sum_{l=n}^{L}\sum_{h=l-n}^{l-1}[|\,B_{l,n,h}(u,\theta+\lambda)\,|\\ &\quad+|\,\bar{r}(\beta+hP)\bar{r}((2l-n-h-1)P+\beta-u)\,|]\end{aligned} \tag{5.40}$$

where

$$B_{l,n,h}(u,\alpha)\stackrel{\triangle}{=}\sum_{k=1}^{P-1}\bar{r}(k+\alpha+hP)\bar{r}((2l-n-h)P+\alpha-k-u).$$

Once the fine symbol timing estimate has been evaluated, the frequency offset estimate can be obtained by (5.19) (referred as NCR estimator) or by the

reduced-complexity expression (5.37) (referred to in the following as NCR-BLU estimator). Note that, unlike the refined symbol timing estimator reported in [19] and referred to in the following as fine-MBL, the proposed algorithm requires neither a channel-dependent timing preadvancement nor a SNR-dependent threshold.

Chapter 6

Numerical Results

In this chapter we the performance of derived blind and data-aided estimators is assessed via computer simulations and compared with that of some estimators previously proposed in literature in presence of AWGN and multipath channel.

6.1 Performance of Blind Estimators

In this section the performance of the proposed blind estimators is assessed via computer simulations and compared with that of MLC estimators, derived in [9], and that of modified MLC (MMLC) estimators, proposed in [5], exploiting only ISI-free samples of the CP to counteract the degrading effects of dispersive channels. In the simulations the values of the arrival time, the normalized CFO and the carrier phase have been fixed at $\theta = 10$, $\epsilon = 1/8$ and $\phi = \frac{\pi}{8}$, respectively. Moreover, 10^5 trials were used to obtain the performance plot.

Note that the MCL0 symbol timing estimator has been derived under the assumption $L_c = 0$. However, since in the following experiments L_c is different from zero, the known bias equal to the CP length L_c is subtracted from the estimates provided by the MCL0 symbol timing estimator. Moreover, to obtain unbiased estimates the CFO estimator (4.38) is multiplied by N/M (see also [44]).

6.1.1 AWGN Channel

In this first set of simulations we have tested the performance of the proposed algorithms as a function of SNR in AWGN channel and for an OFDM system with N=512 DBPSK subcarriers.

The performance of the considered symbol timing estimators is shown in Fig. 6.1 where it is reported the probability $P(\theta) \stackrel{\triangle}{=} P(\{\hat{\theta}<\theta-L_c\} \bigcup \{\hat{\theta}>\theta\})$, that is the probability that an incorrect symbol timing causes ISI and ICI (see Section § **??**). In the figure three different contexts are considered: an observation window of length $W = 2M + N/2$ and a CP length fixed at $L_c = 4$ (dashed lines) and $L_c = 12$ (solid lines) and, moreover, an observation window of length $W = 4M + N/2$ and a CP length fixed at $L_c = 12$ (dotted lines). Note that the markers for NC and MCL0 estimators appear only for $SNR < 0$ dB, since for higher values of SNR both the NC and MCL0 estimates were coincident with the actual value of the symbol timing in all the 10^5 performed experiments. The results show that NC and MCL0 estimators, whose performance is practically unaffected by the value of the CP length, greatly outperform the MLC estimator on the whole range of SNR values.

Fig. 6.2 shows the mean squared error (MSE) of the considered CFO estimators as a function of SNR and for different values of the CP length. In the figure are also reported as benchmark the CRB_{ϵ}^{NC} and the CRB_{ϵ}^{C} derived in Section 4.3 for the case of $L_c = 12$. Note that, although the CRBs have been derived under the assumption of known symbol timing, the performance of the CFO estimators has been obtained without the knowledge of this parameter, that is, in each run the CFO estimate has been obtained by exploiting the corresponding timing estimate. However, it should be emphasized that, as previously stated, NC and MCL0 symbol timing estimates were coincident with the actual value of the symbol timing in all the performed runs for $SNR \geq 0$ dB. The results show that the greater accuracy of the proposed symbol timing estimators has beneficial effects also on the performance of the CFO estimators. In particular, the performance improvement of NC and MCL0 estimators, with respect to the MLC estimator, increases as the CP length decreases. Moreover, the performance of NC and MLC estimators results to be very close to the corresponding CRBs.

By augmenting the observation interval, the considered CFO estimators

provide more accurate estimates and, besides, as shown in Fig. 6.3, the performance gap between the proposed CFO estimators and the MLC estimator increases. Moreover, by a comparison with Fig. 6.2 it follows that the MLC CFO estimator achieves the CRB_{ϵ}^{C} for lower SNR values as the sample size increases. This is in agreement with the fact that the CRB_{ϵ}^{C} has been derived under the assumption of known symbol timing while the performance of the MLC CFO estimator depends on the accuracy of the symbol timing estimate that improves as the sample size increases.

6.1.2 Multipath Channel

The performance of the considered estimators has also been assessed in multipath channel for an OFDM system with $N{=}1024$ DBPSK subcarriers. In each experiment the multipath channel has been modeled to consist of $N_m{+}1{=}11$ independent Rayleigh-fading taps with an exponentially decaying power delay profile. Specifically, $E[|h(l)|^2]{=}Ce^{-\frac{l}{4}}$, $l \in \{0,\ldots,N_m\}$, where C is a constant such that $\sum_{l=0}^{N_m} E[|h(l)|^2] = 1$. Moreover, the channel is fixed in the observation window but independent from one run to another.

Figures 6.4 and 6.5 show the MSE and the probability $P(\theta) \stackrel{\triangle}{=} P(\{\hat{\theta}{<}\theta{-}L_c{+}N_m\}\bigcup\{\hat{\theta}{>}\theta\})$ of NCR, MCL0R, MLC and MMLC symbol timing estimators (defined in (4.53), (4.55), (4.27) and in [5], respectively) for an observation window of length $W{=}2M{+}N/2$ and different CP values. The results show that the proposed NCR estimator and the more practical MCL0R synchronization scheme exhibit nearly the same performance and significantly outperform the MLC algorithm proposed in [9] and its modified version for dispersive channel (MMLC algorithm). In particular, as the number $L_c{-}N_m$ of ISI-free samples decreases, the performance gain of the proposed estimators with respect to the MMLC algorithm increases. Note that the MLC statistic is strongly biased for all examined situations. Moreover, it is worthwhile to emphasize that, unlike the proposed NCR and MCL0R algorithms, the MMLC estimator requires the knowledge of the maximum delay spread N_m.

The results reported in Fig.6.6 show that the feasible-computational MCL0 CFO estimator provides the most accurate estimates. Moreover, as one would expect, only the MMLC algorithm does not present a floor since it exploits

ISI-free samples. However, the figure shows that the MMLC algorithm assures a relevant performance, as the number of ISI-free samples decreases, for higher and higher values of SNR. Moreover, as already underlined, the MMLC algorithm requires the knowledge of the maximum delay spread N_m.

Finally, Fig. 6.7 illustrates the symbol-error rate (SER) performance of NCR, MCL0R, MLC and MMLC algorithms as a function of SNR. The results show that the SER achieved by using NCR and MCL0R estimators is coincident with that obtained in the case of perfect synchronization, while the MMLC estimator assures relevant performance only for $L_c = 16$ and high SNR values. Moreover, the MLC estimator provides a contained performance loss with respect to the case of perfect synchronization only for $L_c = 16$.

6.2 Performance of Data-Aided Estimators

In this section the performance of the proposed estimators based on a training symbol is assessed via computer simulations and compared with that of SS and MBL algorithms derived in [18] and [19], respectively. In all the simulations we consider an OFDM system with N=1024 subcarriers and a prefix length fixed at $L_c = 16$. The actual values of the arrival time, the normalized frequency offset and the carrier phase have been fixed at $\theta = 10$, $\epsilon = 1/8$ and $\phi = \frac{\pi}{8}$, respectively. Moreover, the training symbol used for NC estimators is obtained by transmitting, on the different subcarriers, a maximum length sequence (MLS) of DBPSK data symbols, whereas, for the other schemes, a MLS of DQPSK symbols is exploited. Furthermore, to verify the incidence of the training symbol pattern on the performance we have considered two different cases:

(a) training symbol pattern $\boldsymbol{p} = [1, 1, 1, 1]^T$ (solid lines);

(b) training symbol pattern $\boldsymbol{p} = [1, 1, -1, 1]^T$ (dashed lines).

6.2.1 Timing Metric

Figures 6.8-6.9 show the behavior in a single run of NC, GSC[1] and MBL timing metrics for a noiseless and distortionless transmission of the training

[1]Note that, as previously stated, for the considered number of repeated parts ($L = 4$), the GSC timing metric reduces to the SS timing metric when the training symbol pattern $\boldsymbol{p} =$

symbol. Specifically, in Fig. 6.8 the employed training symbol is made up of four identical parts and with the pattern (a). In this case the NC timing metric presents the sharpest peak at the actual timing $\theta = 0$, whereas MBL and GSC metrics present a large plateau. As showed in the plot, the NC metric exhibits relative maxima, located in $\pm lN/2L$ with $l \in \{1, ..., L\}$. However, these peaks do not interfere with the exact correlation peak provided that the length P of each identical training sequence block is sufficiently large. In Fig. 6.9 the timing metrics corresponding to the training symbol pattern (b) have been considered. The results show that the sign inversion in the transmitted training symbol pattern reduces the undesirable peaks in the NC timing metric and eliminates the plateau effect for GSC and MBL symbol timing metrics. Nevertheless, as we will see, the use of a training sequence made up of identical parts with different signs can introduce in a dispersive channel some performance degradation in the frequency offset estimation.

6.2.2 AWGN Channel

In this first set of simulations we have tested the performance of the proposed algorithms in an AWGN channel. In particular, Fig. 6.10 illustrates the performance of NC, MBL and GSC symbol timing estimators as a function of SNR evaluated in terms of the probability $P(\theta)$ that an incorrect timing causes ISI and ICI. The number of runs for each SNR value is equal to 10^4. The results presented in Fig. 6.10 show that, for both patterns, the NC symbol timing estimator greatly outperforms GSC and MBL estimators. Besides, in the case (a) the plot reveals a degradation in the performance for both MBL and GSC estimators due to the plateau in the metric (see Fig.6.8).
The previous conclusions are further supported by results reported in Fig. 6.11, where the MSE versus SNR for symbol timing estimates is depicted. In particular, in the cases (a) and (b) no errors were observed for the NC estimator in the performed runs for $SNR \geq -5$, while, in the case (a) MBL and GSC estimators present performance floor. In AWGN channel the considered CFO estimators do not reveal significant performance sensitivity to the training sequence pattern. Therefore, for the sake of brevity, we present only the results in the case (a). In particular, in Fig. 6.12 we compare the performance of

$[1, 1, -1, 1]^T$ is considered.

NC, GSC and NC-BLU CFO estimators proposed in (5.19), (5.23) and (5.37), respectively, with that of SS and MBL CFO estimators. Moreover, MSE for the proposed NC-BLU estimator under perfect timing synchronization is also included as reference. The results show that NC and GSC CFO estimators present, for low SNR values, a performance gain with respect to MBL and SS estimators, while NC-BLU CFO estimator assures the best performance at moderate and high SNR values. Note that this performance is very close to that obtained with perfect symbol timing estimation.

6.2.3 Multipath Channel

The performance of the proposed data-aided estimators has also been assessed in a multipath channel. In each experiment the multipath channel has been modeled to consist of $N_m + 1 = 13$ independent Rayleigh-fading taps with an exponentially decaying power delay profile with root mean-squared width corresponding to two samples. The channel is fixed during the transmission of one OFDM symbol but independent from one run to another. The values of the remaining parameters are those used for AWGN channel.
Figures 6.13 and 6.14 show the probability $P(\theta)$ and the MSE, respectively, of NCR, NC, GSC and fine-MBL symbol timing estimators in the cases (a) and (b). We can note that for both patterns the NCR estimator clearly outperforms NC, GSC and fine-MBL estimators. Moreover, GSC and fine-MBL estimators exhibit satisfactory performance only in the case (b).
Figures 6.15 and 6.16 present the MSE of NC, NCR, NCR-BLU, SS, GSC and MBL[2] CFO estimators as a function of SNR. Specifically, Fig. 6.15 illustrates the performance in the case (b). As we can see, the presence of a sign inversion in the training symbol pattern leads to a performance floor in a dispersive channel. Thus, it is necessary fine frequency estimation to counteract this degradation (see [19]). However, except for NC and MBL estimators, no floor effect is observed in Fig. 6.16 in the case of a training pattern without sign inversion. In particular, the NCR-BLU estimator presents the best performance for moderate and high SNR values, while the more complex NCR CFO

[2]To compare coarse CFO estimators the simulated MBL algorithm is that considered in [19] without a subsequent fine frequency estimation. Specifically, this algorithm is a modified version of that proposed in [45].

estimator assures a good estimation accuracy for low SNR values.

Finally, Figures 6.17 and 6.18 illustrate the SER performance versus SNR of the considered OFDM system when the investigated estimators are exploited and the two training symbol patterns are adopted. As shown in the plots, for both cases the proposed NCR and the more feasible NCR-BLU synchronization schemes provide a SER very close to that of the perfectly synchronization system.

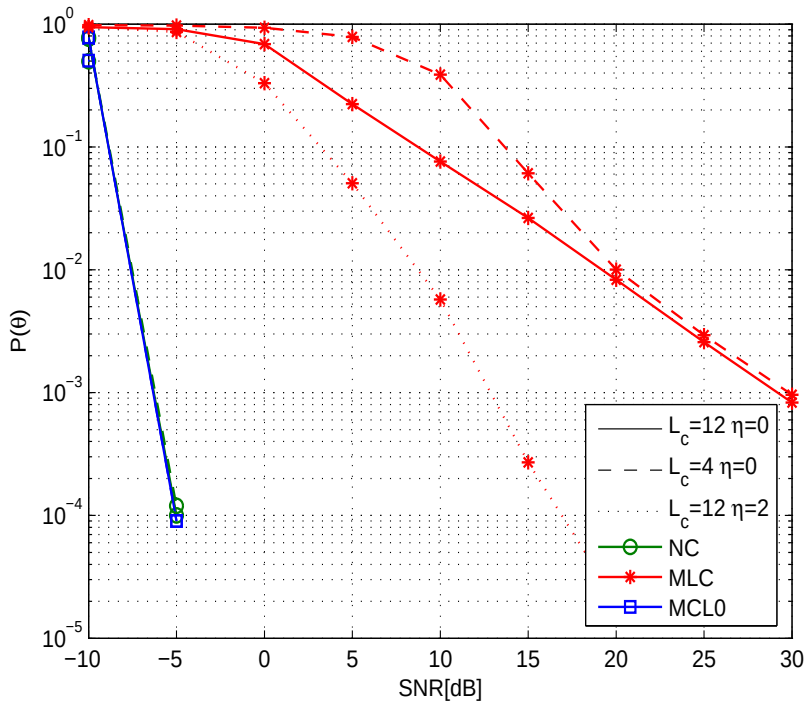

Figure 6.1: Performance of NC, MCL0 and MLC symbol timing estimators in AWGN channel for an observation window length $W = 2M + N/2$ and a CP length fixed at $L_c = 12$ (solid lines) and $L_c = 4$ (dashed lines). Dotted lines refer to an observation window of length $W = 4M + N/2$ and a CP length fixed at $L_c = 12$.

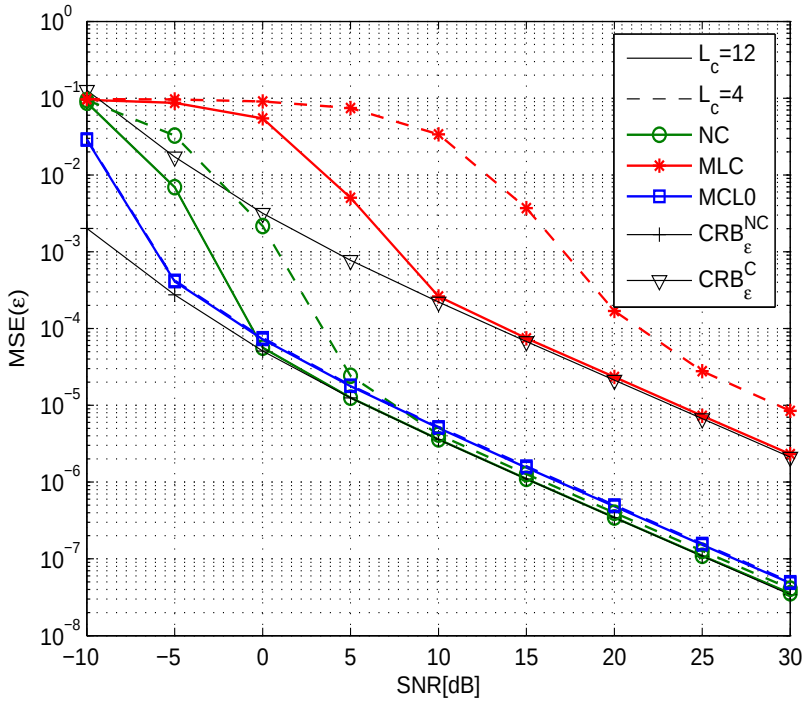

Figure 6.2: MSE of NC, MCL0 and MLC CFO estimators in AWGN channel for an observation window of length $W = 2M + N/2$ and for a CP length fixed at $L_c = 12$ (solid lines) and $L_c = 4$ (dashed lines).

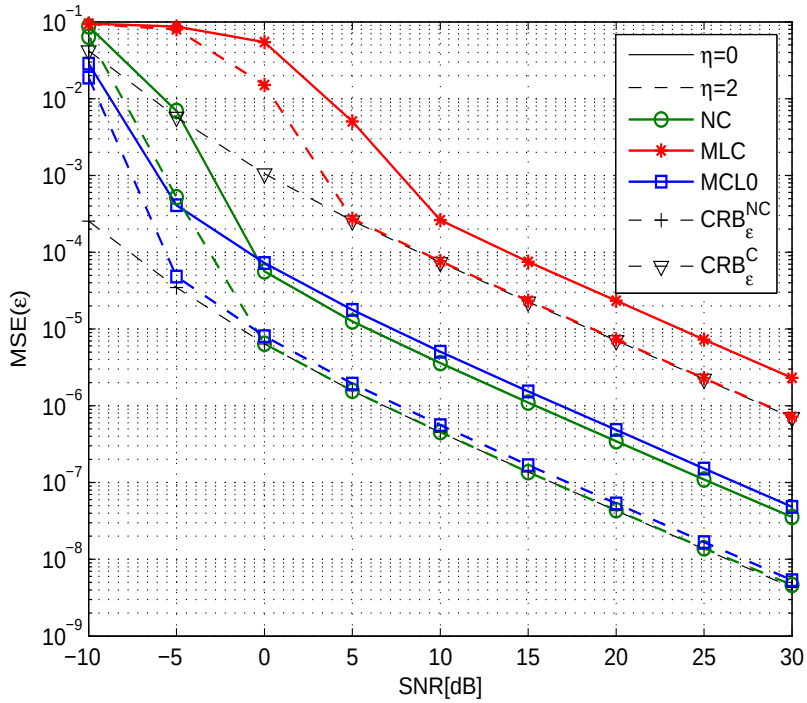

Figure 6.3: MSE of NC, MCL0 and MLC CFO estimators in AWGN channel for a CP length fixed at $L_c = 12$ and for an observation window of length $W = 2M + N/2$ (solid lines) and $W = 4M + N/2$ (dashed lines).

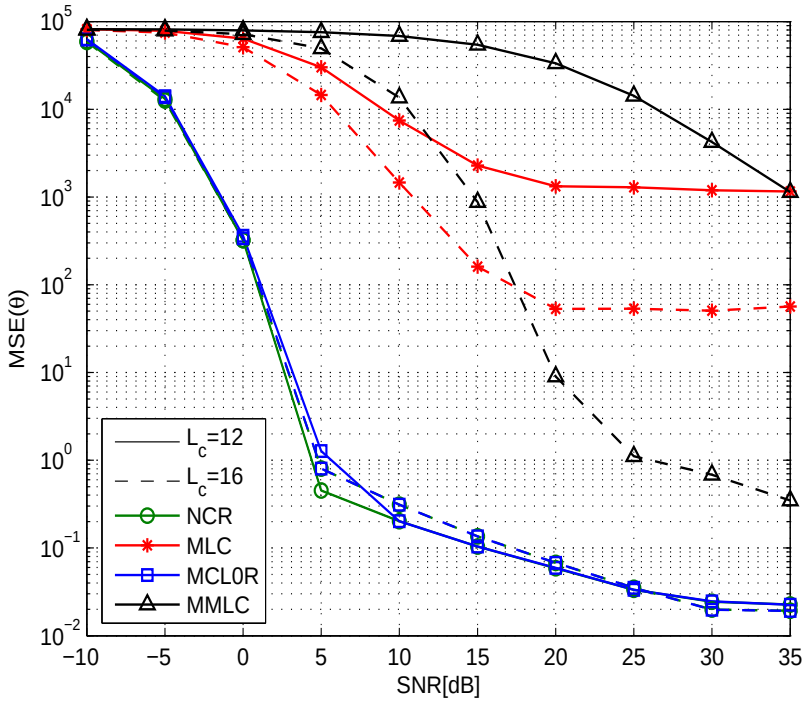

Figure 6.4: MSE of NCR, MCL0R, MLC and MMLC symbol timing estimators in multipath channel for an observation window of length $W = 2M + N/2$ and a CP fixed at $L_c = 12$ (solid lines) and $L_c = 16$ (dashed lines).

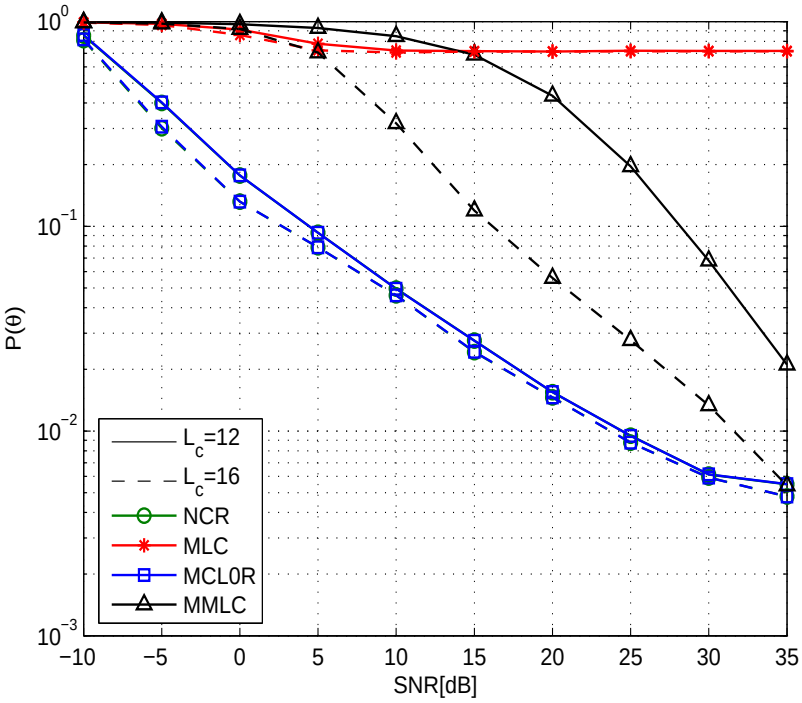

Figure 6.5: Performance of NCR, MCL0R, MLC and MMLC symbol timing estimators in multipath channel for an observation window of length $W = 2M + N/2$ and a CP fixed at $L_c = 12$ (solid lines) and $L_c = 16$ (dashed lines).

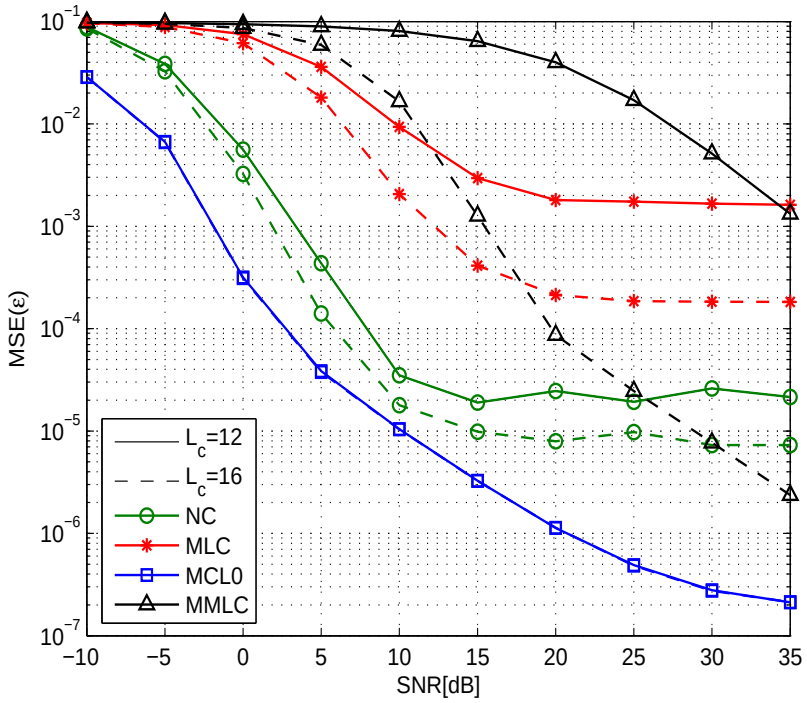

Figure 6.6: Performance of NC, MCL0, MLC and MMLC CFO estimators in multipath channel for an observation window of length $W = 2M + N/2$ and a CP fixed at $L_c = 12$ (solid lines) and $L_c = 16$ (dashed lines).

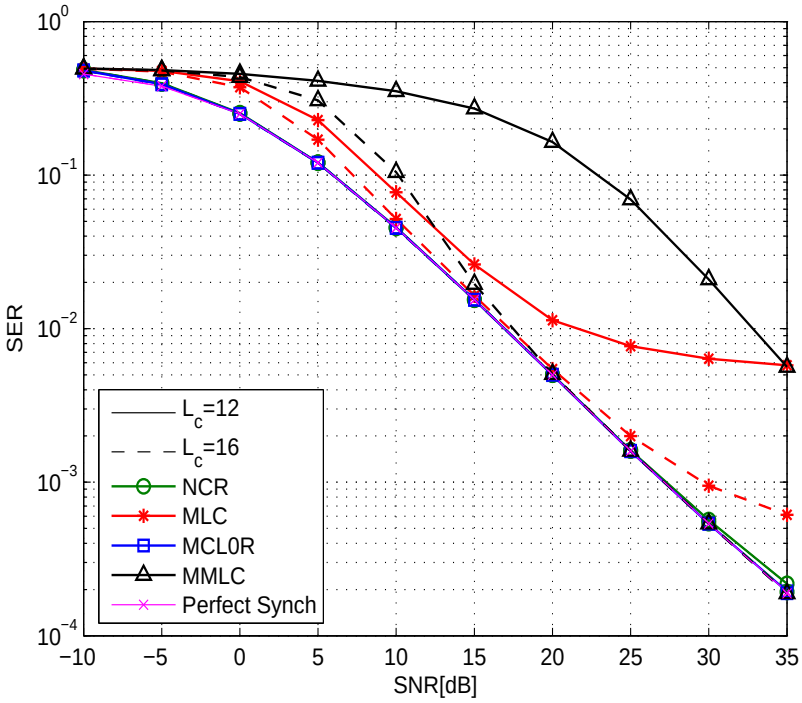

Figure 6.7: SER performance versus SNR of NCR, MCL0R, MLC and MMLC algorithms in multipath channel for an observation window of length $W = 2M + N/2$ and a CP fixed at $L_c = 12$ (solid lines) and $L_c = 16$ (dashed lines).

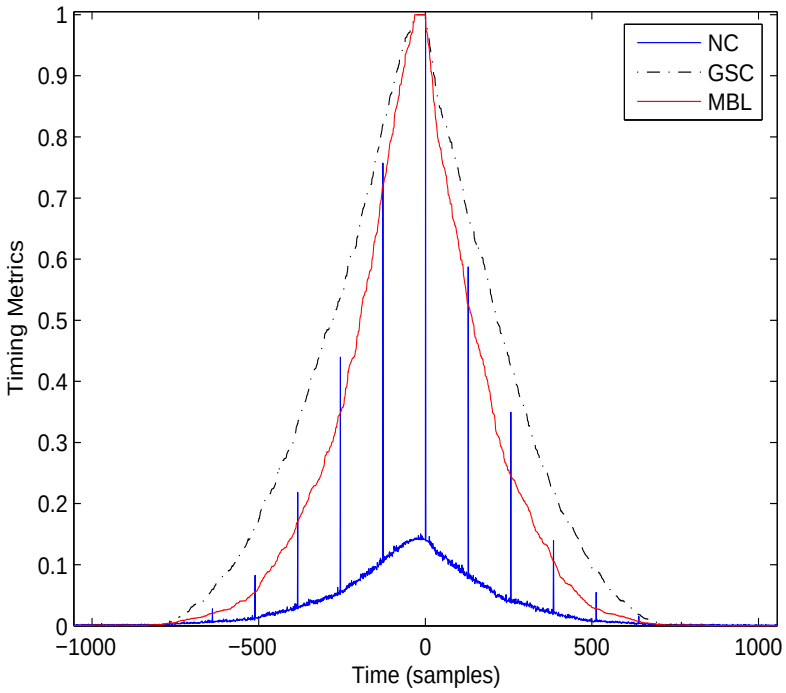

Figure 6.8: Behavior, in a single run, of symbol timing metrics as a function of time [samples] for an OFDM system with $N = 1024$ subcarriers, a CP length $L_c = 16$ and for the training symbol pattern $\boldsymbol{p} = [1, 1, 1, 1]^T$.

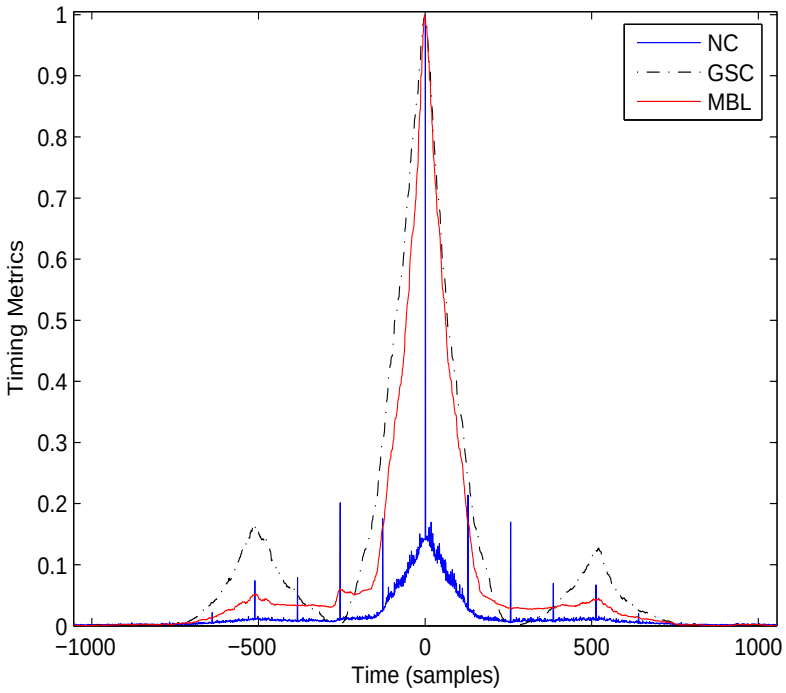

Figure 6.9: Behavior, in a single run, of symbol timing metrics as a function of time [samples] for an OFDM system with $N = 1024$ subcarriers, a CP length $L_c = 16$ and for the training symbol pattern $\boldsymbol{p} = [1, 1, -1, 1]^T$.

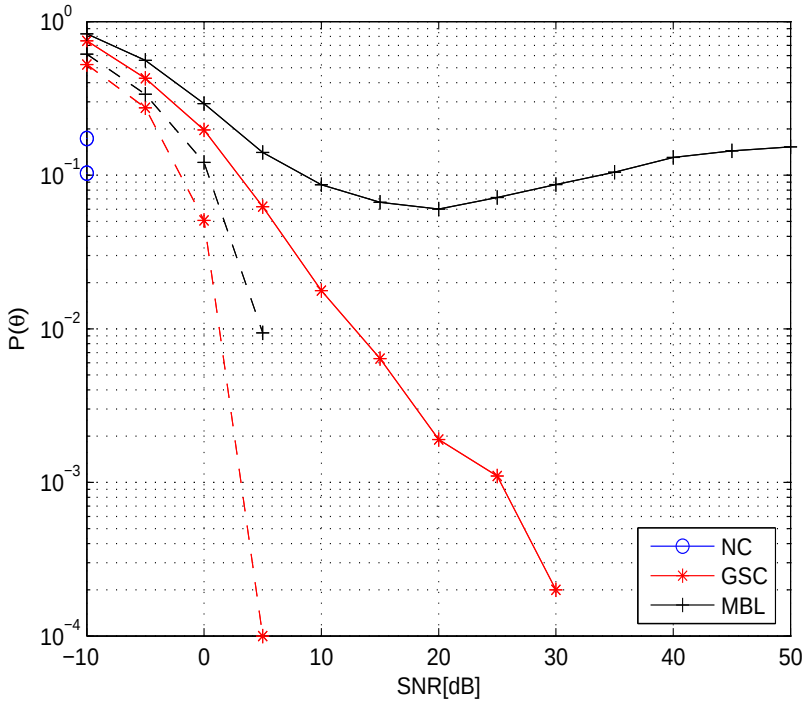

Figure 6.10: Performance of symbol timing estimators as a function of SNR in an AWGN channel ($N = 1024$, $L_c = 16$) for the training symbol patterns $\boldsymbol{p} = [1, 1, -1, 1]^T$ (dashed lines) and $\boldsymbol{p} = [1, 1, 1, 1]^T$ (solid lines).

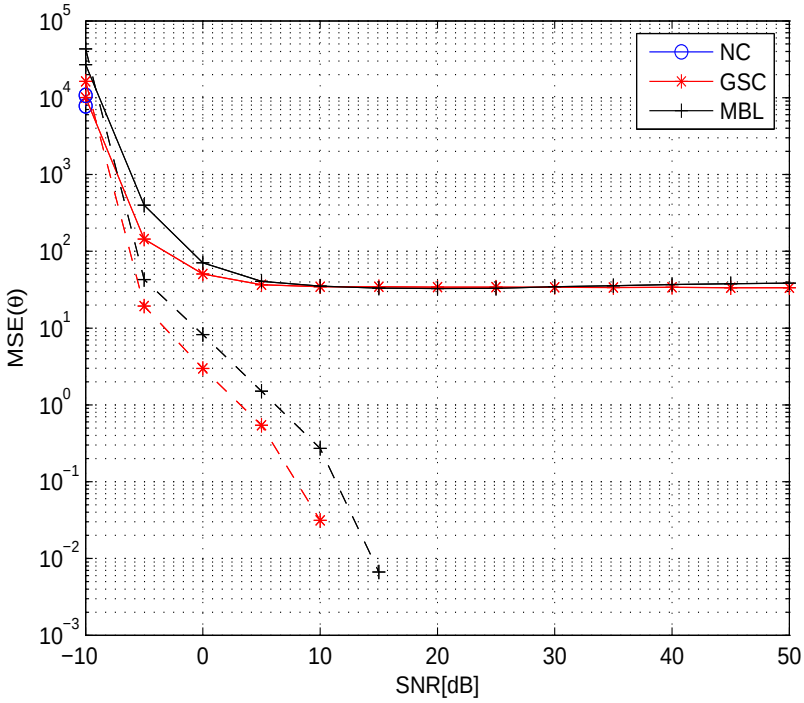

Figure 6.11: MSE of symbol timing estimators as a function of SNR in an AWGN channel ($N = 1024$, $L_c = 16$) for a training symbol pattern $[+ + -+]$ (dashed lines) and for a training sequence without sign inversion (solid lines).

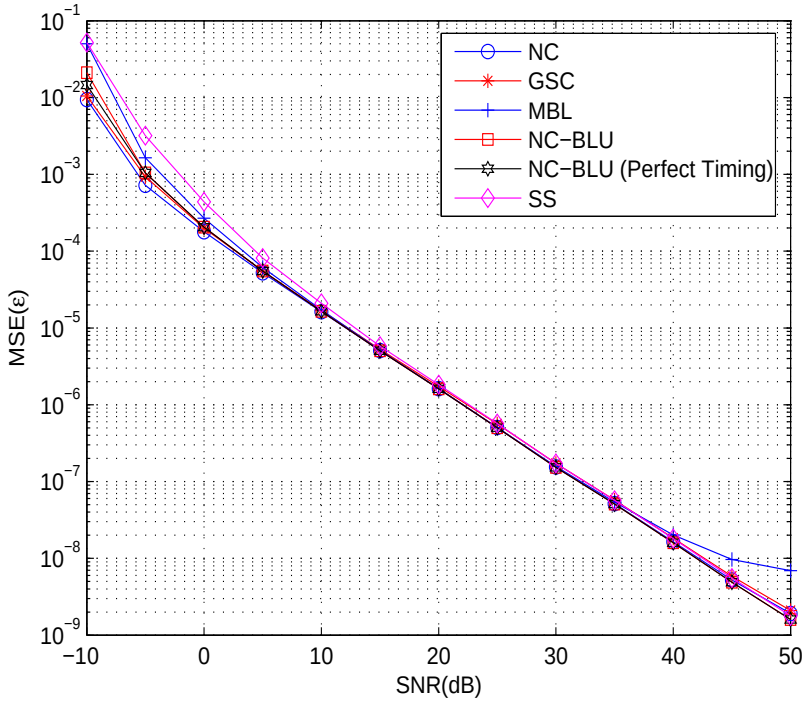

Figure 6.12: MSE of CFO estimators as a function of SNR in an AWGN channel ($N = 1024$, $L_c = 16$) for a training symbol pattern without sign inversion.

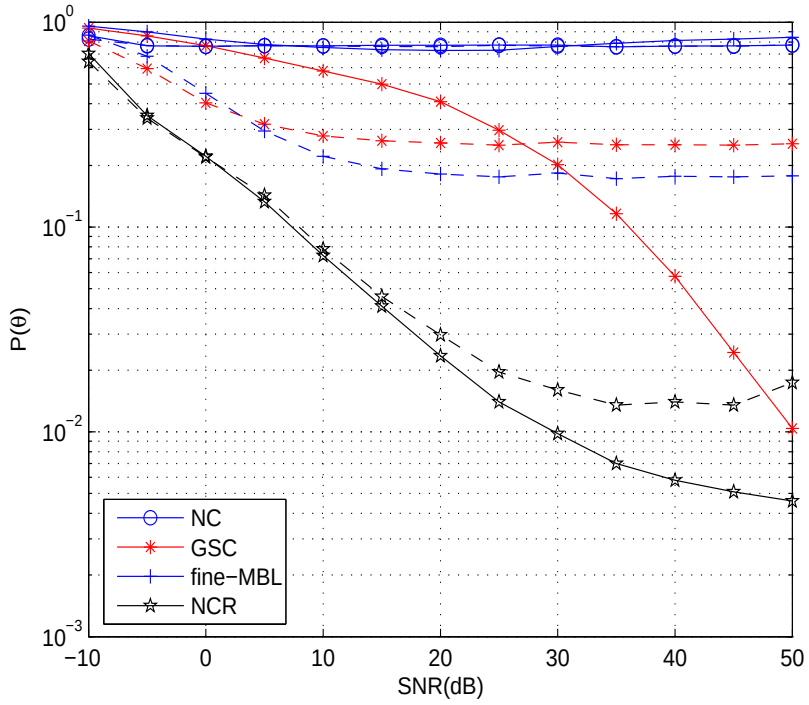

Figure 6.13: Performance of symbol timing estimators as a function of SNR in a multipath channel ($N = 1024$, $L_c = 16$, $N_m = 13$) for the training symbol patterns $\boldsymbol{p} = [1, 1, -1, 1]^T$ (dashed lines) and $\boldsymbol{p} = [1, 1, 1, 1]^T$ (solid lines).

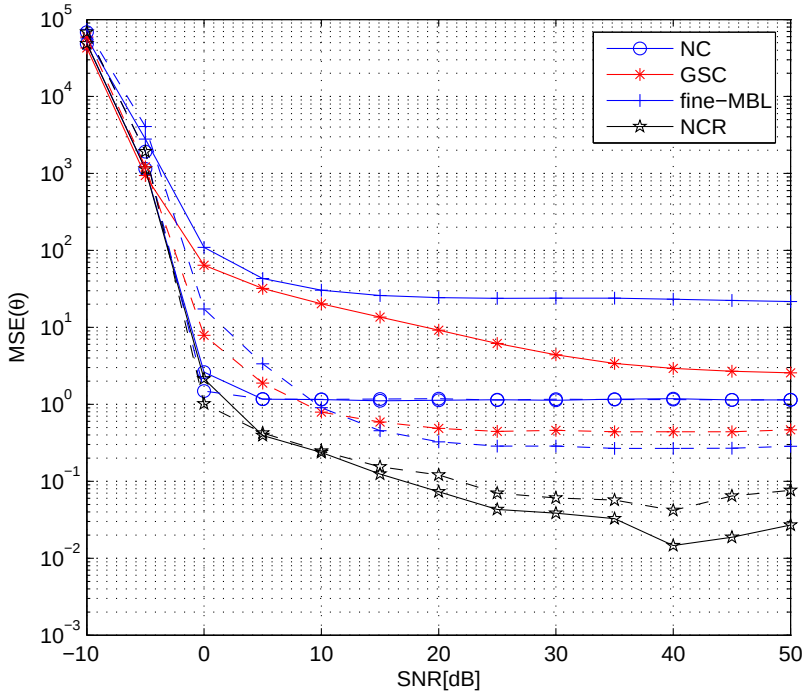

Figure 6.14: MSE of symbol timing estimators as a function of SNR in a multipath channel ($N = 1024$, $L_c = 16$, $N_m = 13$) for the training symbol patterns $\boldsymbol{p} = [1, 1, -1, 1]^T$ (dashed lines) and $\boldsymbol{p} = [1, 1, 1, 1]^T$ (solid lines).

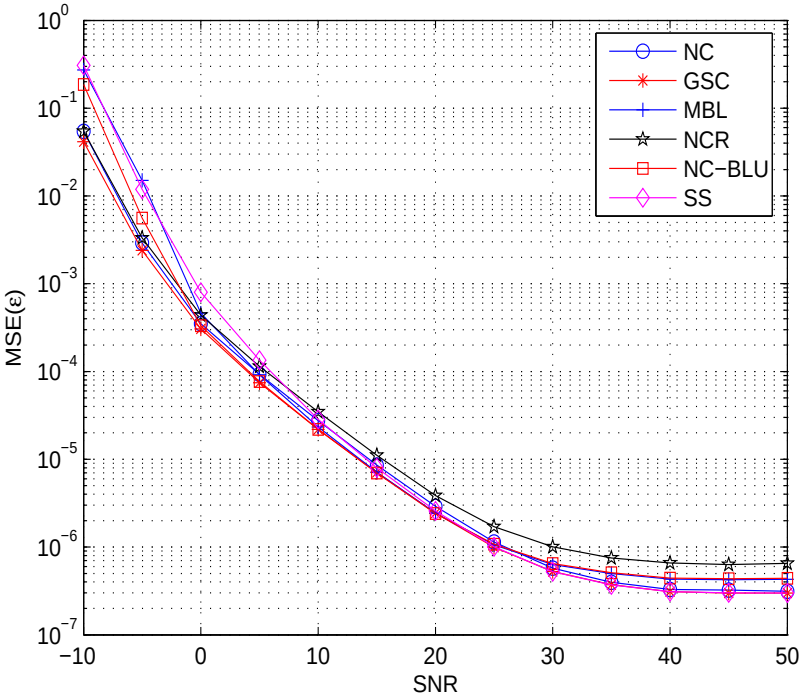

Figure 6.15: Performance of CFO estimators as a function of SNR in a multipath channel ($N = 1024$, $L_c = 16$, $N_m = 13$) for the training symbol pattern $\boldsymbol{p} = [1, 1, -1, 1]^T$.

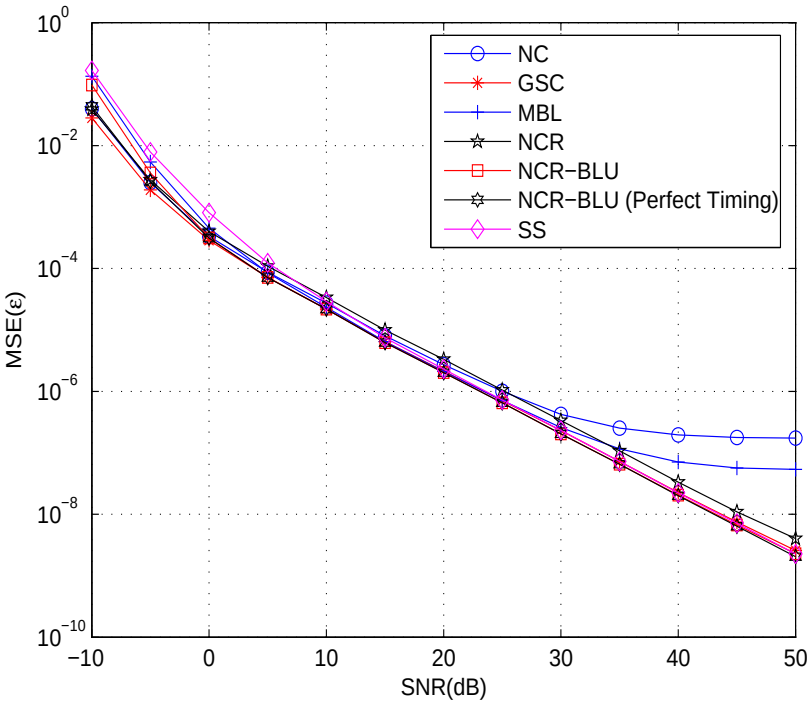

Figure 6.16: Performance of CFO estimators as a function of SNR in a multipath channel ($N = 1024$, $L_c = 16$, $N_m = 13$) for a training symbol pattern without sign inversion.

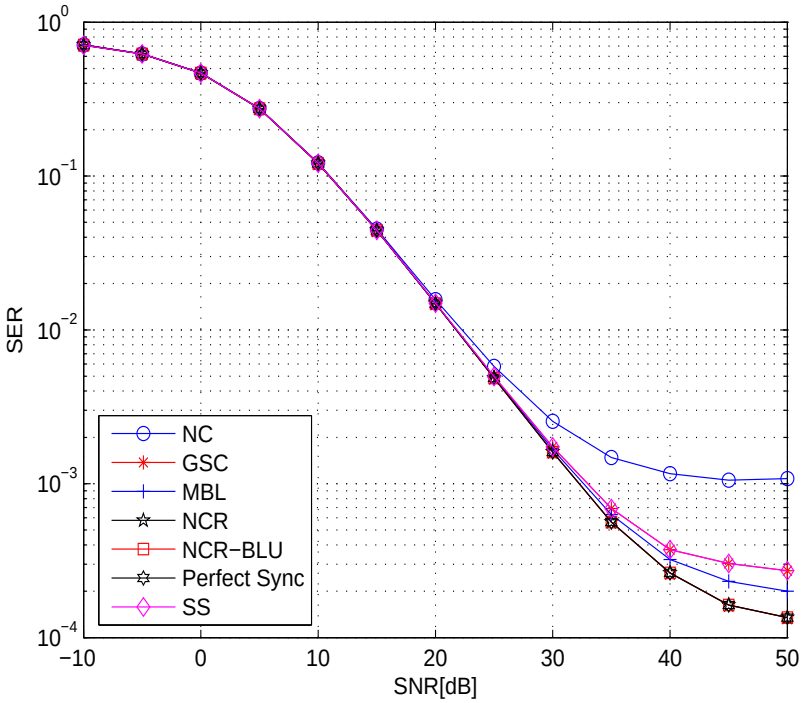

Figure 6.17: SER of considered OFDM system as a function of SNR in a multipath channel ($N = 1024$, $L_c = 16$, $N_m = 13$) for the training symbol pattern and $\boldsymbol{p} = [1, 1, -1, 1]^T$.

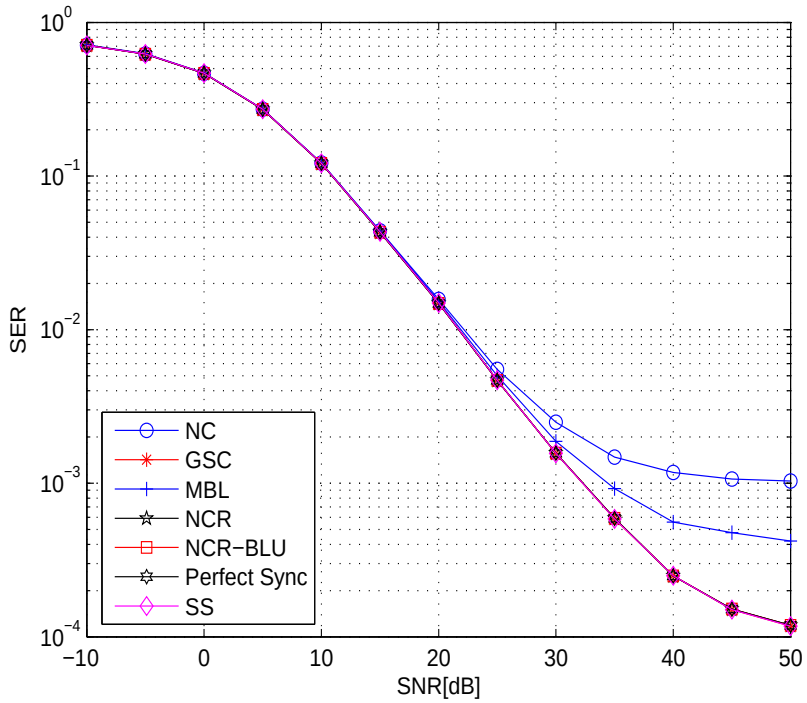

Figure 6.18: SER of considered OFDM system as a function of SNR in a multipath channel ($N = 1024$, $L_c = 16$, $N_m = 13$) for the training symbol pattern $\boldsymbol{p} = [1, 1, 1, 1]^T$.

Chapter 7

Conclusions

7.1 Thesis Summary

The performance of OFDM systems depends on the signal quality seen by the receiver. Good signal integrity is only obtained when the correct timing information is available and system impairment such as CFO is effectively estimated and corrected. This requirement demands properly designed synchronization systems. In this thesis, issues related to symbol timing and CFO synchronization are discussed. In particular, after the presentation of the OFDM system and the analysis of effects of CFO and symbol timing synchronization errors, new blind and data-aided synchronization algorithms have been derived and analyzed.

Precisely, in the chapter § 4 the problem of blind joint symbol timing and CFO estimation in OFDM systems with NC transmissions has been considered and new ML-based synchronization algorithms have been derived. These estimators, unlike MLC estimators based only on the correlation induced by the CP insertion, exploit also the conjugate correlation resulting from the adoption of NC constellations. Due to the computational complexity of ML estimators for NC transmissions, simpler synchronization schemes that can also be used in the absence of CP, have been proposed. Moreover, in this chapter it has been evaluated the CRB on CFO and carrier phase estimation for NC-OFDM systems in the case of known symbol timing and under the Gaussianity assumption on the useful OFDM signal vector. In particular, it has been shown

that according to [41], in the case of NC transmissions and for an observation window including different OFDM symbols, the convergence rate of the phase and the CFO $\triangle F = \epsilon/N$ are $1/N$ and $1/N^3$, respectively. Moreover, the CRB_{ϵ}^{NC} obtained into the case of NC-OFDM transmissions is upper bounded by the associated CRB_{ϵ}^{C} for circular transmissions and, in the examined case, the difference between them is more prominent for low SNR values and, for a fixed SNR value, when the length of the observation window increases.

In the chapter § 5 the problem of data-aided symbol timing and CFO estimation in OFDM systems has been considered. Precisely, a novel synchronization scheme based on a training symbol made up of L identical parts, obtained by transmitting BPSK data symbols on the subcarriers whose indexes are multiple of L and setting zero on the remaining subcarriers, has been proposed. In this case, if the number of subcarriers is sufficiently large, the training symbol can be modeled as an NC-CGRV. By exploiting the joint PDF for improper CGRV's, the joint ML estimator for the parameters of interest has been derived. Since its implementation complexity is high, simpler estimators have been obtained. Moreover, a refined symbol timing estimator, that do not require the knowledge of the maximum channel delay spread or a timing advancement estimate, has been proposed.

In the chapter § 6 the performance of the considered blind and data-aided estimators has been evaluated and compared with that of MLC and MMLC estimators, proposed in [9] and [5], and with that of SS and MBL estimators based on complex training symbol proposed in [18] and in [19], respectively. Computer simulations have shown that:

- Proposed blind ML-based symbol timing and CFO estimators can outperform in AWGN and in multipath channel MLC and MMLC estimators.

- In multipath channel the derived blind estimators assure a SER performance practically coincident with that obtained in the case of perfect synchronization while the adoption of MLC and MMLC schemes leads to a severe performance degradation unless the CP presents a relatively large number of ISI-free samples.

- Proposed data-aided NC symbol timing estimator assures in AWGN channel absence of plateau effect. In particular, in contrast to the meth-

ods considered in [18] and in [19] the proposed symbol timing estimator assures good localization properties independently of the training sequence pattern,

- The proposed NCR and the more feasible NCR-BLU synchronization schemes provide a SER very close to that of the perfectly synchronization system in presence of AWGN and in multipath channel.

7.2 Future Works

In this work, we have investigated the problem of symbol timing and CFO synchronization for OFDM systems by deriving ML-based blind synchronization schemes for OFDM systems with NC transmissions and new estimators based on an NC training symbols. Our suggestions for future work are twofold: they pertain to the application of our analysis method to orthogonal frequency-division multiplexing (OFDM) systems based on offset QAM (OFDM/OQAM) (see [48]), and to the derivation and analysis of synchronization algorithms for NC-OFDM systems with virtual subcarriers. Moreover, all proposed synchronization schemes have been derived under the hypothesis of a non dispersive channel. Nevertheless, in a dispersive channel the proposed symbol timing estimators could not synchronize the receiver to the first arriving multipath component giving rise to imperfect timing recovery. Therefore, to maintain orthogonality between different subcarriers, refined symbol timing estimators have been proposed. Future work could include the study and the analysis of new blind and/or data-aided estimators designed for multipath channels that do not require the refinement process.

Appendix A

Derivation of LLF

In this appendix we present some algebraic detail to derive the expression of the LLF in (4.19).

With reference to the quadratic form in (4.18), we can observe that the inverse of the block diagonal matrix $\bar{\boldsymbol{C}}$, defined in (4.17), is still a block diagonal matrix equal to

$$\bar{\boldsymbol{C}}^{-1}=\text{diag}\Bigg\{\begin{bmatrix}(\sigma_s^2+\sigma_n^2)\boldsymbol{I}_{N/2+L_c+\theta} & \boldsymbol{G}_1\boldsymbol{R}_{\boldsymbol{s}}\boldsymbol{G}_1^T \\ \boldsymbol{G}_1\boldsymbol{R}_{\boldsymbol{s}}^*\boldsymbol{G}_1^T & (\sigma_s^2+\sigma_n^2)\boldsymbol{I}_{N/2+L_c+\theta}\end{bmatrix}^{-1}$$

$$\begin{bmatrix}\boldsymbol{C}_{\boldsymbol{s}}+\sigma_n^2\boldsymbol{I}_M & \boldsymbol{R}_{\boldsymbol{s}} \\ \boldsymbol{R}_{\boldsymbol{s}}^* & \boldsymbol{C}_{\boldsymbol{s}}+\sigma_n^2\boldsymbol{I}_M\end{bmatrix}^{-1}\otimes\boldsymbol{I}_{\eta+1}$$

$$\begin{bmatrix}(\sigma_s^2+\sigma_n^2)\boldsymbol{I}_{N-\theta} & \boldsymbol{G}_2\boldsymbol{R}_{\boldsymbol{s}}\boldsymbol{G}_2^T \\ \boldsymbol{G}_2\boldsymbol{R}_{\boldsymbol{s}}^*\boldsymbol{G}_2^T & (\sigma_s^2+\sigma_n^2)\boldsymbol{I}_{N-\theta}\end{bmatrix}^{-1}\Bigg\},$$

moreover, using the properties of inversion of block matrices, we obtain

$$\bar{\boldsymbol{C}}^{-1}=\mathrm{diag}\Bigg\{\begin{bmatrix} \boldsymbol{P}_{\boldsymbol{s}-1}^{-1} & -\dfrac{\boldsymbol{G}_1\boldsymbol{R}_{\boldsymbol{s}}\boldsymbol{G}_1^T\boldsymbol{P}_{\boldsymbol{s}-1}^{-1}}{\sigma_n^2+\sigma_s^2} \\ -\dfrac{\boldsymbol{G}_1\boldsymbol{R}_{\boldsymbol{s}}^*\boldsymbol{G}_1^T\boldsymbol{P}_{\boldsymbol{s}-1}^{-1}}{\sigma_n^2+\sigma_s^2} & \boldsymbol{P}_{\boldsymbol{s}-1}^{-1} \end{bmatrix}$$

$$\boldsymbol{I}_{\eta+1}\otimes\begin{bmatrix} \boldsymbol{P}_{\boldsymbol{s}}^{-1} & -\left(\boldsymbol{C}_{\boldsymbol{s}}+\sigma_n^2\boldsymbol{I}_M\right)^{-1}\boldsymbol{R}_{\boldsymbol{s}}\boldsymbol{P}_{\boldsymbol{s}}^{-1} \\ -\left(\boldsymbol{C}_{\boldsymbol{s}}+\sigma_n^2\boldsymbol{I}_M\right)^{-1}\boldsymbol{R}_{\boldsymbol{s}}^*\boldsymbol{P}_{\boldsymbol{s}}^{-1} & \boldsymbol{P}_{\boldsymbol{s}}^{-1} \end{bmatrix} \tag{A.1}$$

$$\begin{bmatrix} \boldsymbol{P}_{\boldsymbol{s}+1}^{-1} & -\dfrac{\boldsymbol{G}_2\boldsymbol{R}_{\boldsymbol{s}}\boldsymbol{G}_2^T\boldsymbol{P}_{\boldsymbol{s}+1}^{-1}}{\sigma_n^2+\sigma_s^2} \\ -\dfrac{\boldsymbol{G}_2\boldsymbol{R}_{\boldsymbol{s}}^*\boldsymbol{G}_2^T\boldsymbol{P}_{\boldsymbol{s}+1}^{-1}}{\sigma_n^2+\sigma_s^2} & \boldsymbol{P}_{\boldsymbol{s}+1}^{-1} \end{bmatrix}\Bigg\}$$

where
$\boldsymbol{P}_{\boldsymbol{s}-1}=(\sigma_n^2+\sigma_s^2)\boldsymbol{I}_{N/2+L_c+\theta}-(\sigma_n^2+\sigma_s^2)^{-1}\boldsymbol{G}_1\boldsymbol{R}_{\boldsymbol{s}}(\boldsymbol{G}_1\boldsymbol{R}_{\boldsymbol{s}})^H$,
$\boldsymbol{P}_{\boldsymbol{s}}=(\boldsymbol{C}_{\boldsymbol{s}}+\sigma_n^2\boldsymbol{I}_M)-\boldsymbol{R}_{\boldsymbol{s}}(\boldsymbol{C}_{\boldsymbol{s}}+\sigma_n^2\boldsymbol{I}_M)^{-1}\boldsymbol{R}_{\boldsymbol{s}}^*$ and
$\boldsymbol{P}_{\boldsymbol{s}+1}=(\sigma_n^2+\sigma_s^2)\boldsymbol{I}_{N-\theta}-(\sigma_n^2+\sigma_s^2)^{-1}\boldsymbol{G}_2\boldsymbol{R}_{\boldsymbol{s}}(\boldsymbol{G}_2\boldsymbol{R}_{\boldsymbol{s}})^H$.

Let us define the complex matrices $\boldsymbol{\Upsilon}_{-1}\overset{\triangle}{=}\boldsymbol{G}_1\boldsymbol{\Psi}_{-1}\boldsymbol{G}_1^T$ and $\boldsymbol{\Upsilon}_{\eta+1}\overset{\triangle}{=}\boldsymbol{G}_2\boldsymbol{\Psi}_{\eta+1}\boldsymbol{G}_2^T$. Substituting (A.1) in (4.18) and applying the definition of trace of a block diagonal matrix, the quadratic form (4.18) can be rearranged as

$$\begin{aligned}\Lambda(\boldsymbol{\lambda})=&\Re\Bigg\{\mathrm{Tr}\Bigg[\boldsymbol{\Upsilon}_{-1}\frac{\boldsymbol{G}_1\boldsymbol{R}_{\boldsymbol{s}}\boldsymbol{G}_1^T\boldsymbol{P}_{\boldsymbol{s}-1}^{-1}}{\sigma_n^2+\sigma_s^2}\boldsymbol{\Upsilon}_{-1}\check{\boldsymbol{r}}_{-1}^*\check{\boldsymbol{r}}_{-1}^H\\ &-\boldsymbol{\Upsilon}_{-1}\boldsymbol{P}_{\boldsymbol{s}-1}^{-1}\boldsymbol{\Upsilon}_{-1}^*\check{\boldsymbol{r}}_{-1}\check{\boldsymbol{r}}_{-1}^H-\boldsymbol{\Upsilon}_{\eta+1}\boldsymbol{P}_{\boldsymbol{s}+1}^{-1}\boldsymbol{\Upsilon}_{\eta+1}^*\check{\boldsymbol{r}}_{\eta+1}\check{\boldsymbol{r}}_{\eta+1}^H\\ &+\sum_{i=0}^{\eta}\boldsymbol{\Psi}_i\Big(\left(\boldsymbol{C}_{\boldsymbol{s}}+\sigma_n^2\boldsymbol{I}_M\right)^{-1}\boldsymbol{R}_{\boldsymbol{s}}\boldsymbol{P}_{\boldsymbol{s}}^{-1}\boldsymbol{\Psi}_i\boldsymbol{r}_i^*-\boldsymbol{P}_{\boldsymbol{s}}^{-1}\boldsymbol{\Psi}_i^*\boldsymbol{r}_i\Big)\,\boldsymbol{r}_i^H\\ &+\boldsymbol{\Upsilon}_{\eta+1}\frac{\boldsymbol{G}_2\boldsymbol{R}_{\boldsymbol{s}}\boldsymbol{G}_2^T\boldsymbol{P}_{\boldsymbol{s}+1}^{-1}}{\sigma_n^2+\sigma_s^2}\boldsymbol{\Upsilon}_{\eta+1}\check{\boldsymbol{r}}_{\eta+1}^*\check{\boldsymbol{r}}_{\eta+1}^H\Bigg]\Bigg\},\end{aligned}$$

that, after some algebraic manipulations, can be rewritten as

$$\begin{aligned}\Lambda(\boldsymbol{\lambda})=&T(\theta)+\Re\Bigg\{e^{-j2\pi\epsilon}\sum_{i=0}^{\eta}U_i(\theta)\\ &+\gamma^*\sum_{i=-1}^{\eta+1}\left[V_i(\theta)e^{-j\frac{4\pi}{N}\epsilon iM}+Z_i(\theta)e^{-j\frac{2\pi}{N}\epsilon(2iM+N)}\right]\Bigg\},\end{aligned}$$

where the parameter γ is defined in (4.20),

$$\begin{aligned} T(\theta) \stackrel{\triangle}{=} & -\sum_{l=0}^{\eta}\sum_{k=0}^{M-1} |r_l(k+\theta-L_c)|^2 \left[\boldsymbol{P}_{\boldsymbol{s}}^{-1}\right]_{k,k} \\ & -\sum_{k=0}^{N/2+L_c+\theta-1} |r_{-1}(k+N/2-L_c)|^2 \left[\boldsymbol{P}_{\boldsymbol{s}_{-1}}^{-1}\right]_{k,k} \\ & -\sum_{k=0}^{N-\theta-1} |r_{\eta+1}(k+\theta-L_c)|^2 \left[\boldsymbol{P}_{\boldsymbol{s}_{+1}}^{-1}\right]_{k,k} , \end{aligned} \tag{A.2}$$

$$U_i(\theta) \stackrel{\triangle}{=} -2\sum_{k=0}^{L_c-1} r_i^*(k+\theta-L_c) r_i(k+\theta+N-L_c) \left[\boldsymbol{P}_{\boldsymbol{s}}^{-1}\right]_{k,k+N} , \tag{A.3}$$

for $i = 0, \ldots, \eta$, moreover

$$V_i(\theta) \stackrel{\triangle}{=} \begin{cases} 0 \quad i=-1 \\ \sum_{k=0}^{2L_c} r_i(k+\theta-L_c) r_i(L_c+\theta-k) \times \\ \left[\left(\boldsymbol{C}_{\boldsymbol{s}}+\sigma_n^2\boldsymbol{I}_M\right)^{-1} \boldsymbol{R}_{\boldsymbol{s}}^* \boldsymbol{P}_{\boldsymbol{s}}^{-1}\right]_{k,2L_c-k} \quad i=0,\ldots,\eta \\ \sum_{k=0}^{2L_c} r_i(k+\theta-L_c) r_i(L_c+\theta-k) \times \\ \left[\frac{1}{\sigma_n^2+\sigma_s^2} \boldsymbol{G}_2 \boldsymbol{R}_{\boldsymbol{s}}^* \boldsymbol{G}_2^T \boldsymbol{P}_{\boldsymbol{s}+1}^{-1}\right]_{k,2L_c-k} \quad i=\eta+1 \end{cases} \tag{A.4}$$

and

$$Z_i(\theta)\stackrel{\triangle}{=}\begin{cases}\displaystyle\sum_{k=0}^{2L_c+2\theta} r_i(k+N/2-L_c)r_i(N/2+L_c+2\theta-k)\times \\ \left[\frac{1}{\sigma_n^2+\sigma_s^2}\boldsymbol{G}_1\boldsymbol{R}_{\boldsymbol{s}}^*\boldsymbol{G}_1^T\boldsymbol{P}_{\boldsymbol{s}-1}^{-1}\right]_{k,2L_c+2\theta-k} & i=-1 \\ \displaystyle\sum_{k=L_c+1}^{M-1} r_i(k+\theta-L_c)r_i(M+\theta-k)\times \\ \left[\left(\boldsymbol{C}_{\boldsymbol{s}}+\sigma_n^2\boldsymbol{I}_M\right)^{-1}\boldsymbol{R}_{\boldsymbol{s}}^*\boldsymbol{P}_{\boldsymbol{s}}^{-1}\right]_{k,N+2L_c-k} & i=0,\ldots,\eta \\ \displaystyle\sum_{k=2L_c+\theta+1}^{N-\theta-1} r_i(k+\theta-L_c)r_i(M+\theta-k)\times \\ \left[\frac{1}{\sigma_n^2+\sigma_s^2}\boldsymbol{G}_2\boldsymbol{R}_{\boldsymbol{s}}^*\boldsymbol{G}_2^T\boldsymbol{P}_{\boldsymbol{s}+1}^{-1}\right]_{k,N+2L_c-k} & i=\eta+1.\end{cases} \tag{A.5}$$

Finally, the (l,m)th entries of inverse of the matrices $\boldsymbol{P}_{\boldsymbol{s}-1}$, $\boldsymbol{P}_{\boldsymbol{s}}$ and $\boldsymbol{P}_{\boldsymbol{s}+1}$, appearing in (A.2) - (A.5), are given by

$$\left[\boldsymbol{P}_{\boldsymbol{s}-1}^{-1}\right]_{(l,m)}=\begin{cases}\dfrac{1}{(\sigma_n^2+\sigma_s^2)(1-\rho^2|b|^2)} & l=m \\ \forall\ 0\le l,m\le 2L_c+2\theta, & \\ \dfrac{1}{(\sigma_n^2+\sigma_s^2)} & l=m \\ \forall\ 2L_c+2\theta+1\le l,m\le N/2+L_c+\theta-1, & \\ 0 & \text{otherwise,}\end{cases} \tag{A.6}$$

$$\left[\boldsymbol{P}_{\boldsymbol{s}}^{-1}\right]_{(l,m)} = \begin{cases} c_1(\rho^2|b|^2-1) & l=m \\ \forall\ 0\le l,m\le L_c-1,\ N\le l,m\le M-1 & \\ c_1(\rho^2-1) & l=m \\ \forall\ L_c+1\le l,m\le 2L_c, & \\ \dfrac{1}{(\sigma_n^2+\sigma_s^2)(1-\rho^2|b|^2)} & l=m \\ \forall\ l,m=L_c,\ 2L_c+1\le l,m\le N-1, & \\ c_1\rho(1-\rho|b|^2) & |l-m|=N \\ \forall\ 0\le l,m\le M-1, & \\ 0 & \text{otherwise} \end{cases} \tag{A.7}$$

and

$$\left[\boldsymbol{P}_{\boldsymbol{s}+1}^{-1}\right]_{(l,m)} = \begin{cases} \dfrac{1}{(\sigma_n^2+\sigma_s^2)(1-\rho^2|b|^2)} & l=m \\ \forall\ 0\le l,m\le 2L_c, 2L_c+\theta+1\le l,m\le N-\theta-1, & \\ \dfrac{1}{(\sigma_n^2+\sigma_s^2)} & l=m \\ \forall\ 2L_c+1\le l,m\le 2L_c+\theta, & \\ 0 & \text{otherwise}, \end{cases} \tag{A.8}$$

where

$$c_1 \stackrel{\triangle}{=} \frac{1}{(\sigma_n^2+\sigma_s^2)(-1+2\rho^2|b|^2+\rho^2-2\rho^3|b|^2)}$$

and

$$\rho \stackrel{\triangle}{=} \frac{\sigma_s^2/\sigma_n^2}{1+\sigma_s^2/\sigma_n^2} = \frac{SNR}{1+SNR}. \tag{A.9}$$

Appendix B

Refined Symbol Timing Estimators

In this Appendix we report some details to derive the approximation (4.49). We underline that these approximations are derived to clarify the relationship between the coarse NC and MCL0 symbol timing estimators in (4.23) and (4.37) and their refined version in (4.53) and (4.55), respectively.

Let us substitute the signal model (4.48) into (A.3), then, in the absence of noise and accounting for (4.1), we can write

$$\frac{|U_i(\beta+\theta)|}{N}=\frac{2\rho^2(1-\rho|b|^2)}{(1-\rho)(1+\rho-2\rho^2|b|^2)}\left|\sum_{l_1,l_2=0}^{N_m} h(l_1)h^*(l_2)\right.$$
$$\left.\frac{1}{N^2}\sum_{n_1,n_2=0}^{N-1} a_i^{n_1}(a_i^{n_2})^* e^{j\frac{2\pi}{N}(n_1-n_2)(k-L_c+\beta)} e^{j\frac{2\pi}{N}(n_2l_2-n_1l_1)}\right|.$$

Let us observe that the random variable

$$\frac{1}{N^2}\sum_{n_1,n_2=0}^{N-1} a_i^{n_1}(a_i^{n_2})^* e^{j\frac{2\pi}{N}(n_1-n_2)(k-L_c+\beta)} e^{j\frac{2\pi}{N}(n_2l_2-n_1l_1)}$$

with mean $\mathcal{O}(N^{-1})$ and variance $\mathcal{O}(N^{-2})$, tends to 0 in the mean squared sense by the Markoff's theorem. Then, for $N \gg 1$ and for $i \in \{0,\ldots,\eta\}$

$$\frac{|U_i(\beta+\theta)|}{N} \simeq 0\,. \tag{B.1}$$

Equally, it can be shown that for $i \in \{0, \ldots, \eta+1\}$

$$\frac{|V_i(\beta+\theta)|}{N} \simeq 0 \,. \tag{B.2}$$

Moreover, substituting the signal model (4.48) into (A.5), and accounting for (A.6)-(A.8), after simple manipulations, we can write

$$\frac{1}{N}\sum_{i=-1}^{\eta+1}|Z_i(\beta+\theta)| = \frac{\rho^2|b|}{(1-\rho^2|b|^2)}\left\{w_N(-1)+w_N(\eta+1)+\sum_{i=0}^{\eta}w_N(i)\right\},$$

where

$$w_N(-1) \stackrel{\triangle}{=} \left|\sum_{l_1,l_2=0}^{N_m} h(l_1)h(l_2)\sum_{k=-L_c}^{L_c+2(\theta+\beta)} y_N(k+N/2-\theta-\beta,-1)\right|,$$

$$w_N(\eta+1) \stackrel{\triangle}{=} \left|\sum_{l_1,l_2=0}^{N_m} h(l_1)h(l_2)\sum_{k=L_c+\theta+\beta+1}^{N-L_c-\theta-\beta} y_N(k,\eta+1)\right|$$

and

$$w_N(i) \stackrel{\triangle}{=} \left|\sum_{l_1,l_2=0}^{N_m} h(l_1)h(l_2)\left[\frac{2\rho(|b|^2\rho-1)}{(1+\rho-2\rho^2|b|^2)}\sum_{k=1}^{L_c} y_N(k,i) - y_N(0,i) + \frac{1}{N}\sum_{n=0}^{N-1}(a_i^n)^2 e^{j\frac{2\pi}{N}n(2\beta-l_1-l_2)}\right]\right|$$

with

$$y_N(k,i) \stackrel{\triangle}{=} \frac{1}{N^2}\sum_{n_1,n_2=0}^{N-1}\Big[a_i^{n_1}a_i^{n_2}e^{j\frac{2\pi}{N}(n_1-n_2)k} e^{j\frac{2\pi\beta}{N}(n_1+n_2)}e^{-j\frac{2\pi}{N}(n_1l_1+n_2l_2)}\Big].$$

It can be shown that the random variables $w_N(-1)+w_N(\eta+1)$ and $w_N(i)$, for $i \in \{0, \ldots, \eta\}$ tend to $|b||(h*h)(2\beta)|$ in the mean squared sense . Therefore, for $N \gg 1$ and under the assumption that the channel impulse response $h(n)$

spans over N_m samples (that is $h(n) \neq 0$, $\forall n \in \{0,\ldots,N_m\}$ and $h(n) \equiv 0$, $\forall n \notin \{0,\ldots,N_m\}$), it follows that $\forall \beta \in \{0,\ldots,N_m\}$

$$\frac{1}{N}\sum_{i=-1}^{\eta+1}|Z_i(\beta+\theta)| \simeq \frac{(\eta+2)\rho^2|b|^2|(h*h)(2\beta)|}{(1-\rho^2|b|^2)}\,, \tag{B.3}$$

while $\forall \beta \notin \{0,\ldots,N_m\}$

$$\frac{1}{N}\sum_{i=-1}^{\eta+1}|Z_i(\beta+\theta)| \simeq 0\,. \tag{B.4}$$

Note that in presence of additive noise modeled as a complex circular white Gaussian process it can be easily shown that (B.1)-(B.4) hold true, while the $T(\beta+\theta)/N$ term can be approximated by

$$\begin{aligned}\frac{T(\beta+\theta)}{N} \simeq \; & -\left[\frac{(\eta+2)\rho}{(1-\rho^2|b|^2)}+\frac{\rho}{2}\right]\sum_{l=0}^{N_m}|h(l)|^2 \\ & -\frac{(\eta+2)(1-\rho)}{(1-\rho^2|b|^2)}+\frac{(1-\rho)}{2}.\end{aligned} \tag{B.5}$$

Thus, from (B.1)-(B.5), we obtain (4.49) with $\mu_1 \stackrel{\triangle}{=} \frac{(\eta+2)\rho^2|b|^2}{(1-\rho^2|b|^2)}$ and $\mu_2 \stackrel{\triangle}{=} \left[\frac{(\eta+2)\rho}{(1-\rho^2|b|^2)}+\frac{\rho}{2}\right]\sum_{l=0}^{N_m}|h(l)|^2+\frac{(\eta+2)(1-\rho)}{(1-\rho^2|b|^2)}+\frac{(1-\rho)}{2}$.

Appendix C

Analytical Performance of MCL0

In this Appendix we derive the mean squared error reported in (4.56). Let us evaluate the CFO MCL0 estimator in (4.38) at $\hat{\theta} = \beta$ and let us observe that for $|\hat{\epsilon}_{MCL0} - \epsilon| \ll 1/4\pi$ we can approximate the estimation error as (see [7])

$$\hat{\epsilon}_{MCL0} - \epsilon \simeq \frac{1}{4\pi} \left\{ \frac{\sum_{i=0}^{\eta} \Im \left[e^{-j4\pi\epsilon} Z_{i+1_{L0}}(\beta) / Z_{i_{L0}}(\beta) \right]}{\sum_{i=0}^{\eta} \Re \left[e^{-j4\pi\epsilon} Z_{i+1_{L0}}(\beta) / Z_{i_{L0}}(\beta) \right]} \right\}. \tag{C.1}$$

Let us substitute the signal model (4.48) in (4.33). Then, under the hypothesis $N \gg 1$, by following the lines of Appendix B and for high SNR values, (4.33) can be rewritten as

$$\frac{Z_{i_{L0}}(\beta)}{N} \simeq e^{j\frac{2\pi\epsilon}{N}((2i+1)N+2\beta)} \sigma_s^2 b(h * h)(2\beta) + w_i, \tag{C.2}$$

for $i \in \{0, \ldots, \eta + 1\}$, with

$$\begin{aligned} w_i \stackrel{\triangle}{=} \frac{1}{N} \sum_{k=1}^{N-1} \Bigg[& n_i(k+\beta) e^{-j\frac{2\pi\epsilon}{N}(iN+\beta+k)} \sum_{l=0}^{N_m} s_i(N+\beta-k-l) h(l) \\ & + n_i(N-k+\beta) e^{-j\frac{2\pi\epsilon}{N}((i+1)N+\beta-k)} \sum_{l=0}^{N_m} s_i(\beta+k-l) h(l) \Bigg], \end{aligned}$$

for $i \in \{0, \ldots, \eta\}$, and

$$w_i \stackrel{\triangle}{=} \frac{1}{N} \sum_{k=\beta+1}^{N-\beta-1} \Bigg[n_i(k+\beta) e^{-j\frac{2\pi\epsilon}{N}(iN+\beta+k)} \sum_{l=0}^{N_m} s_i(N+\beta-k-l) h(l) + n_i(N-k+\beta) e^{-j\frac{2\pi\epsilon}{N}((i+1)N+\beta-k)} \sum_{l=0}^{N_m} s_i(\beta+k-l) h(l) \Bigg],$$

for $i = \eta + 1$. Then, accounting for (C.2) and after simple manipulations, it can be shown that

$$\hat{\epsilon}_{MCL0} - \epsilon \simeq \frac{1}{4\pi\sigma_s^2(\eta+1)} \Im \left[\frac{1}{b(h*h)(2\beta)} (w_{\eta+1} - w_0) \right]. \tag{C.3}$$

From (C.3) we obtain $E[(\hat{\epsilon}_{MCL0} - \epsilon)] = 0$, that is, for high SNR values the CFO MCL0 estimate is unbiased. Moreover, the mean squared error is given by

$$\begin{aligned} E[(\hat{\epsilon}_{MCL0} - \epsilon)^2] &\simeq \frac{E[|w_{\eta+1}|^2 + |w_0|^2]}{32\pi^2\sigma_s^4(\eta+1)^2 |b(h*h)(2\beta)|^2} \\ &\qquad (N-\beta-1) \sum_{l=0}^{N_m} |h(l)|^2 \\ &= \frac{}{4\pi^2 SNR(\eta+1)^2 |b|^2 |(h*h)(2\beta)|^2 N^2}, \end{aligned}$$

then, for $N \gg 2N_m + 1$ (4.56) is obtained.

Bibliography

[1] R. van Nee and R. Prasad, "OFDM for Wireless Multimedia Communications," *Boston, MA: Artech House*, 2000.

[2] A. R. S. Bahai and B. R. Saltzberg, "Multi-Carrier Digital Communications. Theory and Applications of OFDM," *Kluwer Academic Publishers*, 1999.

[3] A. Palin and J. Rinne, "Enhanced symbol synchronization method for OFDM system in SFN channels," in Proc. *GLOBECOM 1998*, vol. 5, pp. 2788-2793, November 1998.

[4] L. Da-wei, T. You-xi, S. Dong-sheng and L. Shao-qian, "Impact of timing error on BER performance of TDD pre-equalized OFDM systems," in Proc. *PIMRC 2004*, pp. 714-718, September 2004.

[5] M. Speth, F. Classen and H. Meyr, "Frame synchronization of OFDM systems in frequency selective channels," in Proc. *VTC*, pp. 1807-1811, May 1997.

[6] T. Pollet and M. Moeneclaey, "Synchronizability of OFDM signals," in Proc. *GLOBECOM 1995*, pp. 2054-2058, November 1995.

[7] P. H. Moose, "A techique for orthogonal frequency division multiplexing frequency offset correction," *IEEE Trans. Commun.*, vol. 42, pp. 2908-2914, October 1994.

[8] H. Steendam and M. Moeneclaey, "Sensitivity of orthogonal frequency-division multiplexed systems to carrier and clock synchronization errors," *Signal Processing*, vol. 80, pp. 1217-1229, July 2000.

[9] J.J. van de Beek, M. Sandell and P.O. Börjesson, "ML estimation of time and frequency offset in OFDM systems," *IEEE Trans. Signal Processing*, vol. 45, pp. 1800-1805, July 1997.

[10] B. Picinbono, "On Circularity," *IEEE Trans. Signal Processing*, vol. 42, pp. 3473-3482, December 1994.

[11] F.D. Neeser and J.L. Massey, "Proper complex random processes with applications to information theory," *IEEE Trans. Inform. Theory*, vol. 39, pp. 1293-1302, July 1993.

[12] P. O. Amblard, M. Gaeta and J.L. Lacoume, "Statistics for complex variables and signals-Part I: Variables," *Signal Processing*, vol. 53, pp. 1-13, 1996.

[13] T. Fusco and M. Tanda: "Blind symbol timing, frequency offset and carrier phase estimation in OFDM systems," in Proc. of *Thirty-Seventh Annual Asilomar Conference on Signals, Systems, and Computers*, Pacific Grove, California, 9-12 November 2003.

[14] T. Fusco and M. Tanda, "ML frequency offset and carrier phase estimation in OFDM systems with noncircular transmissions," in Proc. *EUSIPCO 2004*, pp. 897-900, September 2004.

[15] T. Fusco and M. Tanda, "ML-based symbol timing and frequency offset estimation for OFDM systems with noncircular transmissions," to appear in *IEEE Trans. on Signal Processing*.

[16] B. Picinbono, "Second-order complex random vectors and normal distributions," *IEEE Trans. Signal Processing*, vol. 44, pp. 2637-2640, October 1996.

[17] T.M. Schmidl and D.C. Cox, "Robust frequency and timing synchronization for OFDM," *IEEE Trans. Commun.*, vol. 45, December 1997.

[18] K. Shi and E. Serpedin, "Coarse frame and carrier synchronization of OFDM systems: a new metric and comparison," *IEEE Trans. Wireless Commun.*, vol. 3, July 2004.

[19] H. Minn, V.K. Bhargava, and K.B. Letaief, "A robust timing and frequency synchronization for OFDM systems," *IEEE Trans. Wireless Commun.*, vol. 2, pp. 822-839, July 2003.

[20] T. Fusco and M. Tanda, "A timing and frequency synchronization algorithm for OFDM systems," in Proc. of *Seventh International Symposium on Wireless Personal Multimedia Communications* (WPMC 2004), Abano Terme, Padova, 12-15 September 2004.

[21] T. Fusco and M. Tanda, "A pilot-symbol-based timing and frequency offset synchronization algorithm for OFDM systems," Proc. of *International Symposium on Information Theory and its Applications* (ISITA 2004), Parma, 10-13 October 2004.

[22] T. Fusco and M. Tanda, "A data-aided symbol timing and frequency offset estimation algorithm for OFDM systems," *Wireless Personal Commun.*, vol 35, pp 201-212, October 2005.

[23] T. Fusco and M. Tanda, "Symbol timing and frequency offset estimation for OFDM systems," to be submitted to *IEEE Trans. Wireless Commun.*.

[24] S. B. Weinstein and P. M. Ebert, "Data transmission by frequency-division multiplexing using the discrete fourier transform," *IEEE Trans. Commun. Tech.* vol COM-19, pp 628-634, October 1971.

[25] J. S. Chow, J. C. Tu and J. M. Cioffi, "A discrete multitone transceiver system for HDSL applications," *IEEE J. Select. Areas Commun.* vol 9, pp 895-908, August 1991.

[26] A. Ruiz, J. M. Cioffi and S. Kasturia, "Discrete multiple tone modulation with coset coding for the spectrally shaped channel," *IEEE Trans. Commun.* vol 40, pp 1012-1029, June 1992.

[27] J. M. Cioffi, "Very high-speed digital subscriber lines (VDSL)," Proc. of *ISCAS*, pp 590-594, May/June 1998.

[28] K. Taura, M. Tsujishita, M. Takeda, H. Kato, M. Ishida, "Digital audio broadcasting (DAB) receiver," *IEEE Trans. Cons. Electronics*, vol. 42, pp. 45-66, March 1996.

[29] M. Russell and G. L. Stüber, “Terrestrial digital video broadcasting for mobile reception using OFDM ,” *Wireless Personal Commun.*, vol. 2, pp 45-66, March 1995.

[30] J. Heiskala and J. Terry, “OFDM Wireless LANs: A Theoretical and Practical Guide” *Sams Publishing* 2001.

[31] A. Peled and A. Ruiz, “Frequency domain data transmission using reduced computational complexity algorithms,” in Proc. *ICASSP*, pp 964-967, April 1980.

[32] J. H. Gunther, H. Liu, and A. L. Swindlehurst, “A new approach for symbol frame synchronization and carrier frequency estimation in OFDM communications,” in Proc. *ICASSP*, pp. 2725-2728, March 1999.

[33] D. Landström, S. K. Wilson, J. J. van de Beek, P. Ödling and P.O. Börjesson, “Symbol time offset estimation in coherent OFDM systems,” *IEEE Trans. Commun.*, pp. 545-549, April 2002.

[34] H. Bölcskei, “Blind estimation of symbol timing and carrier frequency offset in wireless OFDM systems,” *IEEE Trans. Commun.*, vol. 49, pp. 988-999, June 2001.

[35] ETSI TS 101 761-1 v1.1.1 (2000-04) “Broadband radio access networks (BRAN); HIPERLAN type 2; data link control (DLC) layer; Part 1: basic data transport functions.” http:\\www.etsi.org.

[36] J. Khun-Jush, P. Schramm, U. Wachsmann and F. Wenger, “Structure and performance of the HIPERLAN/2 physical layer”, in Proc. *VTC‘99* Amsterdam, The Netherlands, pp. 2667-2671, September 1999.

[37] T. Thaiupathump, C.D. Murphy, and S.A. Kassam, “Asymmetric signaling constellations for phase estimation,” in Proc. *SSAP*, pp. 161-165, August 2000.

[38] S.M. Kay, “Fundamentals of statistical signal processing: estimation theory,” *Prentice Hall*, 1993.

[39] J.J. van de Beek, P.O. Börjesson, M.L. Boucheret, D. Landström, J.M. Arenas, P. Ödling and S.K. Wilson, “Three non-pilot based time

and frequency estimators for OFDM," *Signal Processing*, vol. 80, pp. 1321-1334, July 2000.

[40] T. Keller, L. Piazzo, P. Mandarini and L. Hanzo, "Orthogonal frequency division multiplex synchronization techniques for frequency-selective fading channels," *IEEE J. Select. Areas Commun.*, vol. 19, pp. 999-1008, June 2001.

[41] P. Ciblat, M. Ghogho, P. Forster and P. Larzabal, "Harmonic retrieval in the presence of non-circular Gaussian multiplicative noise: performance bounds," *Signal Processing*, vol. 85, pp. 737-749, April 2005.

[42] J.P. Delmas and H. Abeida, "Stochastic Cramér-Rao bound for noncircular signals with application to DOA estimation," *IEEE Trans. Signal Processing*, vol. 52, pp. 3192-3199, November 2004.

[43] Y.C. Wu and E. Serpedin, "Comments on "Class of cyclic-based estimators for frequency-offset estimation of OFDM systems"," *IEEE Trans. Commun.*, vol. 53, pp. 413-414, March 2005.

[44] M. Tanda, "Blind symbol timing and frequency offset estimation in OFDM systems with real data symbols," *IEEE Trans. Commun.*, vol. 52, pp. 1609-1612, October 2004.

[45] M. Morelli and U. Mengali, "An improved frequency offset estimator for OFDM applications," *IEEE Trans. Commun. Letters*, vol. 3, March 1999.

[46] D.C. Rife and R.R. Boorstyn, "Single-tone parameter estimation from discrete-time observations," *IEEE Trans. Inform. Theory*, vol. IT-20, September 1974.

[47] Y.V. Zakharov, and T.C. Tozer, "Frequency estimator with dichotomous search of periodoram peak," *IEE Elecron. Letters*, vol. 35, pp. 1608-1609, September 1999.

[48] T. Fusco and M. Tanda, "Blind frequency offset estimation for OFDM/OQAM systems," to be submitted to *IEEE Trans. Signal Processing*.